STRENGTH REQUIREMENTS OF SHEAR DIAPHRAGMS USED TO BRACE STEEL I-BEAMS

A Thesis Submitted to
the Graduate School of Engineering and Sciences of
İzmir Institute of Technology
in Partial Fulfillment of the Requirements for the Degree of

MASTER OF SCIENCE

in Civil Engineering

by
Mustafa VARDAROĞLU

December 2014
İZMİR

We approve the thesis of **Mustafa VARDAROĞLU**

Examining Committee Members:

Assoc. Prof. Dr. Ninel ALVER
Department of Civil Engineering, Ege University

Assoc. Prof. Dr. Engin AKTAŞ
Department of Civil Engineering, İzmir Institute of Technology

Assist. Prof. Dr. İzzet ÖZDEMİR
Department of Civil Engineering, İzmir Institute of Technology

Assoc. Prof. Dr. O. Özgür EĞİLMEZ
Department of Civil Engineering, İzmir University of Economics

Assoc. Prof. Dr. Cemalettin DÖNMEZ
Department of Civil Engineering, İzmir Institute of Technology

12 December 2014

Assoc. Prof. Dr. Cemalettin DÖNMEZ
Supervisor,
Department of Civil Engineering
İzmir Institute of Technology

Assoc. Prof. Dr. O. Özgür EĞİLMEZ
Co-Supervisor,
Department of Civil Engineering
İzmir University of Economics

Prof. Dr. Gökmen TAYFUR
Head of the Department of Civil Engineering

Prof. Dr. Bilge KARAÇALI
Dean of the Graduate School of
Engineering and Sciences

ACKNOWLEDGEMENTS

I would like to first express my appreciation to Assoc. Prof. Dr. Özgür Eğilmez for all of his guidance, advice and friendship through this research and also throughout my graduate education. I would like to give my sincere thanks to Assoc. Prof. Dr. Cemalettin Dönmez for his professional attitude, guidance and advice as my supervisor in IZTECH. I would like to give a special thank to Professor Dr. Metin Tanoğlu for letting us to operate the analyses on the work-station originally operated by the IZTECH Mechanical Engineering Department.

I would like to thank to the members of my dissertation committee; Assoc. Prof. Dr. Ninel Alver, Assoc. Prof. Dr. Engin Aktaş and Assist. Prof. Dr. İzzet Özdemir for providing useful suggestions for my dissertation.

I would also like to thank my colleague, Andaç Akbaba for his friendship, cooperation and the supplementary information through the companion study. Thanks to my colleagues that shared their time and experience in the Laboratory of Civil Engineering Department, IZTECH.

My special thanks to the head of Karabaglar Municipality-Directorate of Technical Works and my colleagues there that supported me through the graduate program.

Finally, I want to thank to my friends, my beloved sister and my family for their encouragement, support during this study and throughout my life.

ABSTRACT

STRENGTH REQUIREMENTS OF SHEAR DIAPHRAGMS USED TO BRACE STEEL I-BEAMS

Lateral torsional buckling, also known as flexural torsional buckling is a failure mode that often controls the design of I-shaped steel beams during construction. In order to increase the lateral torsional buckling capacity of the girders in this stage, discrete or continuous bracing systems are often utilized in building and bridge constructions. Light gauge metal decking acts like a shear diaphragm and provides continuous lateral bracing to the beams. The building industry has long relied on metal decking to laterally support the beam top flanges. Bridge construction industry does not consider metal decking as a brace source due to the flexible connection between the girder and the diaphragm. However, recent studies have shown that metal sheeting can also be used in the bridge industry as construction bracing as long as the flexibility of the connections can be controlled by modifications.

An adequate bracing system must possess sufficient strength and stiffness to control deformations and brace forces. A parametrical study was conducted to investigate the stiffness and strength of shear diaphragms used to brace stocky and slender steel I-beams. This thesis focuses on the strength requirements. The parametrical study consists of eigenvalue buckling analyses and large displacement analyses on a twin girder shear diaphragm system with various girder and metal deck configurations. A three-dimensional finite element analysis program was selected for the analyses. In the model metal deck-girder connections and the connection between adjacent decks are modeled respectively. Finite element model is verified by a full-scale twin-girder buckling test as the part of a previous study. According to the numerical study an equation is proposed for the estimation of the brace forces in the deck connections. The equation is shifted for possible deck and girder configurations.

ÖZET

ÇELİK I-KİRİŞLERİ DESTEKLEMEK İÇİN KULLANILAN KAYMA DİYAFRAMLARININ MUKAVEMET İHTİYACI

Yanal burulmalı burkulma I-kesitli çelik kirişlerin tasarımında dayanımı kontrol eden limit durumlarından biri olarak kabul edilmektedir. Çelik yapı ve köprülerin yapım aşamalarında kirişlerin yanal burulmalı burkulma dayanımını arttırmak için sürekli veya tek noktada etki eden destek sistemleri kullanılmaktadır. Bina inşaatlarında beton döşeme kalıp sistemi, çatı ve cephe kaplamaları olarak sıklıkla kullanılan trapez sac kalıplar kayma diyaframı gibi çalışmakta ve bağlı oldukları kiriş boyunca sürekli yanal destek sağlamaktadır. Çelik yapı endüstrisi sac kalıbın düzlem içindeki yüksek kayma rijitliğini gözönüne almakta ve inşaat aşamasında kirişlere sürekli yanal destek kaynağı olarak kullanılmasına izin vermektedir. Çelik köprü endüstrisinde ise kalıp-kiriş bağlantılarındaki göreceli esneklik buna imkan vermemektedir. Sac kalıp–kiriş bağlantısı üzerine yapılan çalışmalar sonucunda önerilen bir iyileştirme sac kalıbın I-kirişlere sürekli destek sağlamasını mümkün kılmıştır.

Bu çalışmanın amacı narin ve narin olmayan I-kesitli çelik kirişlerin kayma diyaframları ile kiriş boyunca yanal desteklenebilmesi için gerekli ve yeterli mukavemet değerinin belirlenmesidir. Çalışma kapsamında iki I kiriş ve arasında bir kayma diyaframından ibaret olan bir sonlu elemanlar modeli oluşturulmuştur. Kirişler basit mesnetli olup mesnetlerde çarpılma serbestliği verilmiştir. ANSYS sonlu elemanlar yazılımı kullanılarak model üzerinde elastik sınırlar dahilinde burkulma analizleri yapılmıştır. Modelde kalıp bağlantıları vida ile modellenmiş olup kalıp-kiriş arası ve kalıplar arası bağlantılar ayrı ayrı modellenmiştir. Diyafram kayma rijitliği, basınç başlığı genişliği, gövde narinlik değeri ve olası kalıp-kiriş bağlantı dizilimleri göz önüne alınan değişkenler arasındadır. Sonlu eleman modeli daha önce yapılan bir çalışma kapsamında gerçekleştirilmiş olan tam ölçekli burkulma deneyi sonuçları ile karşılaştırılmış ve doğrulanmıştır. Nümerik çalışma sonucunda diyafram vida kuvvetlerinin basitçe hesaplanmasına olanak sağlayacak bir denklem önerilmiştir. Denklem farklı döşeme oluşumları için katsayıları içerecek şekilde genişletilmiştir.

TABLE OF CONTENTS

LIST OF FIGURES

LIST OF TABLES

CHAPTER 1

INTRODUCTION

1.1. General Information

Steel cross-sections could develop their full strength under tensile stresses. On the other side, under compressive stresses they are susceptible to local or global buckling before reaching to ultimate strength. Various types of buckling may occur depending on the geometry of the cross section, the direction of loading or conditions and locations of the supports.

Lateral torsional buckling, also known as flexural torsional buckling is a failure mode that often controls the design of I-shaped steel girders or beams during construction. While the concrete slab is still fresh, the girders or beams have to carry the entire construction loads and the weight of the fresh concrete. In order to increase the buckling capacity of the girders in this stage, discrete or continuous bracing systems are often utilized. In bridge construction discrete bracing systems in the form of cross-frames and diaphragms are generally utilized. Whereas in building construction, continuous bracing systems in the form of stay-in-place deck forms, often named as shear diaphragms, are commonly utilized.

Floor decks are often used in unshored construction of steel structures as formwork for concrete slab. They provide support to fresh concrete until it hardens and composite action initiates between steel girders/beams and concrete slab. Composite floor systems consist of steel beam, shear studs, stay-in-place metal deck forms, and concrete deck as shown in Figure 1.1

The building industry has long relied on metal decking to laterally support the beam top flanges. The deck forms are often treated as shear diaphragms that provide continuous lateral support against flexural torsional buckling. In the building industry, the decks are continuous over the tops of the beams as seen in Figure 1.1 and are generally attached to the top flanges using puddle welds, shear studs or fasteners (Egilmez et. al, 2009).

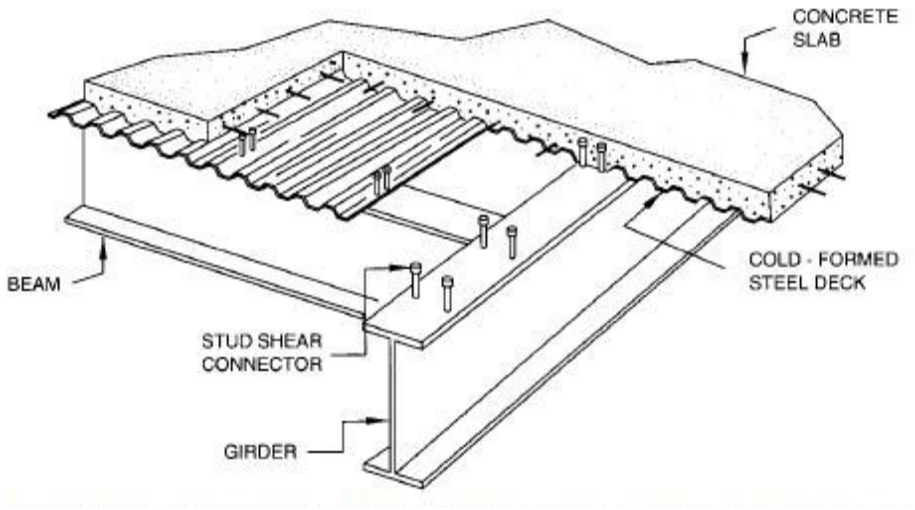

Figure 1.1. Composite floor system
(Source: Owen, 2013)

In the bridge industry, composite girders in positive moment bending regions usually have narrower top flanges with respect to the bottom flanges. This is mainly due to the fact that the final sizes of the girders are often determined by taking composite action into account. In contrast to advantages of the mono-symmetry in ultimate stress design, relatively small top flange weakens the system against lateral torsional buckling. Although reinforced concrete slab along the top flange of the steel girder is a continuous bracing source against lateral torsional buckling after the concrete deck hardens, there is usually a need for additional bracing in the early construction phases, while the concrete deck is still fresh.

American Association of State Highway and Transportation Officials (AASHTO) Load and Resistance Factor Design (LRFD) Bridge Design Specifications (2012) does not currently permit permanent metal deck forms (PMDF) to be relied on as a bracing source against lateral torsional buckling; due to the conventional flexible connection detail. Instead, the specification requires cross frames or diaphragms to be used to increase the lateral torsional buckling capacity of girders. Implementation of discrete bracing by means of cross frames in a bridge deck can be seen in Figure 1.2.

Drawbacks of these discrete bracing systems are fatigue problems encountered in girder-cross frame connections and their relatively higher costs. These drawbacks have led researchers to investigate the conventional flexible connection detail. Modified connection details were developed that significantly improve the stiffness and strength

of the permanent metal deck form systems (Egilmez et. al, 2007 and 2012) used in the bridge industry.

Figure 1.2. Intermediate discrete braces with metal deck forms
(Source: Weeks, 2013)

Following the guidelines from Egilmez et. al (2007 and 2012), two bridges in Houston, Texas were constructed using permanent metal deck forms as construction bracing. Figure 1.3 shows a photograph during the construction phase of these bridges.

Figure 1.3. Diaphragm bracing implementation from Houston, TX, USA

1.2. Forming Systems

Various materials, such as plywood, precast concrete and stay-in-place metal deck are being used for concrete formwork in bridge constructions. However, in steel bridge and building applications due to the high strength and ease of implementation, stay-in-place metal deck forms or permanent metal deck forms (PMDF) are widely chosen as the primary forming system.

PMDF consist of galvanized corrugated sheets that usually change from 60 cm to 90 cm wide. The forms generally change in thickness from 0.91 to 1.52 mm (22 to 16 gauge). PMDF are as light as plywood forms but have relatively larger spans of 2.70 m. to 3.60 m.

Building and bridge applications of PMDF differ in both geometry and connection detail. Bridge forms usually have a deeper profile with considerably thicker sheets than that used in the building industry. Figure 1.4 and Figure 1.5 illustrate deck forms used in building and bridge applications respectively. In building applications forms span over more than two beams and are open ended. Bridge metal deck forms are generally shorter since they only span between adjacent girders. Closed end forms are

used in bridge applications to prevent leaking of the concrete. Types of end closures for bridge applications are seen in Figure 1.6.

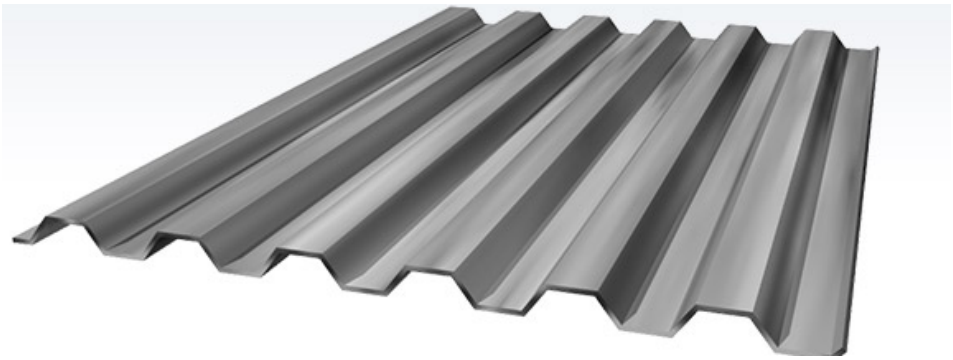

Figure 1.4. PMDF in building industry
(Source: Cordeck, 2014)

US Route 219 – Southern Expressway project by New York City Department of Transportation can be taken as an applied case, Figure 1.5. Entire project consists of 12 sections. Southern Expressway was the 5th section, which consists of two lanes in each direction, northbound and southbound, and nine bridges. The photo was taken before the concrete pouring of a 215 meter span arch bridge deck over the Cattaraugus Creek gorge.

Figure 1.5. PMDF in bridge industry
(Source: New York State Department of Transportation [NYSDOT], 2009)

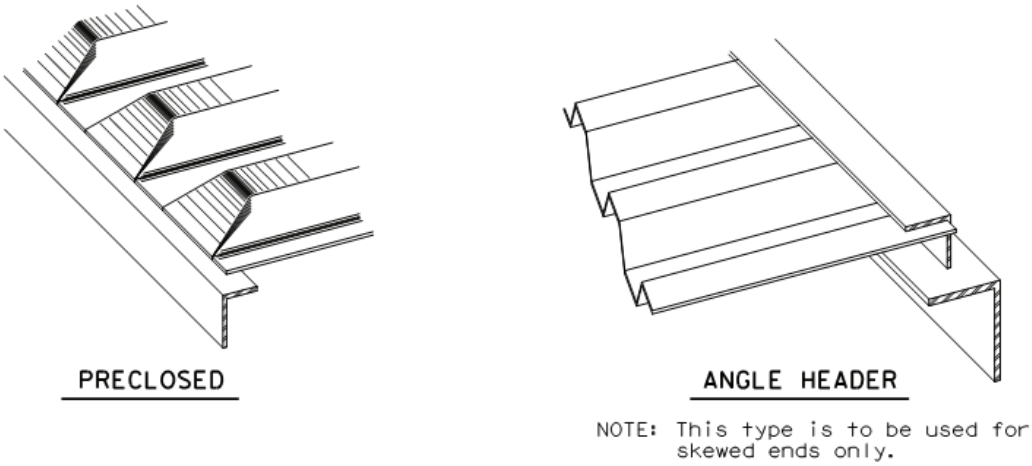

Figure 1.6. Types of PMDF used in bridge industry
(Source: Texas Department of Transportation [TxDOT], 2014)

In building applications forms are attached directly to the top flange by mechanical fasteners, puddle welds or by welding the shear studs through the formwork. Figure 1.7 shows the deck form layout for building applications.

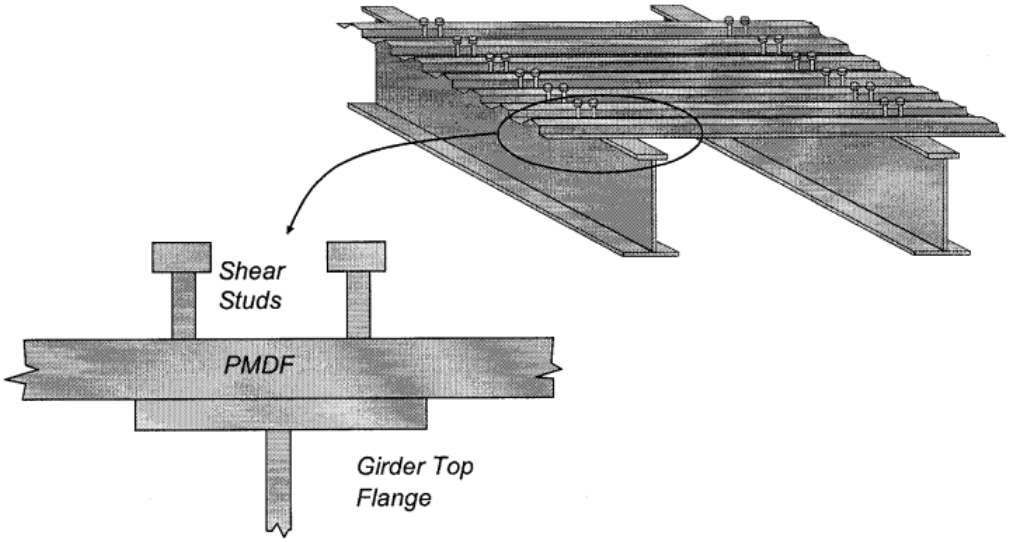

Figure 1.7. Deck form layout for building applications
(Source: Egilmez, 2005)

In bridge applications, due to the differential camber or different flange thicknesses of adjacent girders; deck forms are fastened to cold formed support angles, which are welded to girder top flanges generally with an eccentricity. Figure 1.8 shows deck form arrangement for bridge applications.

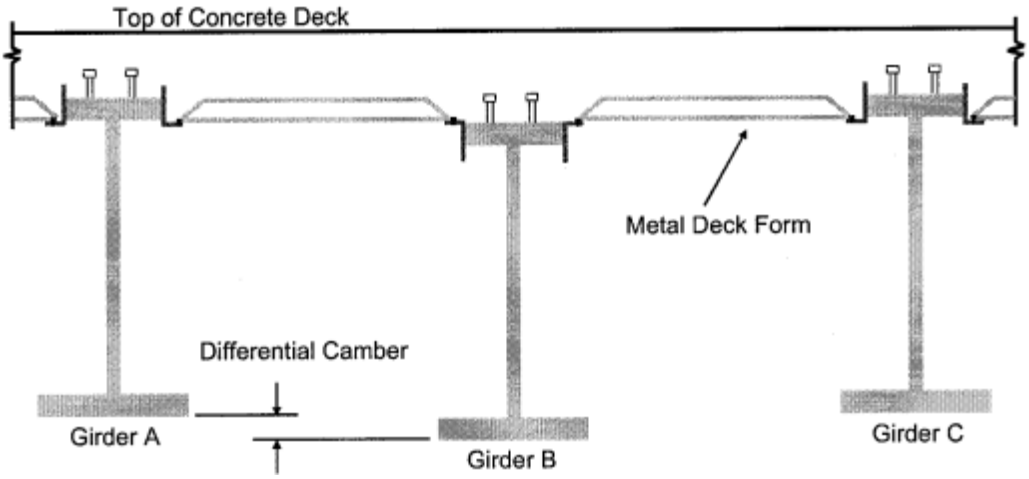

Figure 1.8. Deck form arrangement for bridge applications
(Source: Egilmez, 2005)

As previously mentioned past research has shown that the softening effects of the eccentric cold form support angles can be eliminated by a simple modification to the connection detail (Egilmez et. al, 2007, 2009, and 2012). The modified connection detail consists of transverse stiffening angles that span between adjacent girders, which can be connected directly to the top flanges or indirectly through a gusset plate as shown in Figure 1.9.

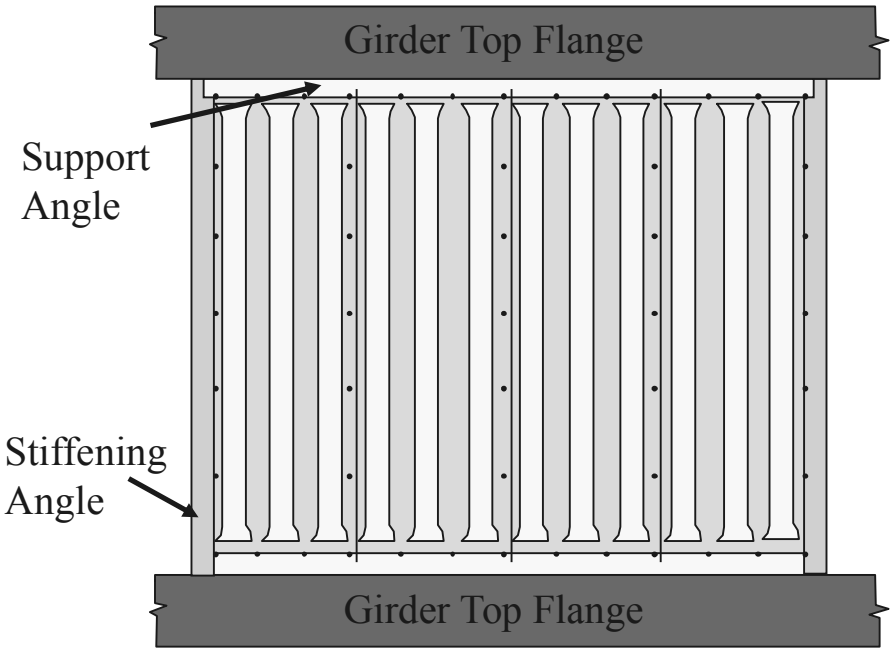

Figure 1.9. Modified connection detail by Egilmez et. al, (2007, 2009, and 2012)
(Source: Egilmez et al, 2014)

According to the Figure 1.9 the stiffening angles are positioned at side-lap locations so the decks are directly fastened to the stiffening angles at side-lap seams.

1.3. Objective and Scope

A research study has been conducted to enhance the understanding of the bracing behavior of shear diaphragms used as PMDF in steel building and bridge construction. Development of stiffness and strength requirements for diaphragm bracing of I-sections are in the scope of the current research studies. Study presented in this thesis mainly focuses and presents results on strength requirements.

A parametric study on a twin girder-shear diaphragm system with finite element approach was conducted by using ANSYS Mechanical APDL (2007). Past studies on diaphragm bracing (Helwig & Yura, 2008) of beams showed that shear strength of a diaphragm is generally controlled by either the shear strength of longitudinal edge connections –sheet to structural member connections along the edges- or shear strength of interior connections between panels –sheet to sheet connections along side laps-. Hence, a finite element model originally developed by Davies and Bryan (1982) was adopted and simply modified to address the forces that developed at both edge and side lap fasteners. The finite element model was validated by the tests conducted at University of Houston, TX by Egilmez (2005). Since an adequate bracing system must possess sufficient stiffness and strength (Winter, 1960), displacements are also taken into account in order to achieve stiffness requirements. Edge and side-lap fasteners were modeled separately; enabling the fastener forces to be directly calculated. Various analyses were conducted in order to obtain the parameters that affect the behavior.

This report consists of seven chapters. Background information with previous studies follows the introduction. Chapter 3 gives information about the finite element model used for the permanent metal deck form systems. Chapter 4 summarizes the numerical study. Chapter 5 summarizes results from stiffness requirements. Chapter 6 gathers the results on strength requirements, Chapter 7 summarizes and concludes the study.

CHAPTER 2

BACKGROUND

2.1. Overview

This chapter gives background information on stability bracing of steel I girders/or beams by shear diaphragms. Basic concepts of structural stability, buckling and lateral torsional buckling phenomena are discussed. Bracing concepts and literature overview of shear diaphragm bracing are reported briefly.

2.2. Stability and Bracing

Stability concept has been in focus of the researchers for a long time ago. Leonhard Euler proposed the critical load concept for members under compression in the 18th century. The critical load or Euler load is the axial force on a member just before it buckles. Elastic critical buckling load of an initially straight and simply supported column is:

$$P_{cr} = P_E = \frac{\pi^2 EI}{L^2} \tag{2.1}$$

where,

P_E = Euler critical buckling load;
EI = Flexural rigidity of the cross section;
L = Unbraced length of the column.

Unbraced length of a member implies the distance between brace locations. If a brace exists at mid-height as shown in Figure 2.1, the elastic critical buckling load of the column increases to four times the Euler buckling load. The significant increase in the buckling capacity clearly shows the importance of the design of bracing members in

a structural system. On the right hand side of Figure 2.1, braces are illustrated by springs with a specific stiffness that should be larger than the required value in order to provide stability to the system. Otherwise system may loose the stability and a sudden collapse may follow.

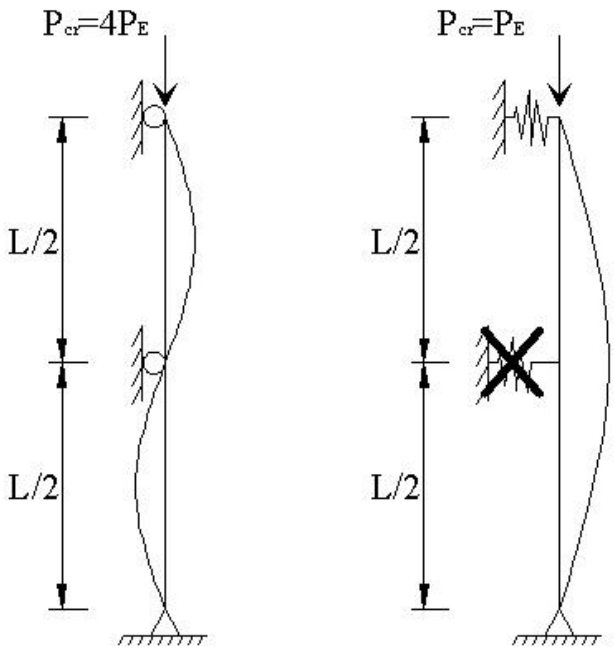

Figure 2.1. Importance of bracing
(Source: Helwig, 2013)

2.3. Lateral Torsional Buckling

According to the Guide to Stability Design Criteria for Metal Structures (2010); lateral torsional buckling is a limit state of structural usefulness where the deformation changes from predominantly in-plane bending to combined lateral deflection and twisting. Lateral torsional buckling involves twist of the cross section around the center of twist - the point where an axis passing through the web of the unbuckled girder intersects the same axis of the buckled girder - and lateral bending of the top flange. Center of twist is illustrated in Figure 2.2.

Lateral torsional buckling involves lateral movement of the compression flange plus twist of the cross-section around the center of twist. Steel I-shaped cross sections are more likely to undergo this failure mode rather than torsionally stiffer box-sections. Lateral torsional buckling is illustrated in Figure 2.3.

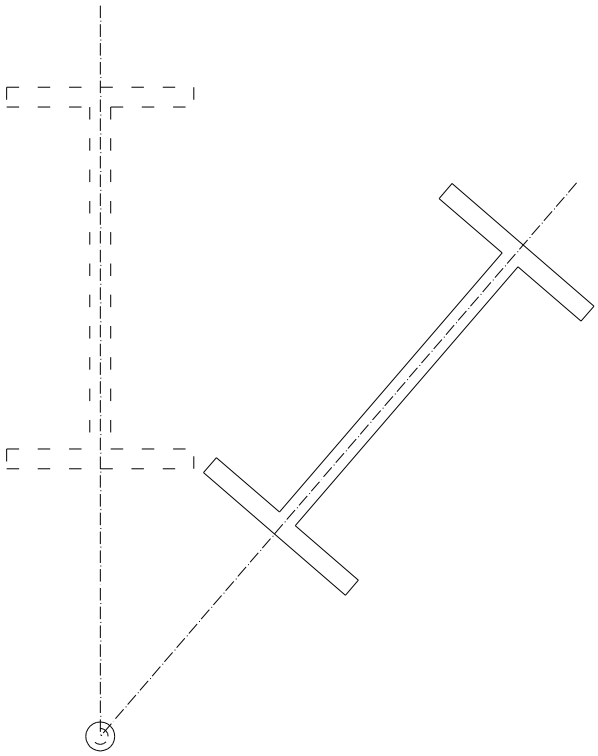

Figure 2.2. Center of twist

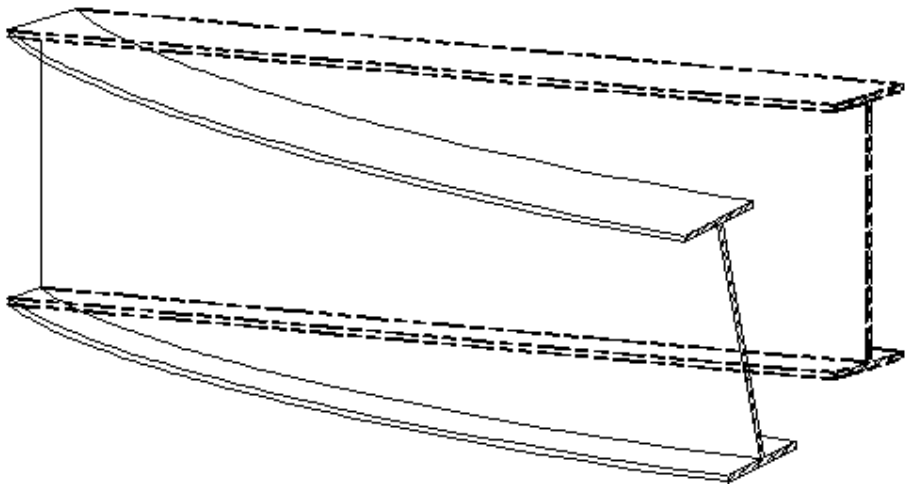

Figure 2.3. Lateral torsional buckling
(Source: U.S. Department of Transportation Federal Highway Administration, 2013)

Lateral torsional buckling capacity of beams has been studied for a long time. Timoshenko and Gere (1961) derived Equation 2.2 for elastic lateral torsional buckling capacity of simply supported, doubly-symmetric beams subjected to uniform moment loading.

$$M_{cr} = \frac{\pi}{L_b}\sqrt{EI_y GJ + \left(\frac{\pi E}{L_b}\right)^2 I_y C_w} \tag{2.2}$$

where,

M_{cr} = Lateral torsional buckling capacity of the beam;
L_b = Unbraced length;
E = Modulus of elasticity;
I_y = Weak axis moment of inertia;
G = Shear modulus;
J = St. Venant's torsional constant;
C_w = Warping constant.

The latest version of the Specification for Structural Steel Buildings (AISC, 2010) utilizes Equation 2.3 for elastic doubly symmetric I-sections. Equation 2.3 is identical Timoshenko's solution with the exception of the moment gradient factor, C_b. Equation 2.3 is applicable to beams under different types of loading.

$$M_n = F_{cr} S_x \tag{2.3a}$$

$$F_{cr} = \frac{C_b \pi^2 E}{\left(\frac{L_b}{r_{ts}}\right)^2}\sqrt{1 + 0.078\frac{Jc}{S_x h_0}\left(\frac{L_b}{r_{ts}}\right)^2} \tag{2.3b}$$

where,

M_n = Nominal flexural strength;
F_{cr} = Critical stress;
S_x = Elastic section modulus taken about the x-axis;

C_b = Lateral torsional buckling modification factor for non-uniform moment diagrams;

E = Modulus of elasticity of steel, 200 000MPa;

L_b = Unbraced Length;

r_{ts} = Effective radius of gyration;

J = St. Venant's torsional constant;

c = A constant dependent on cross-section (1 for doubly sym. I-shapes);

h_0 = Distance between the flange centroids.

Various solutions were proposed for C_b factor up to now. AISC, 2010 specification recommends using the following equation:

$$C_b = \frac{12.5M_{\max}}{2.5M_{\max} + 3M_A + 4M_B + 3M_C} \tag{2.4}$$

where,

M_{max} = Absolute value of maximum moment in the unbraced segment; kN-m;

M_A = Absolute value of moment at quarter point of the unbraced segment; kN-m;

M_B = Absolute value of moment at centerline of the unbraced segment; kN-m;

M_C = Absolute value of moment at three-quarter point of the unbraced segment; kN-m.

Kitipornchai and Trahair (1980) proposed a solution for the lateral torsional buckling capacity of singly symmetric I sections. Design specifications such as American Institute of Steel Construction Specification for Steel Structures (AISC, 2010) utilize more simplified solutions. Buckling capacity solution given by the Specification for Structural Steel Buildings (AISC, 2010) for simply supported singly symmetric cross-sectional girders under uniform moment loading is:

$$M_n = F_{cr} S_{xc} \tag{2.5a}$$

$$F_{cr} = \frac{C_b \pi^2 E}{\left(\frac{L_b}{r_{ts}}\right)^2} \sqrt{1 + 0.078 \frac{Jc}{S_x h_0} \left(\frac{L_b}{r_{ts}}\right)^2} \tag{2.5b}$$

where,

M_n = Nominal flexural strength of a singly symmetric beam;

F_{cr} = Critical stress;

S_{xc} = Elastic section modulus of the compression flange taken about the x-axis;

r_t = Radius of gyration of the flange components in flexural compression plus one-third of the web area in compression due to application of major axis bending moment alone.

Unbraced length, which is the distance between braces, L_b, is an important parameter for the lateral torsional buckling capacity. Type of loading, height of loading in the cross section, support conditions, and restraints at the ends of the beam also affects the capacity.

C_b factor that was already defined above represents the effects of moment gradient. Timoshenko's solution defined in Equation 2.2 was for simply supported, doubly symmetric beams under uniform moment loading. Transverse loading of a beam results in variable moment values along the girder. Solutions for girders under transverse loading are simply the product of uniform moment loading solutions and the C_b factor. Buckling moment capacity of girders with moment gradient is larger than those under uniform moment loading.

All expressions demonstrated up to this point about elastic lateral torsional buckling capacity of beams under transverse loading were all based on an assumption that the load was applied at the shear center. Guide to Stability Design Criteria for Metal Structures, 2010 proposed C_b^* expression instead of typical C_b factor in order to overcome load height effect of doubly and singly symmetric sections and double curvature bending of singly symmetric I-section members. The C_b factor equation that takes load height effect into account is given by:

$$C_b^{*} = C_b(1.4^{2y/h_0})R_m \le 3.0 \tag{2.6a}$$

$$R_m = \begin{matrix} 1.0 \\ or \\ 0.5 + 2\left(\dfrac{I_{y\_top}}{I_y}\right)^2 \end{matrix} \tag{2.6b}$$

where,

y = Height of loading relative to shear center ;

h_0 = Distance between flange centroids;

I_y = Weak axis moment of inertia;

I_{y_top} = Moment of inertia of top flange about minor axis of section.

R_m coefficient in Equation 2.6a represents the single & double curvature effect and should be taken "1" for unbraced lengths subjected to single-curvature bending. Otherwise R_m has to be calculated according to Equation 2.6b

2.4. Initial Imperfections and Ideal Stiffness

As indicated previously, the critical load definition is valid for members that are initially straight overall the full length. But this concept is not realistic for in-situ applications because of the geometrical imperfections on the members due to the effects of lifting, temperature etc.

First major specification in the United States that gives provisions about stability bracing systems is the third edition of American Institute of Steel Construction Load and Resistance Factor Design (AISC 2001). The specification proposed only a design strength requirement for the bracing system which is 2% of the compression force on the member to be braced.

The stiffness requirement of a bracing system can be found by conducting an eigenvalue buckling analysis on initially straight in other words, perfect systems. According to Winter (1960); an adequate brace system requires both strength and stiffness. Winter (1960) showed that brace forces in a system are directly proportional

to the geometrical imperfections of the member to be braced. The brace stiffness that enables the member without an initial imperfection to reach its buckling capacity is often called ideal stiffness.

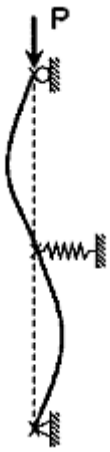

Figure 2.4. Winter's model for column bracing.

Winter (1960) developed a simple model for column bracing. Winter's simple model consists of a column with a lateral single brace located at the mid-height that is seen in Figure 2.4. The lateral brace is represented with a spring. Effects of the initial imperfections on the bracing behavior can be seen in Figure 2.5.

Figure 2.5 demonstrates the relationship between the forces and the buckling deformations on the member to be braced. Vertical axis shows the force level on the system normalized by P_E, the critical buckling load of the system. Horizontal axis shows the maximum deflections, which are proportioned to the initial imperfection. Winter indicated that providing the ideal stiffness, β_i to an initially imperfect system results in excessive deformations at the critical load level. However, a brace with two times the ideal stiffness resulted with a deformation equal to the initial imperfection at the estimated buckling capacity. Further increasing the stiffness resulted with even smaller deformations at the estimated buckling capacity.

Although beam bracing is somewhat more complicated then column bracing, Figure 2.5 also reflects the beam bracing behavior.

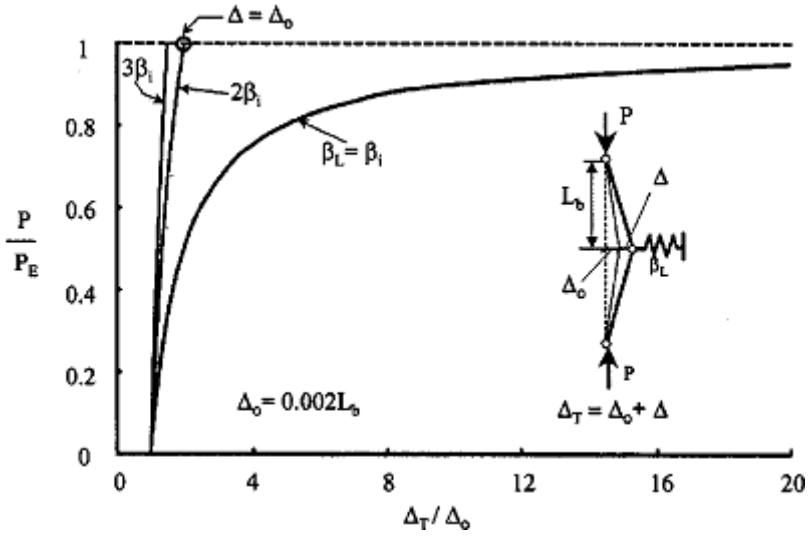

Figure 2.5. Effect of initial imperfections on bracing behavior

Figure 2.6 illustrates the four general types of bracing systems as relative bracing, discrete bracing, continuous bracing and lean-on bracing. Relative bracing systems control the deformation of a point along the length of the member to be braced with respect to another point. A truss inside the steel frames designed for earthquake is a general example for relative bracing. A discrete brace controls the movement of the point that it is attached to. Cross frames between adjacent girders in bridge systems are an example of discrete bracing. Diaphragm bracing of beams, a siding attached to the columns are examples of continuous bracing. One can understand from the name that there is no unbraced length for continuous bracing systems. Buckling of a member that requires the buckling of an adjacent member is lean on buckling.

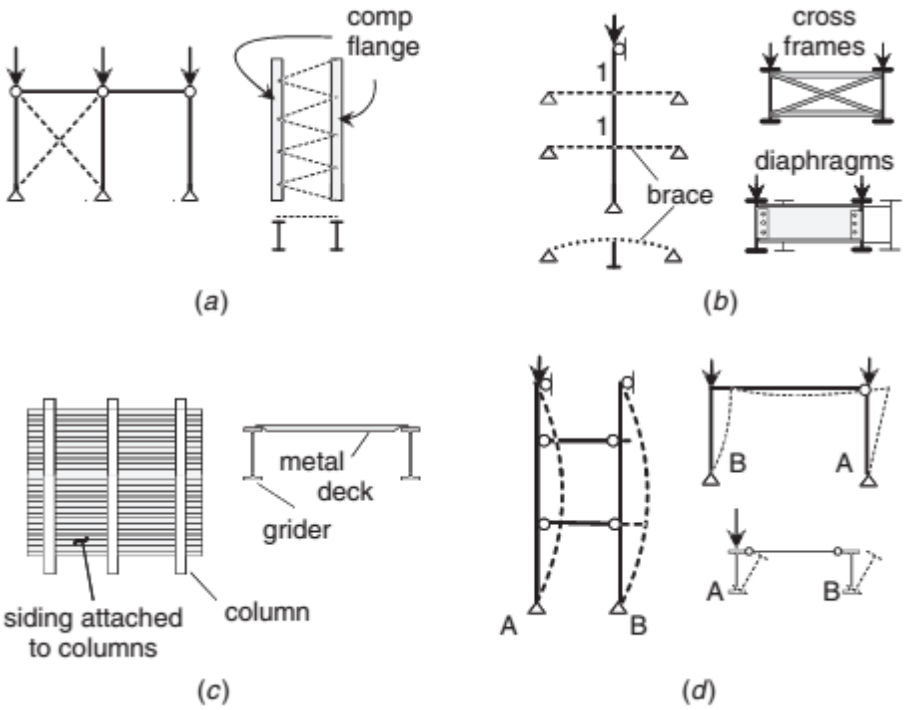

Figure 2.6. Types of bracing systems: (a) relative (b) discrete (c) continuous (d) lean-on (Source: Guide to Stability Design Criteria for Metal Structures, 2010)

2.5. Beam Bracing

Beam bracing is available by either lateral braces or torsional braces. Beam braces must prevent the twist of the cross section that is generated with the relative displacement of the top and bottom flanges (Guide to Stability Design Criteria for Metal Structures, 2010). Lateral braces restrain the lateral movement of the cross section. Joists attached to the compression flange of a simply supported beam are examples of beam lateral bracing. Torsional braces restrain the twist of the cross section. Cross frames or diaphragms attached to both top and bottom flanges of adjacent girders at mid-span are examples of beam torsional bracing. By this way unbraced length is reduced to half of the overall beam length. In steel building frames or steel bridge deck systems hardened concrete slab attached to the girder with shear studs provides lateral and torsional bracing simultaneously.

2.6. Stability Bracing of Girders by Shear Diaphragms

Compression in the top flange develops lateral torsional buckling and causes lateral movement of the top flange accompanied by the twist of the cross section around center of twist. Lateral movement of the top flange results with shear deformations on the metal deck. Metal deck form between the girders with high in-plane shear stiffness resists the lateral movement of the top flanges and generates the diaphragm action as seen in Figure 2.7.

Although larger top flanges may work as well, shear diaphragms considered as continuous bracing source may keep the top flange narrower and provide economy to the system.

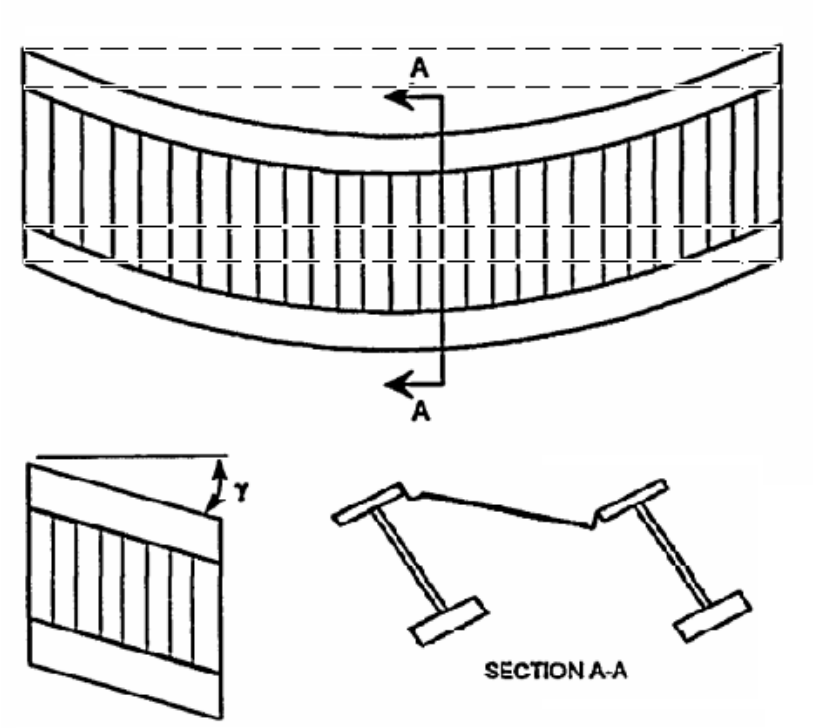

Figure 2.7. Diaphragm bracing analogy
(Source: Helwig, 1994)

The major property of a shear diaphragm in girder bracing is shear rigidity, Q which has units of kN/rad. Helwig & Yura (2008-I) stated the shear rigidity as resistance of the diaphragm along the beam length for a 1 rad shear strain. Shear rigidity of the diaphragm is calculated as follows;

$$Q = G' * s_d \tag{2.7a}$$

$$s_d = \left(\frac{n-1}{n}\right) * s_g \tag{2.7b}$$

where,

G' = Effective shear modulus of the deck;

s_d = Tributary width of a deck bracing a single beam;

n = Number of girders in the system;

s_g = Spacing between girders.

The effective shear modulus, G' can be obtained by performing a shear test on a cantilever test frame illustrated in Figure 2.8. For design phase Steel Deck Institute Diaphragm Design Manual (Luthrell, 2004) provides a set of equations to calculate the effective shear modulus of various types of metal forms.

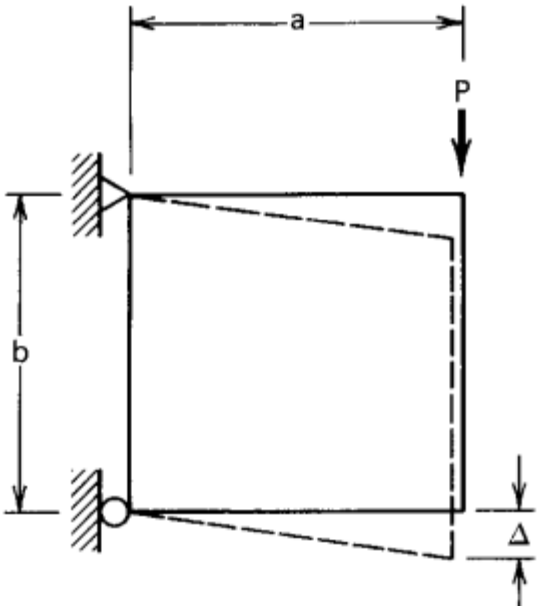

Figure 2.8. Cantilever test frame
(Source: Luthrell, 2004)

According to Figure 2.8:

$$G' = \frac{\tau'}{\gamma} = \frac{\frac{P}{b}}{\frac{\Delta}{a}} \tag{2.8}$$

where,

G' = Effective shear modulus of the deck;
τ' = Average effective shear stress;
γ = Average shear strain in the system.

It's noted in the Diaphragm Design Manual (Luthrell, 2004) that classical shear modulus, G, is not used since the metal sheet is not a thick flat plate material. Detailed information about cantilever test frame and shear modulus can be obtained from the Diaphragm Design Manual (Luthrell, 2004).

Detailed information about previous studies on shear diaphragm bracing of girders in a historical sequence is given in the following part.

2.7. Previous Studies on Diaphragm Bracing

There have been a number of previous works on the bracing behavior of shear diaphragms used for stability bracing of beams or girders since the beginning of the latter half of the 20th century.

Winter (1960) showed that adequate stability bracing requires both sufficient stiffness and strength. During 1960's a significant work was conducted at Cornell University. In the scope of an extensive research; Errera and Apparao (1976) presented a procedure for the design of I-section girders with diaphragm bracing. As a result of this study Errera and Apparao (1976) proposed the closed-form solution below for the buckling capacity of beams with uniform moment loading and bracing by a shear diaphragm on the top flange:

$$M_{cr} = \sqrt{\left(\frac{\pi^2 EI_y}{L^2} + Q\right)\left[\frac{\pi^2 EC_w}{L^2} + GJ + Qe^2\right]} + Qe \qquad (2.9)$$

where,

EI_y = Weak axis bending rigidity;
EC_w = Warping rigidity;
GJ = Torsional rigidity;
e = The distance between the center of gravity of the beam and the plane of the diaphragm;
n = A constant for different end support conditions.

It's notable that; for simplicity, Errera and Apparao (1976) limited the design procedure to "fully" braced beams and columns according to Winter (1960). Full bracing implies a restraint that allows no twist at a point (Helwig, 1994). In addition; a sinusoidal shaped lateral displacement and twist of the cross section was assumed in the solution.

Since Equation 2.9 is a little bit complicated for the design phase, Errera and Apparo (1976) as well as Nethercot and Trahair (1975) simplified the expression to:

$$M_{cr} = M_g + 2Qe \qquad (2.10)$$

where,

M_g = Buckling capacity of the girder alone;
Q = Shear rigidity of the shear diaphragm;
e =Distance from center of gravity of the beam to plane of shear diaphragm.

Later, Helwig and Frank (1999) compared the energy based solution (Equation 2.9) with the simplified solution (Equation 2.10) for a W30x90 (US) section with a span to depth ratio (L/d) of 20 and uniform loading with a shear diaphragm for bracing. The comparison resulted with a very good match for both solutions.

Lawson and Nethercot (1985) evaluated Equation 2.9 and Equation 2.10 and re-defined "*e*" as the distance between the plane of decking and the shear centre of the beam.

Since Equation 2.9 and Equation 2.10 are valid for beams with uniform moment loading, Lawson and Nethercot (1985) proposed the following equation for the buckling capacity of beams with transverse loading and bracing by a shear diaphragm on the top flange;

$$M_{cr} = C_b d \left[\frac{\left(Q\frac{(1-g)}{2} - \frac{P_e g}{2} \right) + }{\sqrt{\left(-\frac{P_e g}{2} + Q\frac{(1-g)}{2} \right)^2 - \frac{Q^2}{4} + \left(\frac{P_e}{2} + \frac{Q}{2} \right) \left(\frac{P_e}{2} + 2P_T + \frac{Q}{2} \right)}} \right] \quad (2.11)$$

where,

C_b = Factor for moment gradient;

d = Depth of the girders;

g =Factor to take into account load height;

P_e = Weak axis Euler buckling load;

G = Shear modulus of the beam material;

J = Torsional constant of the beam;

Q = Shear rigidity of the shear diaphragm;

$P_e = \frac{\pi^2 E I_y}{L^2}$;

$P_T = \frac{GJ}{d^2}$.

A computational study that consisted of a finite element approach was conducted by Helwig and Frank (1999) on the way to investigate the ability of metal deck forms to provide lateral bracing to I-shaped girders. They modified the simplified uniform moment solution (Equation 2.10) of Errera and Apparo (1976) and Nethercot and Trahair (1975) to be applicable for both uniform moment loading cases and cases with moment gradients caused by transverse loading applied at different load heights. They modeled the shear diaphragm with panels constructed from four-node shell

elements stiffened by beam elements that only have out-of-plane stiffness. They focused on simply supported girders that were also free to warp at the supports. Various slender web plate girder cross sections were analyzed in the study with a web slenderness ratio of 96 and 160. They also investigated singly symmetric cross sections. Unlike doubly symmetric sections; shear centre and gravity center of the singly symmetric cross sections do not coincide on each other and may either be above or below mid height of the section. Eventually they proposed the following equation for the buckling capacity of I-beams braced by a shear diaphragm at the top flange and compression in the top flange:

$$M_{cr} = C_b^* M_g + mQd \tag{2.12}$$

where,

M_{cr} = Buckling capacity of a diaphragm-braced beam;
C_b^* = Moment gradient factor that considers load height effects;
M_g = Buckling capacity of the girder alone;
m = Factor for load type and load height effects;
Q = Shear rigidity of the shear diaphragm;
d = Depth of the beam.

Helwig and Frank (1999) redefined the parameter "*e*" in Equation 2.10 as the distance from mid height of the beam to the plane of shear diaphragm for both singly symmetric and doubly symmetric beams. In Equation 2.11 by Nethercot and Trahair (1975), C_b factor represents the moment gradient factor due to transverse loading and is applied to the buckling capacity of both girder and shear diaphragm. Helwig and Frank (1999) reevaluated the moment gradient concept and applied the C_b factor only to the buckling component of the girder, M_g. They utilized center of twist concept to show that the deck is less effective for cases with moment gradient factor caused by transverse loading with respect to cases with uniform moment loading.

Center of twist may lie below or within the depth of the girder depending on the loading type as well as the existence of bracing. As the center of twist comes up to the top flange, bracing implemented at the top flange becomes less effective since the buckled shape of the girder does not have as much lateral movement at the top flange.

Consequently, top flange loading results in lower buckling capacities compared with mid height loading. Helwig and Frank (1999) showed that center of twist is below the bottom flange through the girder under uniform moment loading. With a moment gradient caused by the transverse loading applied at the mid height; center of twist is again below the bottom flange without bracing but elevates to the depth of the girder by the existence of bracing. They also showed that top flange loading additionally decreases the effectiveness of the bracing with an over-closure of the center of the twist to the top flange.

Helwig and Frank (1999) reflected the load type and load height effect on bracing behavior of the deck with an "*m*" factor applied to the deck contribution in Equation 2.10. They recommended "*m*" values of 5/8 for mid height loading and 3/8 for top flange loading. They adopted the load height effect factor of Helwig et al. (1997) and Galambos (1998) on the girder buckling capacity with a $C_b^* = C_b/1.4$ for top flange loading in which C_b is the typical moment gradient factor for mid height loading.

Equation 2.12 can be used to determine the required shear diaphragm stiffness for a specific design load or buckling capacity that is often called "ideal stiffness". For discrete and relative bracing systems ideal stiffness is defined by Helwig & Yura (2008-I) as the required stiffness to force a perfectly straight beam to buckle between brace points. Since structural elements like girders and beams naturally involve an initial imperfection, as discussed in Section 2.4 Winter (1960) showed that a larger stiffness than the ideal value is required to control deformations and brace forces.

Helwig & Yura (2008-I and 2008-II) performed parametric studies on stability bracing of a twin-girder system with shear diaphragms. Results for both stiffness and strength behavior of shear diaphragm bracing of stocky beams were demonstrated. The effects of load type and load position were also considered. Helwig & Yura (2008-I) dealt with the behavior of the general stability bracing behavior of the system. Helwig & Yura (2008-II) outlined the design requirements for shear diaphragm bracing and mainly focused on stiffness and strength requirements of shear diaphragms used to brace steel beams.

Helwig & Yura (2008-I) considered the stiffness requirements to control girder deformations and brace forces. They rearranged the "*m*" values of Equation 2.12 for stocky beams that were already proposed by Helwig and Frank (1999) for slender plate girders. They also conducted analyses with a cross frame at mid-span. Since the

magnitude of the brace force is a function of the initial imperfection in the member to be braced, they used an initial beam twist of:

$$\theta_0 = (\frac{L_b}{500d}) \tag{2.13}$$

where,

θ_0 = Initial twist in radians;
L_b = Spacing between points of zero twist;
d = Depth of the beam.

Initial twist expression in Equation 2.13 depends on an assumption that top flange of the beam has a lateral sweep of $L_b/500$ whereas bottom flange is kept straight along the beam length. This value is twice the value defined in the Specification for Structural Steel Buildings (AISC 2005a). Helwig & Yura (2008-I) conducted both eigenvalue buckling analyses in order to determine ideal stiffness of the shear diaphragm to reach a prescribed load level in a perfectly straight beam and large displacement analyses in order to determine brace strength requirements. They modeled the shear diaphragm with panels built up from two-node truss elements and arranged the shear rigidity of the diaphragm by changing the cross-sectional area of the truss elements. They verified the truss element model with the shell element diaphragm model of Helwig and Frank (1999). According to the results by Helwig & Yura (2008-I); intermediate discrete bracing greatly reduced the effects of top flange loading. They rearranged the "*m*" values for stocky beams that were previously proposed by Helwig and Frank (1999) for slender web plate girders. These values are presented in Table 2.1.

Table 2.1. *m* values
(Source: Helwig & Yura (2008-I))

	Stocky		***Slender***	
Bracing Condition	Centroid loading	Top flange loading	Centroid loading	Top flange loading
No intermediate discrete bracing	0.85	0.5	0.5	0.375
With intermediate discrete bracing	0.85	0.85	0.5	0.375

They conducted large displacement analysis on girders with initial imperfections to obtain stiffness and strength requirements of diaphragm bracing. Although additional analyses with stiffer diaphragms were conducted, a stiffness of four times the ideal value was deemed sufficient to control deformations and brace forces. The stiffness requirement was given by:

$$Q_{req} = 4 \times Q_i = 4 \frac{M_u - C_b \times M_g}{md} \tag{2.14}$$

where,

M_u = Maximum design moment of a diaphragm-braced beam;
C_b^* = Moment gradient factor that considers load height effects;
M_g = Buckling capacity of the girder alone;
m = Factor for load type and load height effects;
Q = Shear rigidity of the shear diaphragm;
d = Depth of the beam.

Helwig & Yura (2008-II) conducted large displacement analyses on stocky cross sections and reported the brace forces in the shear diaphragm along the girder length by means of the warping restraining moment per unit length along the longitudinal axis of the beam, M_{br}' as seen in Figure 2.9. Consequently they recommended utilizing the following expression for M_{br}'.

$$M_{br}' = 0.001 \frac{M_u L}{d^2} \tag{2.15}$$

where,

M_u = Maximum design moment of a diaphragm-braced beam;
M_{br}' = Warping restraining moment per unit length along the longitudinal axis of the beam;
L = Spacing between discrete bracing points;
d = Depth of the beam.

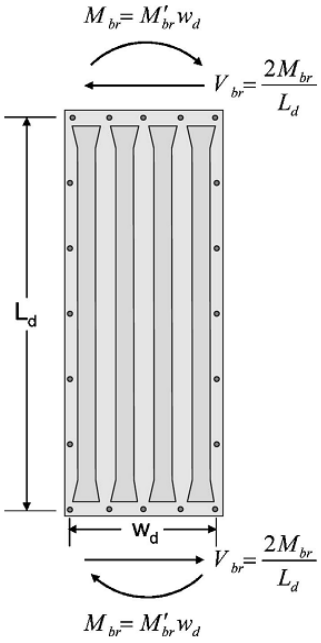

Figure 2.9. Brace moment and shear on corrugated sheet.
(Source: Helwig & Yura, 2008-II)

As seen in Figure 2.9. each corrugated sheet is fastened to both structural element by edge fasteners and adjacent sheets by side-lap fasteners. Since they modeled each sheet by a truss element they assumed that the shear force in the sheet-girder connection is resisted equally by the edge fasteners. In order to carry out the assumption, they converted the brace moment per length, M_{br}' to a moment on a corrugated sheet M_{br} as seen in Figure 2.9. From equilibrium on the panel, Helwig & Yura (2008-II) proposed the expressions for the shear force in an edge fastener as;

$$F_v = \frac{V_{br}}{n_e} = \frac{2M_{br}}{L_d n_e} = \frac{2M_{br}' w_d}{L_d n_e} = 2\left(0.001 \frac{M_u L w_d}{L_d n_e d^2}\right) \tag{2.16}$$

$$F_M = \left(0.001 \frac{M_u L}{1.25 d^2}\right) \tag{2.17}$$

where,

F_V = Component of brace force parallel to beam longitudinal axis;

F_M = Component of brace force perpendicular to beam longitudinal axis;

V_{br} = Brace shear in diaphragm truss panel;

n_e = Number of fasteners per panel along end of diaphragm sheeting;

M_{br} = Brace moment in diaphragm truss panel;

M_{br}' = warping restraining moment per unit length along the longitudinal axis of the beam;

L_d = Spacing between discrete bracing points;

w_d = width of diaphragm sheet;

M_u = Maximum design moment of a diaphragm-braced beam;

L = Total span of a beam;

d = Depth of the beam.

Note that F_M was proposed for five fasteners along end of diaphragm sheeting and they did not propose any expressions for the forces on the side-lap fasteners.

CHAPTER 3

FINITE ELEMENT MODEL

3.1. Overview

This parametrical study consists of numerical analyses on lateral-torsional buckling capacity of I-shaped steel twin girder system with a metal deck form attached to the compression flange. The system to be modeled is illustrated in Figure 3.1.

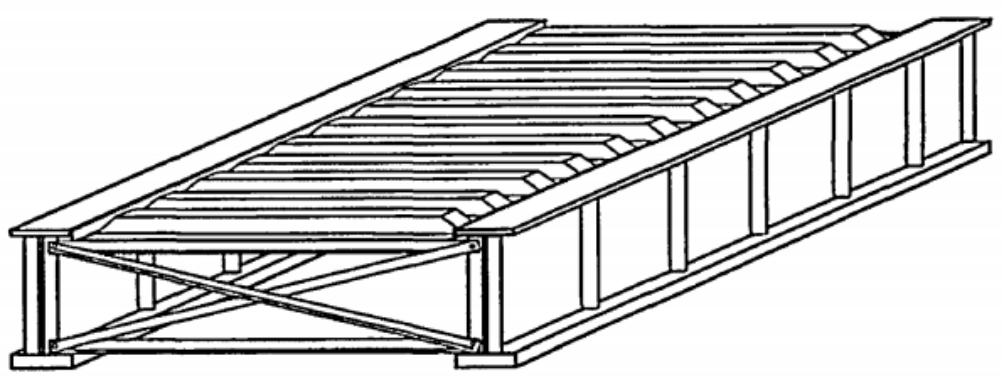

Figure 3.1. Twin girder and metal deck form system
(Source: Helwig, 1994)

Three-dimensional finite element analysis (FEA) program ANSYS Mechanical APDL (2007) was used throughout the study to perform eigenvalue buckling and large displacement analyses. Both doubly symmetric and singly symmetric cross sections with various deck configurations were analyzed. Analyses with a torsional brace at mid-span were also conducted.

In the finite element analysis (FEA) model both girders and shear diaphragm were modeled using elements that possess linear elastic material behavior. Since initial imperfection of the beams play an important role in the strength behavior of diaphragm bracing, geometrical non-linearity of steel I girders were taken into account. Figure 3.2 is the ANSYS (2007) output for the twin girder-metal deck form system.

This chapter gives basic information on finite element modeling of twin girders, shear diaphragm, fasteners, cantilever test frame and verification of the finite element model.

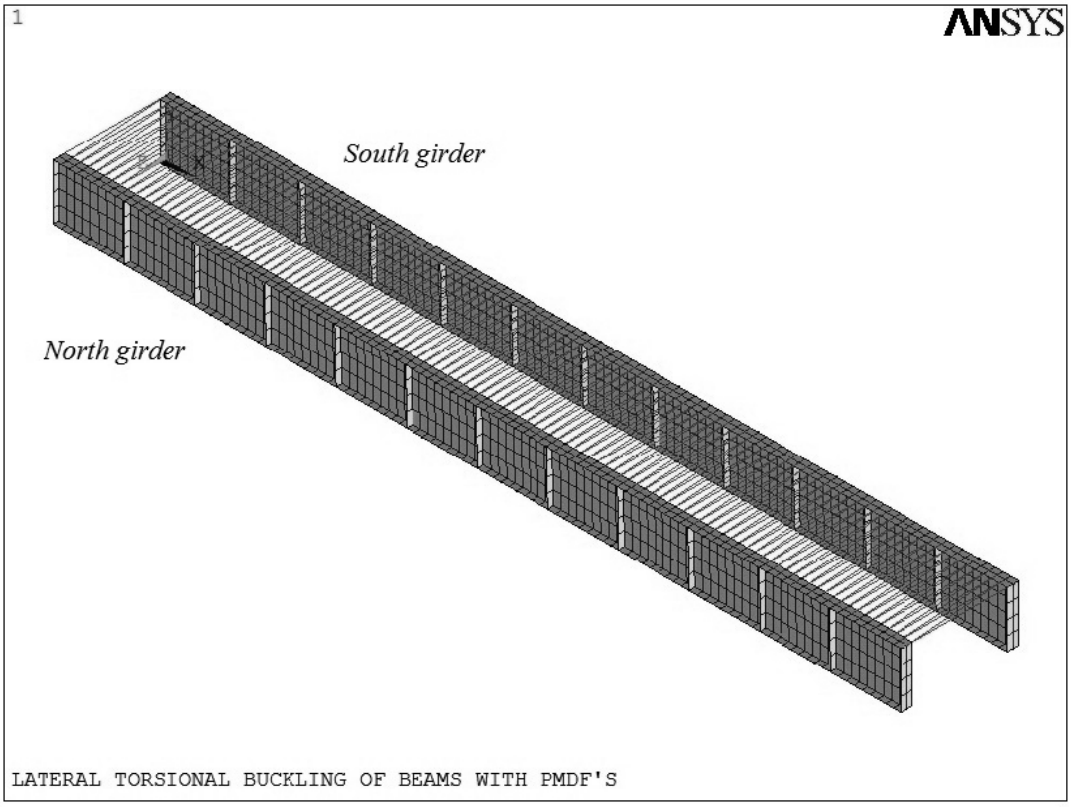

Figure 3.2. Twin girder system FEA model

3.2. Finite Element Model of Girders and Loading Procedure

Twin girders shown in Figure 3.2 were named as south and the north girder with respect to the z-axis. South girder was located through x-axis at z=0 and north girder was located through x-axis shifted by an amount equal to the girder spacing from the south girder. The girders were simply supported in flexure. Bottom flange mid node displacement is restrained in three directions at one support and restrained for displacements in y and z-axis at the other support. Girders were torsionally simply supported at the supports, i.e. free to warp at the supports but out of plane translation of the cross section was restrained at the top and bottom of the web at the both ends to prevent girder twist. In other words top flange mid node displacement is restrained in z-

direction at both ends. Twin girders were stiffened by transverse web stiffeners at least at the supports for concentrated force effects or throughout the slender girder length.

Girders and transverse web stiffeners were modeled with SHELL93, structural shell element from the ANSYS (2007) element library. Flanges were divided into two corresponding elements through the girder length. Webs and transverse web stiffeners were meshed into four elements. Common node of web and flange shell elements was rigidly coupled to each other.

SHELL93 is an 8 noded structural shell in quadrilateral geometry. SHELL93 has plasticity, stress stiffening, large deflection, and large strain capabilities. SHELL 93 has six degrees of freedom at each node; translations in the nodal x, y and z directions and rotations about the nodal x, y and z-axes. SHELL93 element is illustrated in Figure 3.3.

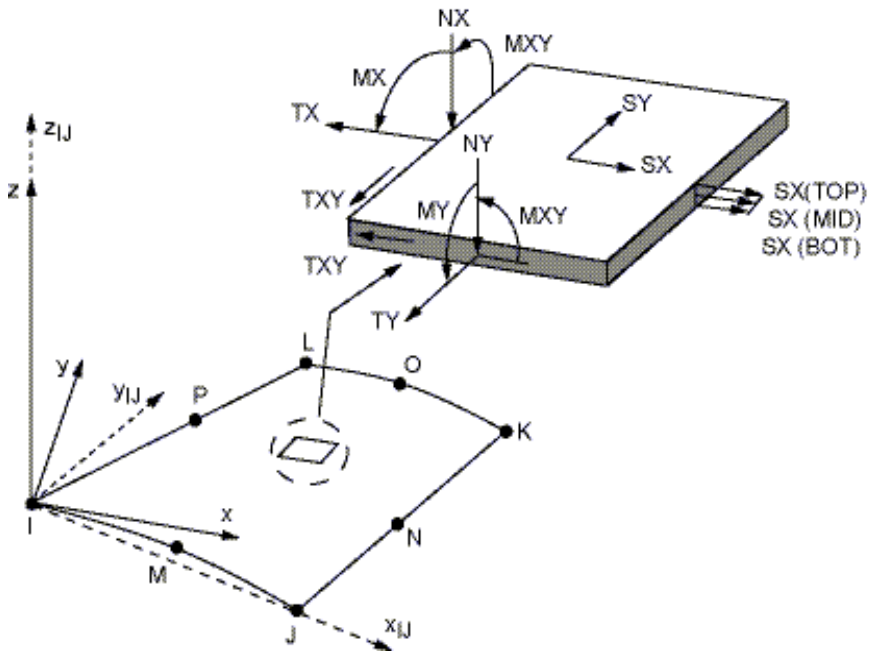

Figure 3.3. SHELL93 geometry and stress output
(Source: ANSYS, 2007 Finite Element Model Users Manual)

Aspect ratio of the elements used in the model was in the range of one and three. Effect of element quantity on the results was also investigated. Use of four elements along the height of the webs not only resulted with an efficient behavior compared to finer meshes like eight elements, but also provided a considerable reduction in process times. Properties of the cross sections are tabulated in the following chapter and in the Appendix A with element aspect ratios.

Mesh geometry of the north girder at the support is demonstrated in Figure 3.4.

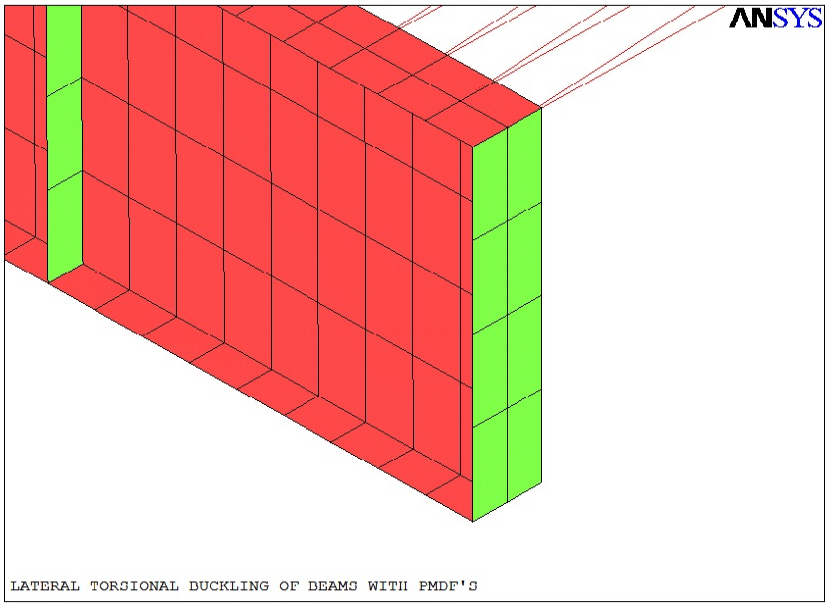

Figure 3.4. North girder mesh.

Parametrical studies were simulated with ANSYS (2007) Batch environment. Girders were modeled according to the ASTM A992 grade steel. Elastic modulus and Poisson's ratio were taken as 205 000 MPa and 0.3 respectively.

As indicated in the previous chapter initial imperfections play a critical role in bracing behavior. Wang and Helwig (2005) focused on choosing the most critical imperfection shape and the distribution of the imperfection along the girder for torsional and lateral bracing systems. Wang and Helwig (2005) especially investigated the effect of initial imperfections on stability brace forces of bridge girder systems. Wang and Helwig (2005) reported that the critical imperfection which is expected to occur in practice is a cross-sectional twist resulting from a lateral displacement of one flange while the other flange remains straight. In this study; same shape and magnitude of initial imperfections recommended by Wang & Helwig (2005) and Helwig &Yura (2008-I) was adopted where bottom flange is straight and top flange is laterally displaced throughout the girder as shown in Figure 3.5. According to the Figure 3.5, initial twist of the cross section follows a sinusoidal path which is zero at the supports and reaches the maximum value at mid-span with the value of;

$$\theta_0 = \frac{L_b}{500d} \tag{3.1}$$

where,

θ_0 = Maximum initial twist of the girder at mid-span;

L_b = Unbraced length of the beam;

d = Depth of the beam.

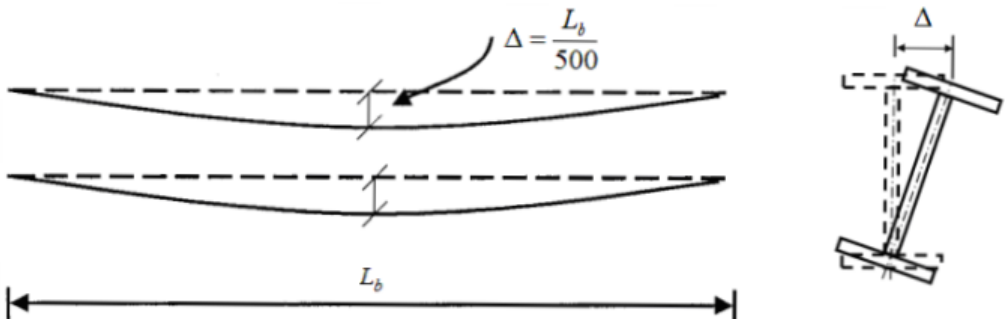

Figure 3.5. Shape and plan view of girder imperfections used in the study.
(Source: Egilmez, 2005)

Twin girder-shear diaphragm system was subjected to uniformly distributed loading in gravitational direction at each mid node of the top flange through the girder. Load was applied in 12 steps: 3 steps with 20% increment, 2 steps with 10% increment, 2 steps with 5% increment and 5 steps with 2% increment. Each load step involved 105 sub steps. In each sub step displacement, force and moment convergence criteria were checked by means of equilibrium iterations. Newton-Raphson procedure was utilized for the solution. Some analyses were terminated due to insufficient convergence criteria.

3.3. Finite Element Model of Shear Diaphragm

Various types of shear diaphragm models were used in previous studies that are aforementioned in the previous chapters. In this study, a shear diaphragm model originally developed by Davies and Bryan (1982) was adopted and simply modified. Shear diaphragm model utilized in this study is illustrated in Figure 3.7**.**

Figure 3.7 represents a twin girder-shear diaphragm system that consists of four metal deck forms. Metal deck sheet profiles modeled in the study represent a typical sheet form with three corrugations used in both building and bridge industry.

In the model each metal sheet consists of four transverse and three diagonal 3-D axial elements as seen in Figure 3.7. Axial elements in the transverse direction have sufficiently high stiffness that enables the axial strain to be neglected. In addition, the ends of the girders at the supports are generally connected to each other by transverse diaphragms as seen in Figure 3.6 to prevent rotation at the supports. In current applications metal deck forms are generally connected to these transverse diaphragms at the supports. The stiffness of the connection was reflected to the model by additional dimensionless spring elements located in the mid node of the girder top flange at both ends.

Figure 3.6 Transverse diaphragm between the girders

On the other hand connection of the adjacent sheets was modeled with additional transverse axial elements named as side-laps. Side-laps are illustrated with seams in Figure 3.7. However seams and transverse axial elements are illustrated apart from each other for visual concerns, they are over lapped on each other in the finite element model. Consequently, while transverse rigid elements transfer the loads from one girder to other and connect diagonals to each other, diagonal axial members provided the unique shear stiffness source of the decks. To achieve a certain amount of stiffness, the area of the diagonal members were altered. In order to determine the required area of the diagonal members, a shear test frame was also simulated which is discussed a few pages later.

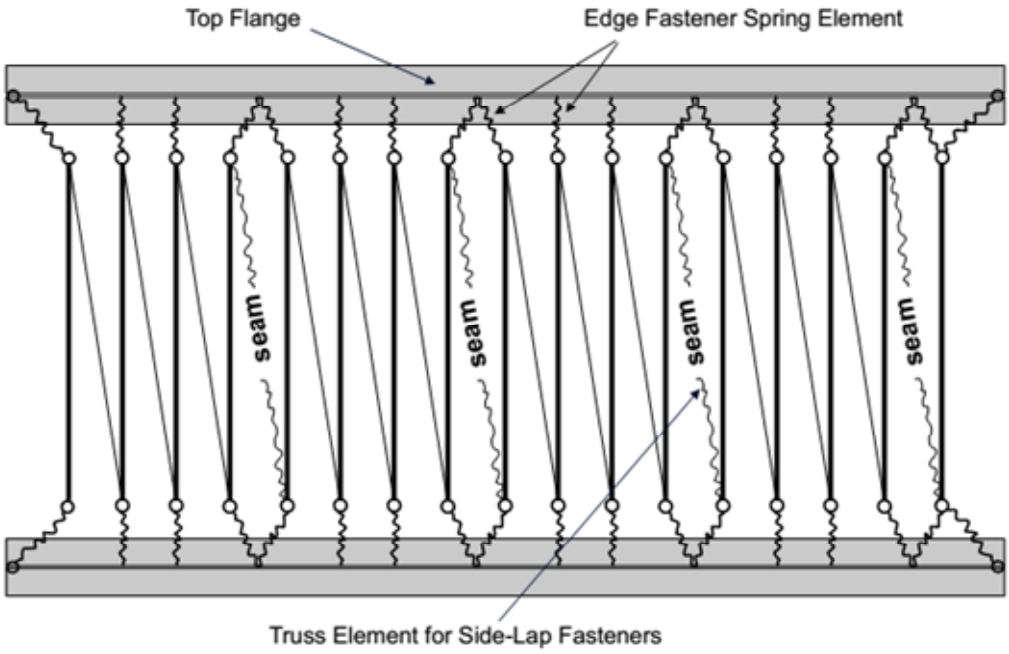

Figure 3.7. Shear diaphragm finite element model
(Source: Egilmez et al., 2014)

Axial elements were modeled with LINK8 element from the ANSYS (2007) element library. LINK8 was utilized as a uni-axial tension compression member without considering any bending. LINK8 has three degrees of freedom at each node; translation in the nodal x, y and z directions. LINK8 geometry and displacement output is illustrated in Figure 3.8.

Representation of the metal deck form by these axial elements enables to model deck to girder connection and monitor the brace forces in the fasteners due to shear diaphragm action. Number of axial elements can be arranged according to the number of fasteners used in shear diaphragm-twin girder connection.

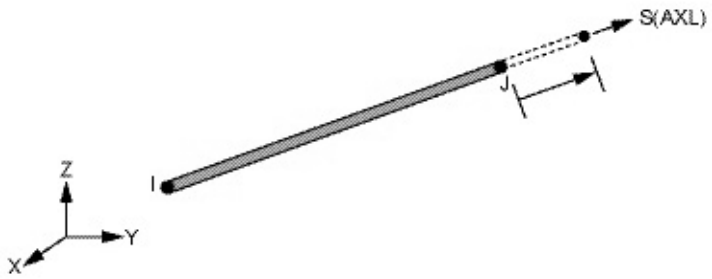

Figure 3.8. LINK8 geometry and displacement output
(Source: ANSYS, 2007 Finite Element Model Users Manual)

3.4. Finite Element Model of Fasteners

Diaphragm sheets can be connected to the structural member or adjacent sheet by welds, screws, power driven pins etc. Connection type has a major effect on diaphragm strength and stiffness (Luthrell, 2004). In this study sheet to girder and side-lap connections were assumed to be constructed by screws. Fastener layout and connection forces generated within a single deck sheet is illustrated in Figure 3.9.

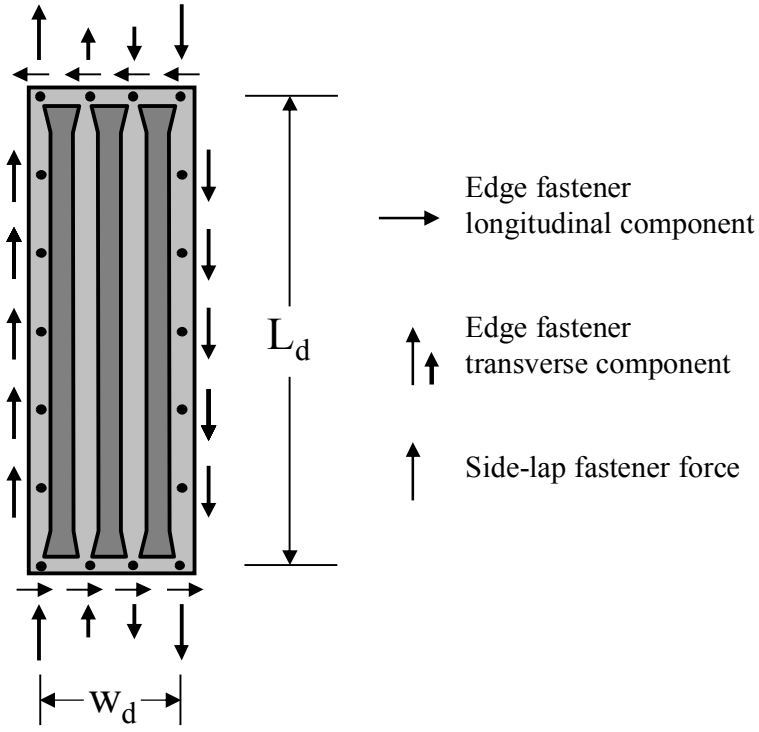

Figure 3.9. Brace forces that develop in a single deck sheet
(Source: Egilmez et al., 2014)

In the finite element model sheet to girder connections were modeled by means of dimensionless spring elements that possess equal stiffness in x and z directions. At sheet to girder connections dimensionless spring elements were attached to the end of the axial members. This connection was assembled on the mid node of the top flange. Although these spring elements are illustrated with a finite length in Figure 3.7, in fact they are dimensionless.

These dimensionless spring elements were modeled with mass free COMBIN14 elements from the ANSYS (2007) element library. COMBIN14 is modeled as a uniaxial tension compression member without considering any bending or torsion by utilizing

longitudinal spring-damper mode capability. COMBIN14 geometry and stress output is illustrated in Figure 3.10.

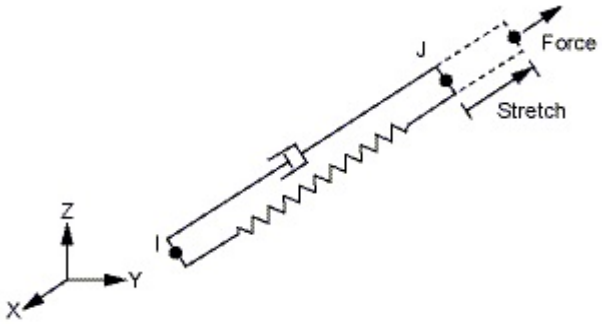

Figure 3.10. COMBIN14 geometry and stress output
(Source: ANSYS, 2007 Finite Element Model Users Manual)

In the finite element model, side-lap connections were modeled with a transverse axial member at the side-lap seams on Figure 3.7 that connects opposite edges of adjacent sheets. The stiffness of these transverse axial members was taken equal to summation of stiffness of the total number of side-lap fasteners at a seam as discussed in the following paragraph. Seams are connected to the girders by means of dimensionless fasteners that already connects the transverse truss elements to the girders.

Strength and stiffness values of the connections were taken from Luthrell (2004). Structural connections were modeled according to the Buildex BX-12 or Buildex BX-14 screws and side-lap connections were modeled according to the #12 screws. Stiffness equations used for structural fasteners and side-lap fasteners in terms of mm/kN from Luthrell (2004) are listed in Equation 3.2 respectively.

$$K_f = \frac{1000\sqrt{t}}{37.4} \tag{3.2a}$$

$$K_s = \frac{1000\sqrt{t}}{86.3} \tag{3.2b}$$

where,

t = Base sheet metal thickness in mm.

Strength equations used for structural fasteners and side-lap fasteners in terms of kN from Luthrell (2004) are listed in Equation 3.3 respectively. Shear strength results according to the Equation 3.3 must be modified by resistance factors (Φ) per the "Load and Resistance Factor Design" (LRFD) or by safety factors per the "Allowable Stress Design" (ASD) to account for reasonable design conditions (Luthrell, 2004).

$$Q_f = \frac{F_y t}{31.5}\left(1 - \frac{F_y}{1380}\right) \tag{3.3a}$$

$$Qs = 0.793 d * t \tag{3.3b}$$

where,

t = Base sheet metal thickness in *mm*;

F_y = Yield strength of sheet steel in *MPa;*

d = Major diameter of the screw in *mm*.

3.5. Finite Element Model of Cantilever Test Frame

As mentioned in finite element modeling of the shear diaphragm, shear stiffness of a metal deck form is provided by the diagonal axial elements of the trusses. Various shear stiffness values can be obtained directly by changing the cross sectional area of these diagonal members. In order to do that a test frame was modeled similar to the twin girder-shear diaphragm model according to the Luthrell (2004). Finite element model of the test frame is illustrated by ANSYS (2007) output in Figure 3.11.

Test frame shown with end conditions in Figure 3.11 consisted of 2 beams in the perimeter and 8 metal sheets inside. Test Frame was loaded as seen in the figure. Beams were modeled with BEAM3 elements from the ANSYS (2007) element library. BEAM3 is a uniaxial element with tension, compression and bending capabilities. The element has 3 degree of freedom at each node; translations in local x and y-axes and rotation about the local z axis. BEAM3 elements are connected to each other with a pinned connection. Metal sheets were modeled with LINK8 elements as in the twin girder model. Since vertical axial elements were rigid, only diagonal axial elements constituted the shear stiffness of the diaphragm. Fastener connections were modeled with the same procedure of twin girder-shear diaphragm model.

Since these diaphragms were fastened to the girders edge wise, the decking system was only exposed to shear deformations when girders displaced.

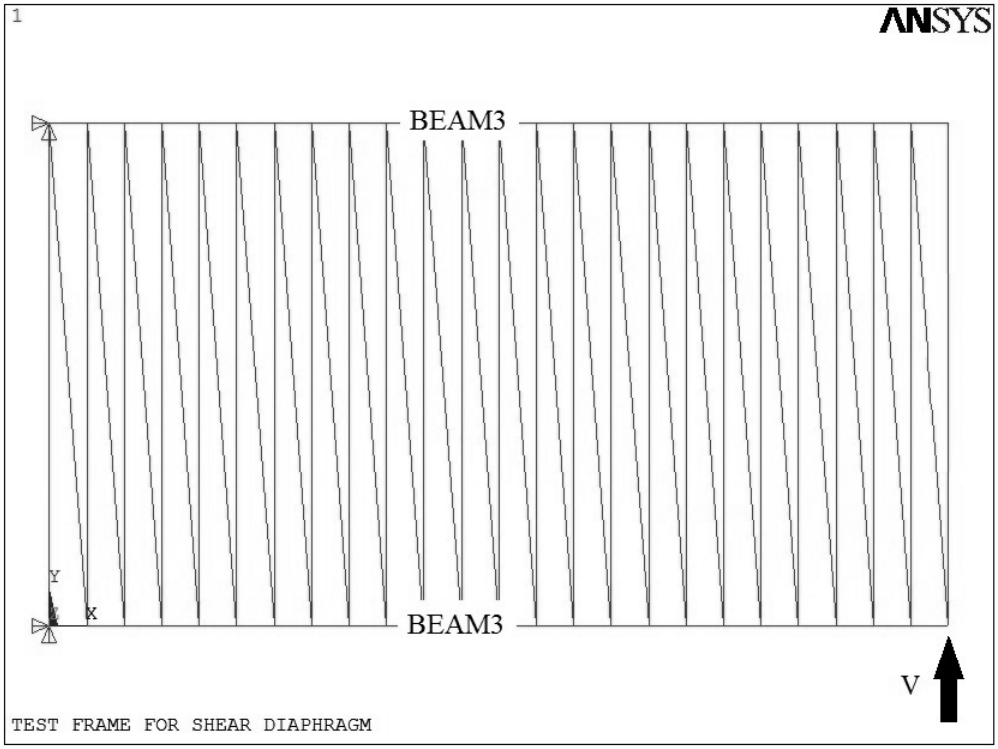

Figure 3.11. Test frame output by ANSYS

3.6. Verification of the Finite Element Model

Finite element model was verified by a full-scale twin-girder buckling test conducted by Egilmez (2005) at the structural engineering laboratory of University of Houston, Texas. Twin girders were 14.63 m. long -48 ft-singly symmetric I-shaped sections that were flame cut from original W760x134 US wide flange beams. Top flanges were narrowed to 158.8 mm's that corresponds to a ρ; I_{yc}/I_y-moment of inertia ratio of the top flange to the entire cross section about the weak axis- of 0.18.The metal deck forms were 610 mm. wide, 1.22 mm -18 gauge - thick and supported to the twin girders with a modified connection detail that diminishes the flexibility of the connection. Measured shear stiffness of the metal deck form was 9842 kN/rad that corresponds to 5.4 times the ideal stiffness of a deck brace system under 210 MPa stress level. Girders were subjected to point loads at one thirds of the total span. Detailed information is available at Egilmez et al. (2005).

Laboratory test and finite element model results are compared in Figure 3.12. Vertical axis in the figure demonstrates the mid-span bending moment level. Horizontal axis demonstrates the ratio of mid-span total twist and the initial twist of the girder. According to the results finite element model predicted the rotation behavior 4.9% higher that the rotations observed in the test.

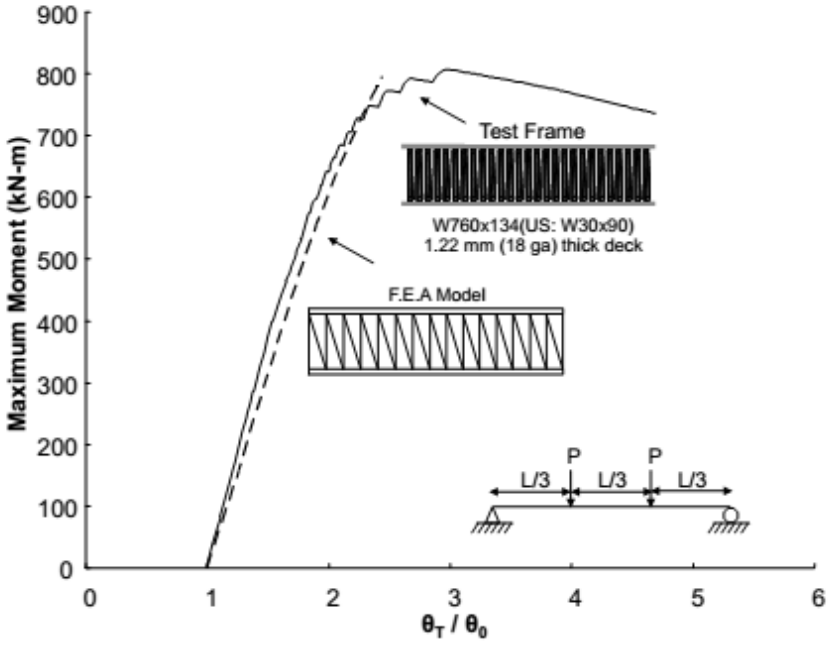

Figure 3.12. Comparison of FEM and laboratory test results
(Source: Egilmez et al., 2014)

CHAPTER 4

OVERVIEW OF THE STUDY

4.1. Introduction

This chapter presents an overview of the study. The steel sections utilized in the analyses, the parameters that are investigated, and the procedure followed in the analyses is briefly presented.

The study consists of eigenvalue buckling analyses, test frame shear-displacement analyses and large displacement analysis on various steel I- sections to observe the stiffness and strength behavior of shear diaphragm. Analyses were conducted by ANSYS Mechanical APDL (2007). Output from the analyses consists of nodal displacements, rotations, element forces, stresses etc. Analysis results are used to investigate the behavior of the twin girder-shear diaphragm system and to propose stiffness and strength requirements of the shear deck. For this purpose rotation of the mid-span around the x-axis with respect to center of twist, brace forces in the structural connectors on longitudinal and transverse direction and, side-lap connector forces on transverse direction were processed. Since ANSYS (2007) post process data is in a raw condition, a commercial software package (MATLAB 7.12, The MathWorks Inc., 2011) was used for data processing.

Results of the study are reported in two parts. The first part mainly focuses on the general stiffness behavior of diaphragm bracing. Detailed results and discussion on the first part will be available in the on-going thesis work of Akbaba (2015). The second part focuses on the strength behavior of diaphragm bracing. This thesis concentrates in the second part. The objective is approached through large displacement analyses on twin girder-deck system with different configurations. Eigenvalue buckling analysis and test frame analysis procedures are also covered briefly since they are a supplementary component of the whole study.

4.2. Parameters

In this study; stocky, doubly and singly symmetric I-shaped girders were analyzed. Detailed information about the girder cross sections is available in Table 4.1.

Table 4.1. Sections of the study

SECTION DESIGNATION	b_T(mm)	b_B(mm)	h_{TOTAL}(mm)	t_{web}(mm)	t_{TF}(mm)	t_{BF}(mm)	λ_{web}	$\lambda_{top\ flange}$	$\lambda_{top\ flange}$
Stocky#1	140	140	366	6	9	9	58.00	7.78	7.78
Stocky#2	280	280	732	12	18	18	58.00	7.78	7.78
Slender-100#1	300	300	1464	14.14	25	25	100.00	6.00	6.00
Slender-160#1	300	300	1464	8.84	25	25	159.95	6.00	6.00
Slender-100#2	300	300	1830	17.8	25	25	100.00	6.00	6.00
Slender-160#2	300	300	1830	11.13	25	25	159.93	6.00	6.00
SS-100# 19	210	300	1464	14.21	17.5	25	100.04	6.00	6.00
SS-100# 29	240	300	1464	14.19	20	25	100.00	6.00	6.00
SS-100# 39	270	300	1464	14.16	22.5	25	100.04	6.00	6.00
SS-160# 19	210	300	1464	8.88	17.5	25	160.08	6.00	6.00
SS-160# 29	240	300	1464	8.87	20	25	159.98	6.00	6.00
SS-160# 39	270	300	1464	8.85	22.5	25	160.06	6.00	6.00

Girders considered in this study are simply illustrated in Figure 4.1.

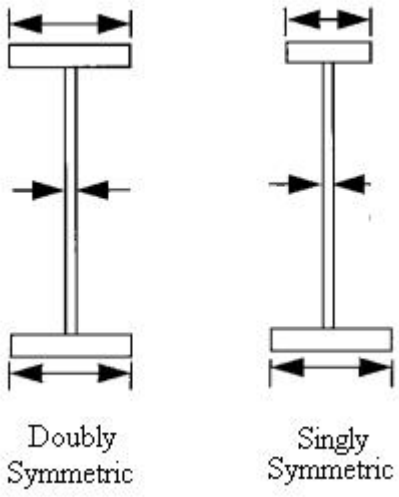

Figure 4.1. Sections considered in the study

Doubly symmetric sections were mainly named according to the web slenderness ratio. A doubly symmetric section with web slenderness ratio smaller than 60 was named as “Stocky Section”, otherwise “Slender Section” designation was used. Slender sections were named according to the web slenderness ratio and web height. Slender sections had two different web slenderness ratio of 100 and 160 and two different total girder depth of 1464 mm and 1830 mm. Slender section flange width was taken constant as 300 mm according to the requirements on AASHTO Standard Specifications (2012).

Singly symmetric sections were named according to the web slenderness ratio and top flange beam width. A singly symmetric section was obtained by changing the width and thickness of the compression flange. Singly symmetric sections were divided into two main groups according to the web slenderness ratio: 100 and 160. Each group consists of three non symmetric sections with a constant bottom flange of 300 mm – same with doubly symmetric sections-. However, the width of the top flange was changed to achieve mono-symmetry ratios of 0.19, 0.29, and 0.39. Mono symmetry ratio is the ratio of top flange second moment of inertia to the overall cross-sectional second moment of inertia around weak axis.

Due to concentrated force effects on the supports, both stocky and slender sections had transverse web stiffeners at the supports. Additionally, slender sections had transverse web stiffeners throughout the girder. These stiffeners are spaced with a distance equal to the girder depth. Web stiffener thickness was constant as 20 mm.

Span to depth ratio, “L/d” of the analyses with stocky sections was altered from 15 to 20, 25 and 30. Span to depth ratio of the analyses with slender sections was 10 and 15.

As explained in the previous chapter; in the study performed by Helwig & Yura (2008) uniform loading was applied through the girder at the top flange since bracing is least effective under top flange loading. Only uniformly distributed loading was considered in the study since it is a good representative of the loading characteristics of a concrete pour during construction. In this study, a uniform load that causes a maximum flexural stress level of 210 MPa at the extreme fiber of the section is applied. The selected 210 MPa stress level is a reasonable estimate of the expected stress levels during construction. Load values are available in the design example presented in the Appendix B. Analyses according to a stress level of 300 and 345 MPa were also

conducted in order to make a comparison with Helwig (2008-I) and inspect the behavior at the yield point of the beams.

In order to investigate the effects of deck thickness on brace forces three different deck thicknesses were considered: 16 gauge (1.52 mm), 18 gauge (1.22 mm) and 20 gauge (0.91 mm).

Deck stiffness is a major parameter in the study. The brace stiffness required for a structural member to reach a specific load level or buckling capacity is often called the "ideal stiffness". Since utilizing a brace stiffness equal to the ideal stiffness results in large deformations and brace forces (Winter, 1960), analyses were conducted with diaphragm stiffnesses of two ($2Q_i$), three ($3Q_i$), four ($4Q_i$), five($5Q_i$) and six times the ideal stiffness ($6Q_i$) of the diaphragms. Various analysis with 3, 4, 5 edge fasteners; 4, 5 and 6 side-lap fasteners were conducted.

The effects of wider decks and mid-span cross frame were also investigated. A list of analyses conducted throughout the study is represented in the Appendix A.

4.3. Numerical Analysis Process

Numerical study started with the definition of the finite element model. Girders, shear diaphragm, diaphragm-girder connectors, side-lap connectors and cross frame (if exists) were modeled respectively. After that, load value of each node corresponding to a bending stress level of 210 MPa is calculated. Following this preliminary step numerical analysis by ANSYS (2007) performed with 3 consecutive steps:

4.3.1. Eigenvalue Buckling Analyses

Eigenvalue buckling analyses provided elastic bifurcation loads of perfectly straight members, in other words a member without any initial imperfection. Eigenvalue buckling analyses were conducted on each configuration. First of all eigenvalue buckling analyses were conducted on a single perfectly straight girder. Analysis output of section Slender-160#1 with a span to depth ratio of 10 is given in Figure 4.2. Slender-160#1 demonstrated lateral torsional buckling as the top flange translated in lateral direction and the web rotated through the girder.

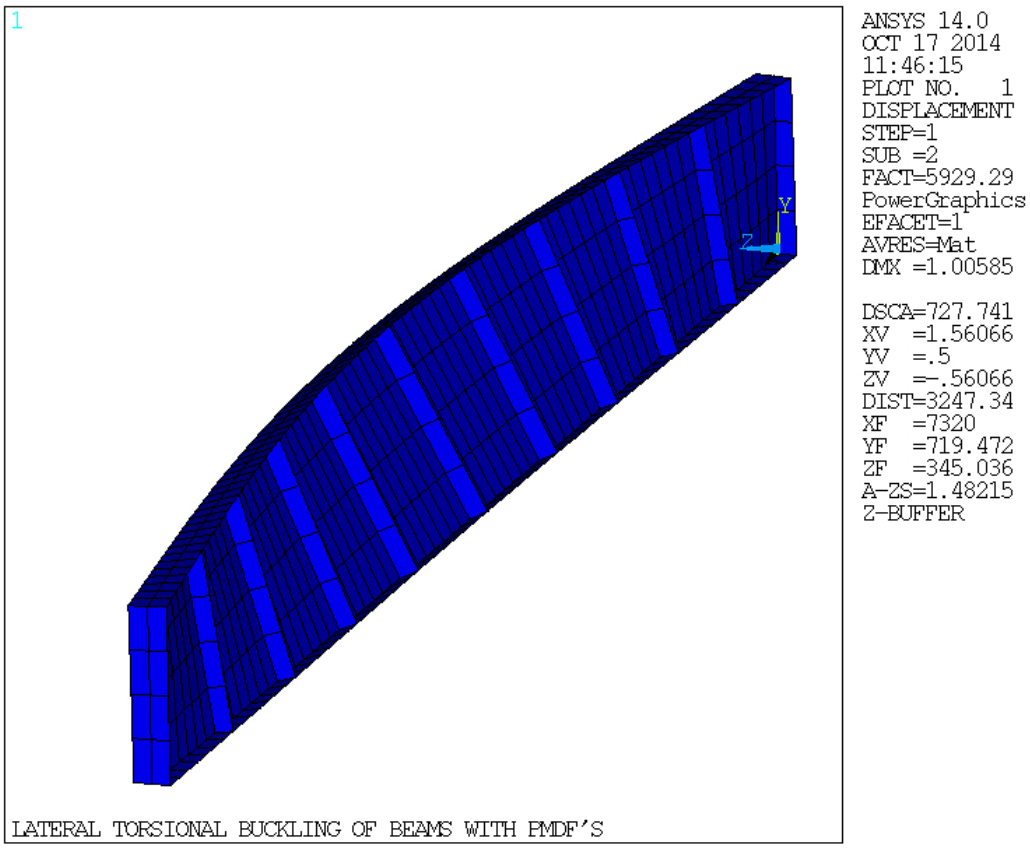

Figure 4.2. Single girder eigenvalue buckling analysis output

The purpose of conducting eigenvalue buckling analyses on single girders initially was to get an estimate for the buckling load inputted in ANSYS (2007). Following this analyses twin-girder systems with shear diaphragm bracing were conducted. The area of the diagonal truss elements of the shear diaphragm FEA model was increased incrementally until the buckling load created a bending stress of 210 MPa at the midspan extreme fiber.

Eigenvalue buckling analysis on the twin girder system with Slender-160#1 section and an L/d ratio of 10 pointed out with a factored load level of 21032.1 Newton's. The factored load level corresponds to a 210 MPa bending stress level in the girders. And the corresponding stiffness is 2320 kN/rad. This value is the ideal stiffness, Q_i of the shear diaphragm.

4.3.2. Shear Frame Analyses

Large displacement analyses were conducted on twin girder systems with diaphragm stiffnesses of two, three, four, five, and six times the ideal stiffness. Shear displacement tests were conducted on a cantilever test frame FEA model in order to calculate the area of the diagonal truss elements that correspond to the specific diaphragm stiffnesses Again for Slender-160#1 section with an L/d ratio of 10; twice the ideal stiffness, $2Q_i$ is equal to 4640 kN/rad. Test frame analysis output is given in Figure 4.3. In Figure 4.3 non-displaced state and displaced state of a test frame analysis are demonstrated together. Shear displacement is noticeable in Y direction with the amount of 0.53 mm's. By using the amount of displacement and Equation 2.8 and 2.7, 4640 kN/rad stiffness was calculated consequently.

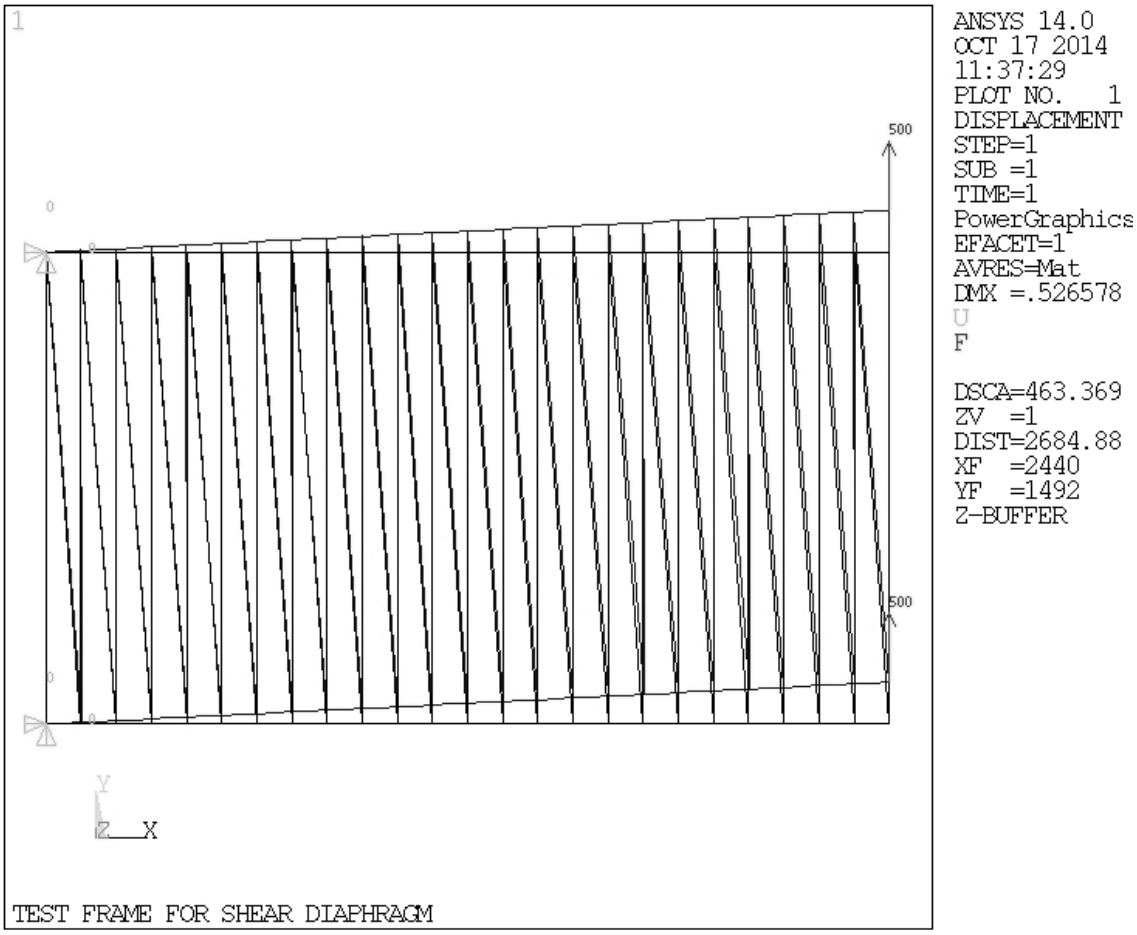

Figure 4.3. Test frame analysis output

4.3.3. Large Displacement Analyses

After gathering the diagonal truss member area for specific stiffness values, large displacement analyses on imperfect girders were conducted. Figure 4.4 demonstrates the support conditions, loads and the entire geometry of section Slender-160#1. Figure 4.5 is the large displacement analysis output of section Slender-160#1 with an L/d ratio of 10 and twice the ideal stiffness. Displaced state in Figure 4.5 is scaled up 5 times the original. The contour plot demonstrates the displacement in z-direction.

Twin girder-shear diaphragm system was subjected to uniformly distributed loading in gravitational direction at each mid node of the top flange through the girder. Load was applied in 12 steps: 3 steps with 20% increment, 2 steps with 10% increment, 2 steps with 5% increment and 5 steps with 2% increment. Each load step involved 105 sub steps. In each sub step; displacement, force and moment convergence criteria were checked. Some analyses were terminated due to insufficient convergence criteria.

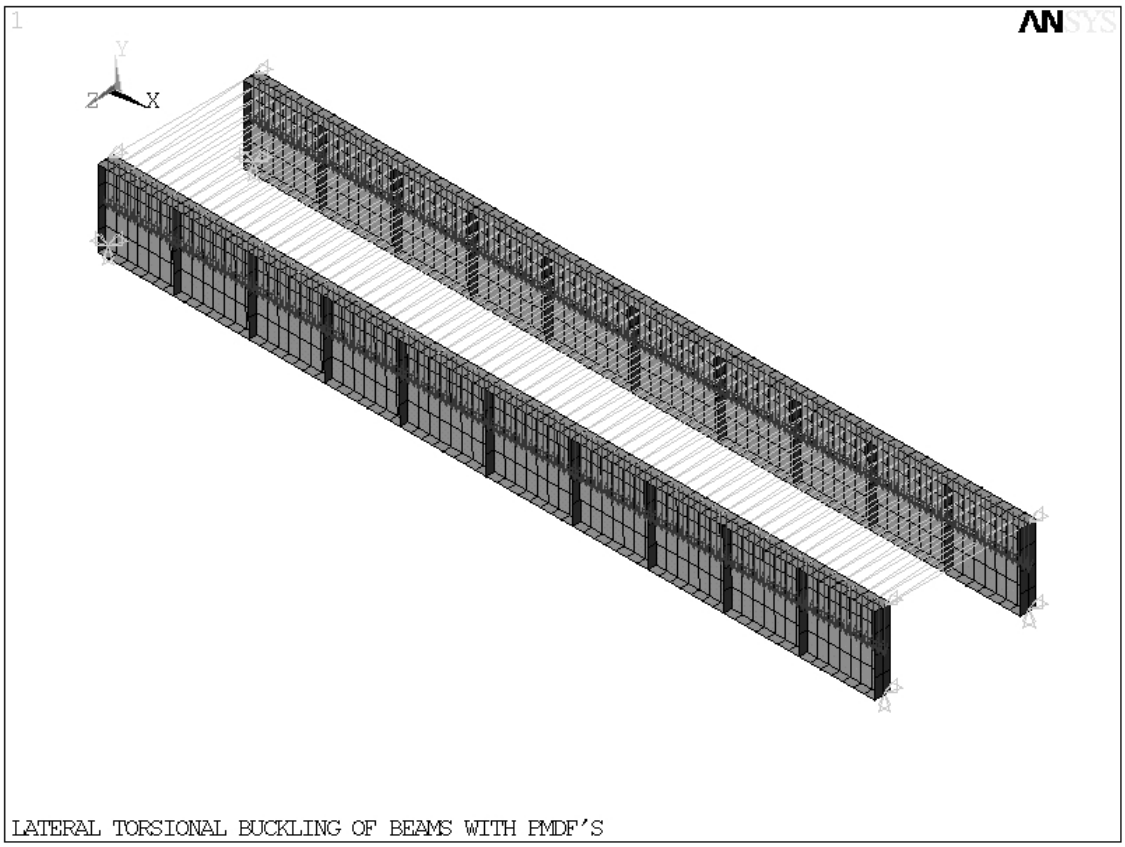

Figure 4.4. Slender-160#1 pre-processed state

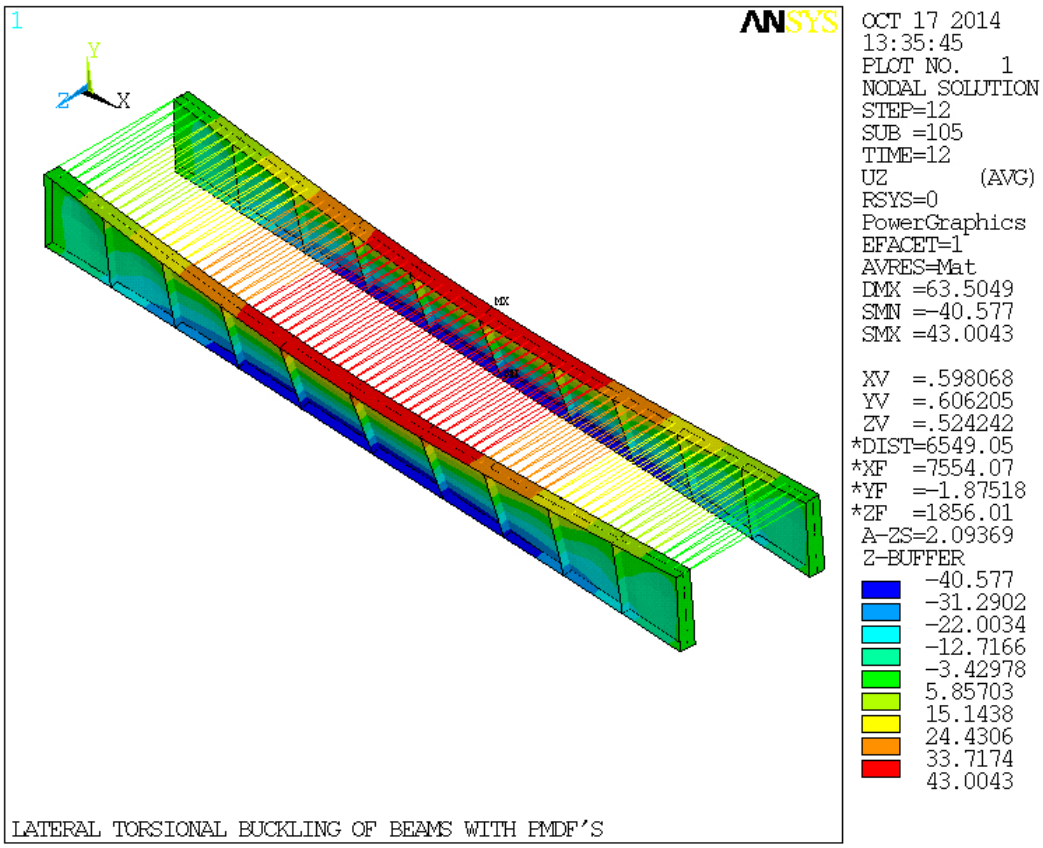

Figure 4.5. Slender-160#1 post-processed state

CHAPTER 5

CALCULATED STIFFNESS REQUIREMENTS

5.1. Introduction

The general philosophy for the design of stability bracing systems is to enable the braced member to support the design load while controlling deformations. In order to achieve this, an adequate bracing system must have sufficient strength and stiffness (Winter, 1960). Strength requirements for bracing members are often developed for specific brace stiffness.

In this part related results on stiffness of the deck systems obtained by Akbaba (2015) in a parallel companion study are reported in order to provide integrity on the presentation.

5.2. Results

Table 5.1 and Table 5.2 demonstrates the midspan twist ratio and edge fastener maximum resultant brace force, side-lap fastener maximum brace force results of stocky doubly symmetric sections respectively.

Mid-span twist ratio was calculated as the amount of rotation at the mid-span section around the x-axis with respect to center of twist to the amount of initial imperfection. Maximum force of a fastener occurred at the end of 12th load step that corresponds to a bending stress level of 210 MPa.

Although several cases were analyzed for the twin girder-shear diaphragm system, most of the analyses were performed in a standard configuration. A standard twin girder-shear diaphragm system consists of 16 gauge thick deck sheets with 4 edge fasteners on both sides connecting each deck sheet to the girder and 5 side-lap fasteners on each sheet-to-sheet connection. Results presented in the following tables were constructed on the standard configured systems.

Table 5.1. Stocky sections mid-span twist ratio

Section Designation	Section Properties	L/d	θ_T/θ_o			
			$2Q_{ideal}$	$3Q_{ideal}$	$4Q_{ideal}$	$5Q_{ideal}$
Stocky#1 (SEC2)	b_f = 140 mm	15	4.29	2.84	2.37	2.15
	d = 366 mm	20	4.37	2.90	2.46	2.24
		25	5.39	3.25	2.73	2.48
	WSR = 60	30	X	4.02	3.22	2.89
Stocky#2 (SEC3)	b_f = 280 mm	15	4.10	2.77	2.34	2.13
	d = 732 mm	20	4.38	2.92	2.48	2.27
		25	5.79	3.38	2.82	2.57
	WSR = 60	30	X	4.51	3.49	3.11

Table 5.2. Stocky sections brace forces

Section Designation	Section Properties	L/d	$F_{br\text{-}edge}$ (N)				$F_{br\text{-}side}$ (N)			
			$2Q_{ideal}$	$3Q_{ideal}$	$4Q_{ideal}$	$5Q_{ideal}$	$2Q_{ideal}$	$3Q_{ideal}$	$4Q_{ideal}$	$5Q_{ideal}$
Stocky#1 (SEC2)	b_f = 140 mm	15	1971	1445	1281	1204	7704	5542	4832	4494
	d = 366 mm	20	2251	1598	1412	1327	8786	6184	5407	5069
		25	2927	1852	1601	1490	11489	7265	6251	5812
	WSR = 60	30	X	2360	1938	1768	X	9157	7502	6826
Stocky#2 (SEC3)	b_f = 280 mm	15	7739	5683	5019	4715	30345	22100	19531	18349
	d = 732 mm	20	9046	6408	5650	5303	35447	24972	21931	20545
		25	12425	7631	6575	6108	48761	29872	25681	23857
	WSR = 60	30	X	10296	8199	7420	X	40212	32000	28959

Cross marks in the last row of the Table 5.1 and Table 5.2 implies that Stocky #1 and Stocky#2 section analysis with an L/d ratio of 30 did not converge with two times the ideal stiffness.

Table 5.3 and Table 5.4 demonstrate the midspan twist ratio and edge fastener maximum resultant brace force, side-lap fastener maximum brace force results of slender doubly symmetric sections respectively. Table 5.5 and Table 5.6 demonstrate the results for singly symmetric sections in the same way with doubly symmetric sections.

Table 5.3. Slender doubly symmetric sections mid-span twist ratio

Section Designation	Section Properties	L/d	θ_T/θ_o			
			$2Q_{ideal}$	$3Q_{ideal}$	$4Q_{ideal}$	$5Q_{ideal}$
Slender-100#1	b_f = 300 mm	10	3.57	2.57	2.24	2.08
	d = 1464 mm	15	3.99	2.87	2.50	2.33
Slender-160#1	b_f = 300 mm	10	3.83	2.72	2.36	2.18
	d = 1464 mm	15	4.22	2.98	2.59	2.40
Slender-100#2	b_f = 300 mm	10	3.74	2.73	2.39	2.22
	d = 1464 mm	15	4.38	3.13	2.74	2.55
Slender-160#2	b_f = 300 mm	10	3.96	2.88	2.52	2.34
	d = 1464 mm	15	4.74	3.30	2.87	2.66

Table 5.4. Slender doubly symmetric sections brace forces

Section Designation	Section Properties	L/d	$F_{br\text{-}edge}$ (N)				$F_{br\text{-}side}$ (N)			
			$2Q_{ideal}$	$3Q_{ideal}$	$4Q_{ideal}$	$5Q_{ideal}$	$2Q_{ideal}$	$3Q_{ideal}$	$4Q_{ideal}$	$5Q_{ideal}$
Slender-100#1	b_f = 300 mm	10	13110	9989	8990	8549	10225	7758	6981	6618
	d = 1464 mm	15	15857	11861	10613	9989	12354	9212	8238	7779
Slender-160#1	b_f = 300 mm	10	12486	9364	8365	7991	9759	7319	6549	6191
	d = 1464 mm	15	14608	10738	9614	8990	11476	8407	7475	7042
Slender-100#2	b_f = 300 mm	10	17405	13222	11899	11275	13591	10306	9266	8772
	d = 1464 mm	15	21725	15982	14234	13344	17011	12483	11090	10424
Slender-160#2	b_f = 300 mm	10	15520	11724	10525	9976	12124	9151	8205	7772
	d = 1464 mm	15	19603	13984	12361	11612	15348	10969	9705	9117

Table 5.5. Slender singly symmetric sections mid-span twist ratio

Section Designation	Section Properties	L/d	θ_T/θ_o			
			$2Q_{ideal}$	$3Q_{ideal}$	$4Q_{ideal}$	$5Q_{ideal}$
SS-100# 19	b_{cf} = 210 mm I_{yc}/I_y = 0.19 d = 1464 mm WSR = 100	10	3.24	2.34	2.05	1.90
		15	3.73	2.66	2.32	2.16
SS-100# 29	b_{cf} = 240 mm I_{yc}/I_y = 0.29 d = 1464 mm WSR = 100	10	3.33	2.41	2.10	1.95
		15	3.84	2.73	2.38	2.21
SS-100# 39	b_{cf} = 270 mm I_{yc}/I_y = 0.39 d = 1464 mm WSR = 100	10	3.49	2.50	2.18	2.02
		15	3.96	2.81	2.45	2.28
SS-160# 19	b_{cf} = 210 mm I_{yc}/I_y = 0.19 d = 1464 mm WSR = 160	10	3.51	2.46	2.13	1.97
		15	4.02	2.77	2.39	2.21
SS-160# 29	b_{cf} = 240 mm I_{yc}/I_y = 0.29 d = 1464 mm WSR = 160	10	3.57	2.52	2.19	2.03
		15	4.01	2.81	2.44	2.26
SS-160# 39	b_{cf} = 270 mm I_{yc}/I_y = 0.39 d = 1464 mm WSR = 160	10	3.66	2.61	2.26	2.10
		15	4.16	2.91	2.52	2.34

Table 5.6. Slender singly symmetric sections brace forces

Section Designation	Section Properties	L/d	$F_{br\text{-}edge}$ (N)				$F_{br\text{-}side}$ (N)			
			$2Q_{ideal}$	$3Q_{ideal}$	$4Q_{ideal}$	$5Q_{ideal}$	$2Q_{ideal}$	$3Q_{ideal}$	$4Q_{ideal}$	$5Q_{ideal}$
SS-100# 19	b_{cf} = 210 mm I_{yc}/I_y = 0.19 d = 1464 mm WSR = 100	10	9701	7254	6493	6143	7576	5657	5055	4771
		15	11512	8390	7441	6992	8982	6535	5792	5447
SS-100# 29	b_{cf} = 240 mm I_{yc}/I_y = 0.29 d = 1464 mm WSR = 100	10	10675	8066	7229	6842	8319	6265	5616	5312
		15	12848	9427	8365	7878	10016	7346	6522	6137
SS-100# 39	b_{cf} = 270 mm I_{yc}/I_y = 0.39 d = 1464 mm WSR = 100	10	11974	9027	8103	7666	9320	7002	6278	5941
		15	14409	10600	9427	8877	11246	8259	7353	6920
SS-160# 19	b_{cf} = 210 mm I_{yc}/I_y = 0.19 d = 1464 mm WSR = 160	10	8852	6430	5693	5356	6914	5021	4454	4190
		15	10376	7279	6393	5981	8076	5697	5001	4683
SS-160# 29	b_{cf} = 240 mm I_{yc}/I_y = 0.29 d = 1464 mm WSR = 160	10	9801	7229	6443	6068	7657	5636	5015	4731
		15	11325	8178	7242	6792	8880	6407	5663	5319
SS-160# 39	b_{cf} = 270 mm I_{yc}/I_y = 0.39 d = 1464 mm WSR = 160	10	10925	8178	7317	6917	8563	6380	5704	5386
		15	12985	9402	8328	7829	10171	7353	6515	6116

According to the results in the Table 5.1 to Table 5.6; providing twice the ideal stiffness results in relatively large normalized mid-span twist ratio with respect to three, four and five times the ideal stiffness. For twice the ideal stiffness; in Table 5.1 sections with span to depth ratio of 30 resulted with a mid-span twist ratio almost six. Increasing the diaphragm stiffness to three times the ideal stiffness (a 50% increase in brace stiffness with respect to twice the ideal stiffness), decreased the mid-span twist ratio of the same sections by approximately 40%, 28%, and 29% for stocky, slender doubly symmetric and slender singly symmetric sections, respectively. However, twist ratio still exceeds three. Following that, increasing the diaphragm stiffness to four times the ideal stiffness (a 33% increase in brace stiffness with respect to three times the ideal

stiffness); decreased the mid-span twist ratio of the same sections by approximately 17%, 13%, 13%. In case of five times the ideal stiffness, mid-span twist ratio results are decreased by at least 8% with respect to four times the ideal stiffness. It was concluded in the study of Akbaba (2015) that providing four times the ideal stiffness was sufficient to control the deformations. Further increasing the stiffness to five times the ideal value (a 25% increase in brace stiffness with respect to four times the ideal stiffness) decreased the rotations by only 8%.

According to Table 5.2, Table 5.4 and Table 5.6 above; analyses with larger diaphragm stiffness resulted with lower brace force values. On the other hand, increasing the span to depth ratio resulted in larger brace force values, which implies an increase of the required diaphragm stiffness. It can also be observed in the tables that side-lap connections are more critical than edge connections. The side-lap fastener forces are higher than the edge fastener connections and the capacity of side-lap connections is smaller than that of the edge fastener connections. In addition; among the three section types, the highest brace forces develop in doubly-symmetric slender sections since these sections could sustain higher moments, therefore higher compression forces, due to larger moment of inertias.

Increasing the diaphragm stiffness to three times the ideal stiffness (a 50% increase in brace stiffness with respect to twice the ideal stiffness) resulted in a decrease in edge and side-lap fastener brace forces with equal amounts of 35%, 26%, and 26% for stocky, slender doubly symmetric and slender singly symmetric sections, respectively. Increasing the diaphragm stiffness to four times the ideal value, further decreased edge and side-lap fastener brace forces for an equal amount of 14%, 11% and 11% with respect to three times the ideal stiffness. In case of five times the ideal stiffness (a 25% increase in brace forces with respect to four times the ideal stiffness), edge and side-lap fastener brace forces decreased an additional amount of approximately 6% with respect to four times the ideal stiffness. It was reported that increasing the diaphragm stiffness to six times the ideal stiffness reduced the brace forces 4%. Similar to the results of mid-span twist ratio, providing a diaphragm stiffness of four times the ideal value was sufficient to control the brace forces.

According to the results on both twists and brace forces, a diaphragm stiffness equal to four times the ideal value was recommended to control deformations and brace forces for shear diaphragms bracing steel I-beams.

CHAPTER 6

CALCULATED STRENGTH REQUIREMENTS

6.1. Introduction

This chapter presents finite element analysis results that are used to develop strength requirements for stocky and slender steel I-beams that are braced by shear diaphragms. Past studies (Luttrell, 1981; Davies & Bryans, 1982) on strength and stiffness of shear diaphragms showed that the shear strength of a diaphragm is generally controlled by either the shear strength of the longitudinal edge connections (sheet to structural member connection along the edges) or shear strength at interior connections between panels (sheet to sheet connections along side-laps). Hence, strength requirements for shear diaphragms should address both edge and side-lap fasteners. In order to investigate the strength requirements a numerical study that involves large displacement analyses is conducted. Noting that global directions are clearly available in Figure 4.4 and Figure 4.5. Results of the large displacement analyses related to strength requirements mainly consist of the following data:

- Fastener brace forces in the deck-girder connection through global z-axis,
- Fastener brace forces in the deck-girder connection through global x-axis,
- Fastener brace forces in side-lap (deck to deck) connections through global z axis,

Upon completion of analysis, the data output was stored in an Excel data sheet and Matlab (2012) was used for processing the data.

In order to make generalizations about the behavior and compare the results of various analyses on the same basis, deck brace forces were normalized. Through normalization process brace force requirements for both deck to girder connection fasteners and sheet to sheet connection fasteners were obtained. Brace force requirements for different deck configurations were also sought. Prior to the normalization process, brace force distributions through the girder are plotted on the

following pages for both edge and side-lap connections. Consecutively, normalized brace force distribution plots are given.

As indicated in Chapter 5.2, figures in this Chapter were also plotted according to the standard twin girder-shear diaphragm system analyzes. As previously explained the standard twin girder-shear diaphragm system consists of a deck system with a stiffness of four times the ideal stiffness, 1.52 mm (16 gauge) thick decks, 4 edge fasteners on both sides connecting each deck sheet to the girder, and 5 side-lap fasteners on each sheet-to-sheet connection.

Table 6.1 presents the properties of the sections utilized in the study.

Table 6.1. Section properties

SECTION DESIGNATION	λ_{web}	d (mm)	I_{major} (mm^4)	$M_{210\ MPa}$ (kNm)
Stocky#1	58.0	366	101381976	116.34
Stocky#2	58.0	732	1622111616	930.72
Slender-100#1	100.0	1464	11097305304	3183.65
Slender-160#1	160.0	1464	9848060190	2825.26
Slender-100#2	100.0	1830	20584007133	4724.20
Slender-160#2	159.9	1830	17446895083	4004.21
SS-100# 19	100.0	1464	8981140031	2308.88
SS-100# 29	100.0	1464	9655128756	2566.65
SS-100# 39	100.0	1464	10363586836	2857.93
SS-160# 19	160.1	1464	7626892659	1895.27
SS-160# 29	160.0	1464	8352439423	2169.96
SS-160# 39	160.1	1464	9096758487	2479.72

6.2. A Closer Look to a Deck Sheet

In this part the displacement and brace force results in the fasteners of a single deck sheet is presented to clarify the force distribution in a single deck. Figure 6.1 presents the total displacement contour plot of Slender-100#2 section with an L/d ratio of 10. The single deck location which is investigated here is indicated with a thunder mark on the figure.

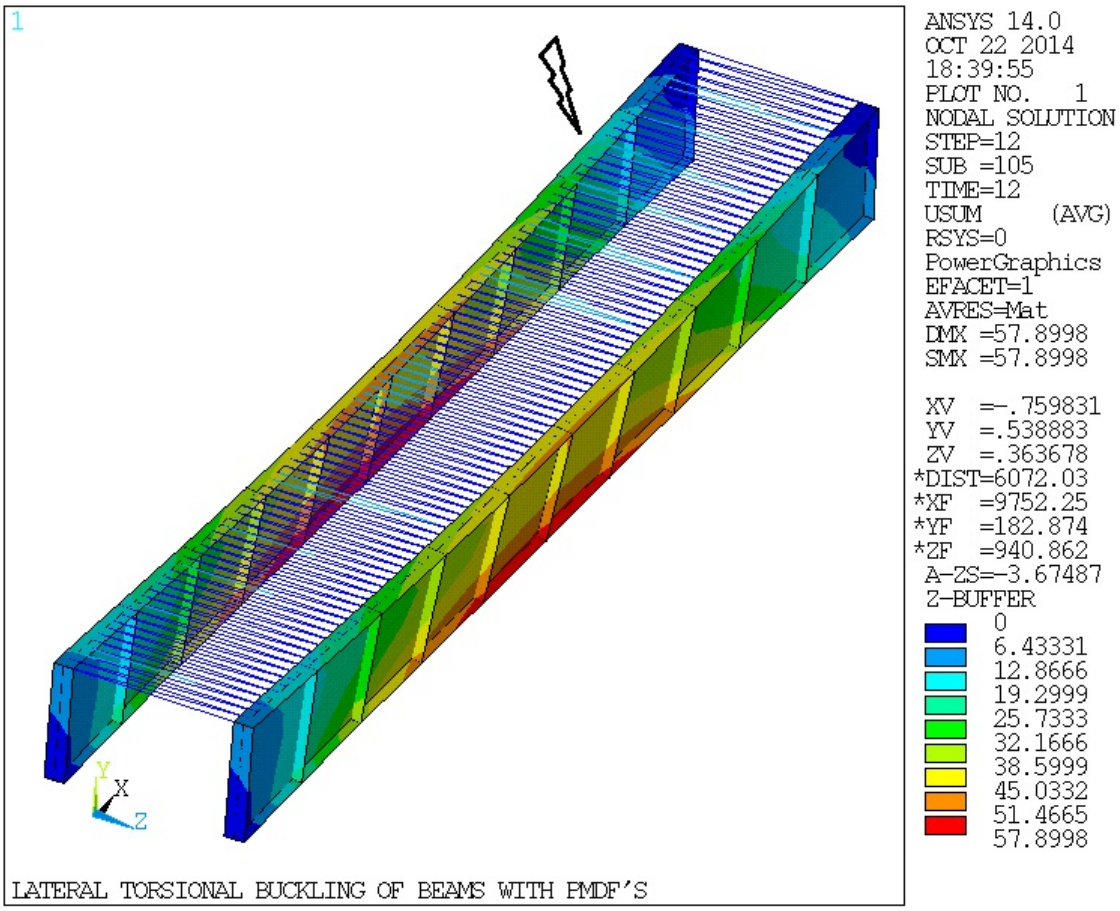

Figure 6.1. Total displacement contour plot of Slender-100#2 section with L/d 10

Figure 6.2 demonstrates the single deck sheet with finite element identification numbers representing each fastener on the left hand side and the fastener brace forces on the right hand side. Table 6.2 presents the displacement and the brace force results of the fastener elements.

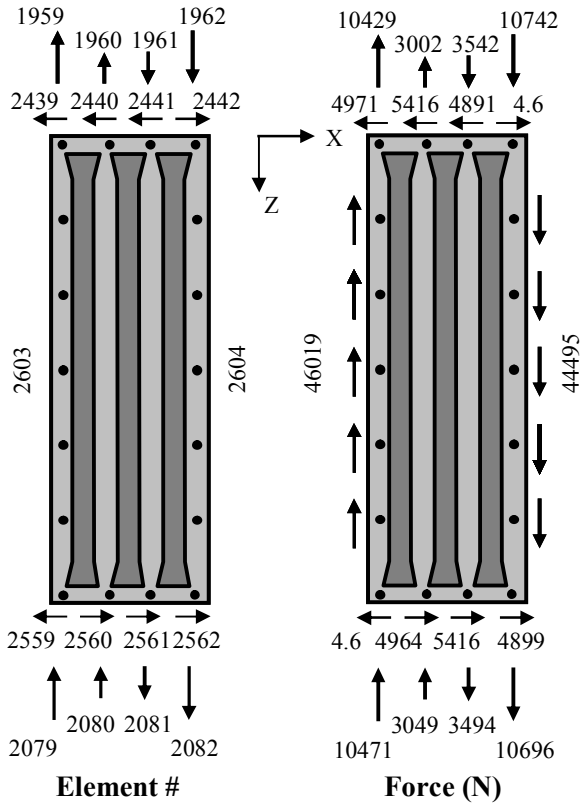

Figure 6.2. Fastener brace forces in a single deck

Table 6.2. Displacement and brace force values of fasteners in a single deck

Element #	Node #		U_x (mm)			U_z (mm)			F_x (N)		F_z (N)	
	i	j	i	j	Δ_{j-i}	i	j	Δ_{j-i}	i	j	i	j
1959	2853	7499	0.61142	0.46076	-0.1507	6.1954	5.8794	-0.316			-10429.0	10429.0
1960	2891	7500	0.49433	0.33019	-0.1641	5.7257	5.6347	-0.091	X		-3002.3	3002.3
1961	2929	7501	0.38375	0.23551	-0.1482	5.2615	5.3688	0.1073			3542.2	-3542.2
1962	2967	7502	0.2799	0.28004	0.00014	4.7999	5.1254	0.3255			10742.0	-10742.0
2439	2853	7499	0.61142	0.46076	-0.1507	6.1954	5.8794	-0.316	-4971.0	4971.0		
2440	2891	7500	0.49433	0.33019	-0.1641	5.7257	5.6347	-0.091	-5416.0	5416.0	X	
2441	2929	7501	0.38375	0.23551	-0.1482	5.2615	5.3688	0.1073	-4891.0	4891.0		
2442	2967	7502	0.2799	0.28004	0.00014	4.7999	5.1254	0.3255	4.6	-4.6		
2603	7498	7619	0.61157	0.99454	0.38297	6.523	5.8791	-0.6439	-6.4	6.4	-46019.0	46019.0
2604	7502	7623	0.28004	0.68484	0.4048	5.1254	4.5029	-0.6225	-6.6	6.6	-44495.0	44495.0
2079	6292	7619	0.99467	0.99454	-0.0001	6.1965	5.8791	-0.3174			-10471.0	10471.0
2080	6330	7620	0.88548	1.0359	0.15042	5.7269	5.6345	-0.0924	X		-3049.0	3049.0
2081	6368	7621	0.78219	0.94633	0.16414	5.2627	5.3686	0.1059			3494.8	-3494.8
2082	6406	7622	0.68497	0.83343	0.14846	4.8011	5.1252	0.3241			10696.0	-10696.0
2559	6292	7619	0.99467	0.99454	-0.0001	6.1965	5.8791	-0.3174	-4.6	4.6		
2560	6330	7620	0.88548	1.0359	0.15042	5.7269	5.6345	-0.0924	4964.5	-4964.5	X	
2561	6368	7621	0.78219	0.94633	0.16414	5.2627	5.3686	0.1059	5416.2	-5416.2		
2562	6406	7622	0.68497	0.83343	0.14846	4.8011	5.1252	0.3241	4898.6	-4898.6		

First column in Table 6.2 identifies fastener element identification numbers in the finite element model. These numbers are associated with the actual locations in Figure 6.2. Table 6.2 consists of eight dimensionless spring elements in the south girder – element # 1959:1962 in z direction and element # 2439:2442 in x direction-; two axial elements, element # 2603-2604 which represents the connection to the adjacent sheets on both sides; eight dimensionless springs in the north girder- element # 2079:2082 in z direction and element # 2559:2562 in x direction-. Following two columns on the table displays first and last node of each element. Following columns display the displacement of the first and the last node of the each element, the difference of the nodal displacements respectively for both directions. Last columns are the fastener brace forces in global directions. These values are the brace forces generated in the deck-girder connections due to the shear displacement of the deck. Note that the values related to side-lap forces are the total of 5 side-lap fasteners. Consequently equilibrium of the forces and the moment with respect to deck mid is calculated as follows:

$\mathbf{\Sigma F_y}$=46019+10429+3002+10471+3049-3542-10742-44495-3494-10696=**0 → OK**

$\mathbf{\Sigma F_x}$= 4964+5416+4899+4.6-4971-5416-4891-4.6=**0 → OK**

$\mathbf{\Sigma M_{deck\text{-}mid}}$= 46019*0.61/2+44495*0.61/2+10429*0.61/2+3002*0.61/6+3542*0.61/6
+10742*0.61/2+10471*0.61/2+3049*0.61/6+3494*0.61/6+10696*0.61/2-
(4971+5416+4891-4.6)*2.74/2-(4964+5416+4899-4.6)*2.74/2=**0 → OK**

6.3. Results on Stocky Sections

6.3.1. Fastener Force Distribution

Figure 6.3 presents the edge fastener resultant force distribution of stocky sections. Only the results of Stocky#1 L/d 30 and Stocky#2 L/d 30 configurations were plotted to present a clear picture. In Figure 6.3 horizontal axis represents the fastener locations through the girder. Vertical axis represents the resultant brace forces of z and x directions. In the figure Stocky#1 section is represented with asterisk. Circle markers indicate the Stocky#2 section. In the figure each deck is represented with a continuous line with 4 markers, since each deck and girder connection was provided with 4 fasteners.

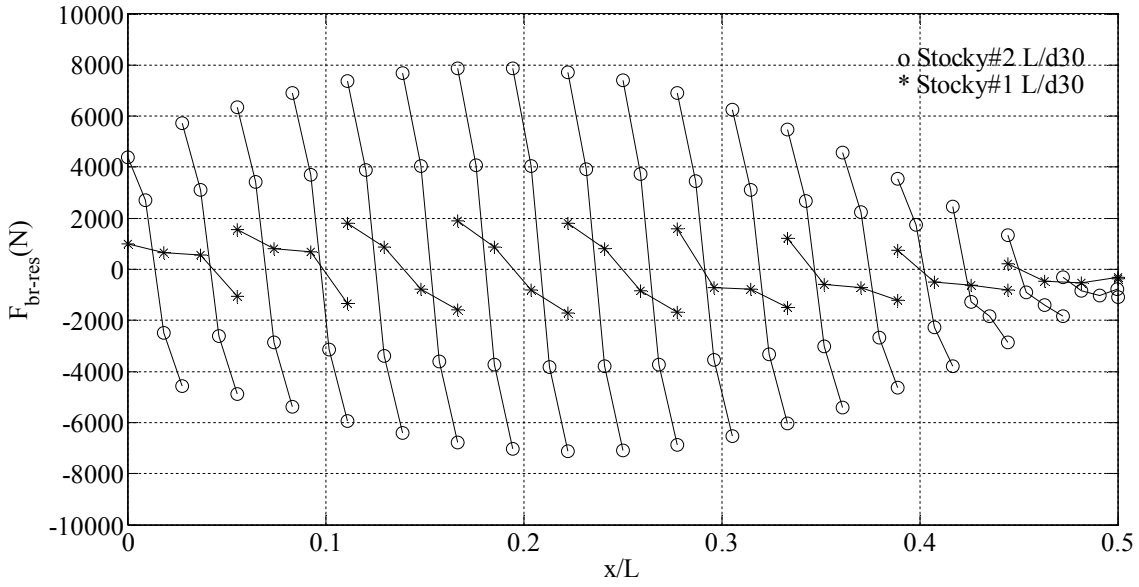

Figure 6.3. Stocky sections edge fastener resultant brace force distribution

In Figure 6.3 horizontal axis is limited to the half-span since the distribution of brace forces is symmetrical with respect to mid-span. According to the Figure 6.3, the maximum brace force of the edge fasteners in a single deck generates within the 1st and the last fasteners. Figure 6.3 also validates the edge fastener force distribution as aforementioned in Figure 3.9. It is notable that considerably higher brace forces develop in Stocky#2 section as compared to those that develop in Stocky#1 section, as previously indicated in Chapter 5.

Figure 6.4 presents the side-lap fastener brace force distribution of stocky sections. In this figure results of remaining configurations, which were not shown in Figure 6.3, are also added to the L/d 30 results. Horizontal axis represents the side-lap fastener locations through the girder in Figure 6.4. Markers located at x=0 indicates the brace force value that develop in deck to diaphragm fasteners, which were represented by additional spring elements that connect the girder mid-points at the support to end of the transverse diagonal truss element of the shear diaphragm FEA model. As previously mentioned in Chapter 3 the ends of the girders at the supports are generally connected to each other by transverse diaphragms. At the supports metal deck forms are generally connected to these diaphragms. Vertical axis represents the brace force of a single side-lap fastener in z direction.

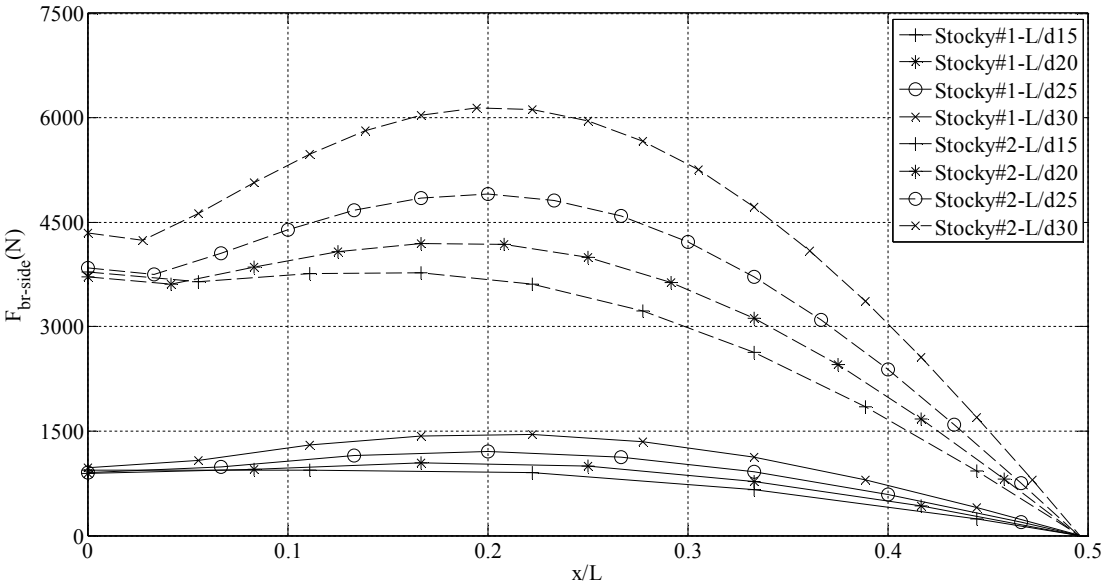

Figure 6.4. Stocky sections side-lap fastener brace force distribution

According to Figure 6.3 and Figure 6.4; brace forces tend to increase with increasing girder span length. It can also be seen in both figures that along the length of the beam maximum brace forces occur around quarter span, where the shear deformations are maximum.

6.3.2. Normalized Fastener Force Distribution

Fastener brace force distribution in Figure 6.3 and Figure 6.4 can be used to estimate the maximum fastener brace force value in diaphragm systems that brace steel I-girders. Many parameters affect the bracing behavior of the diaphragm in steel girder-diaphragm systems. Helwig & Yura (2008-II) used span-to-depth ratio, girder moment of inertia in bending and the cross sectional depth to normalize the brace forces. In this part brace forces are normalized in the same practice with Helwig & Yura (2008-II). Normalization is demonstrated step by step in the following figures.

Before the normalization process; Figure 6.3 is enlarged to Figure 6.5. As distinct from Figure 6.3, Figure 6.5 involves all the stocky section analysis results with the standard deck fastener configuration. Since it is obvious that maximum resultant brace force occurs within the first edge fastener in a deck sheet; each deck is represented only with the first edge fastener result in Figure 6.5.

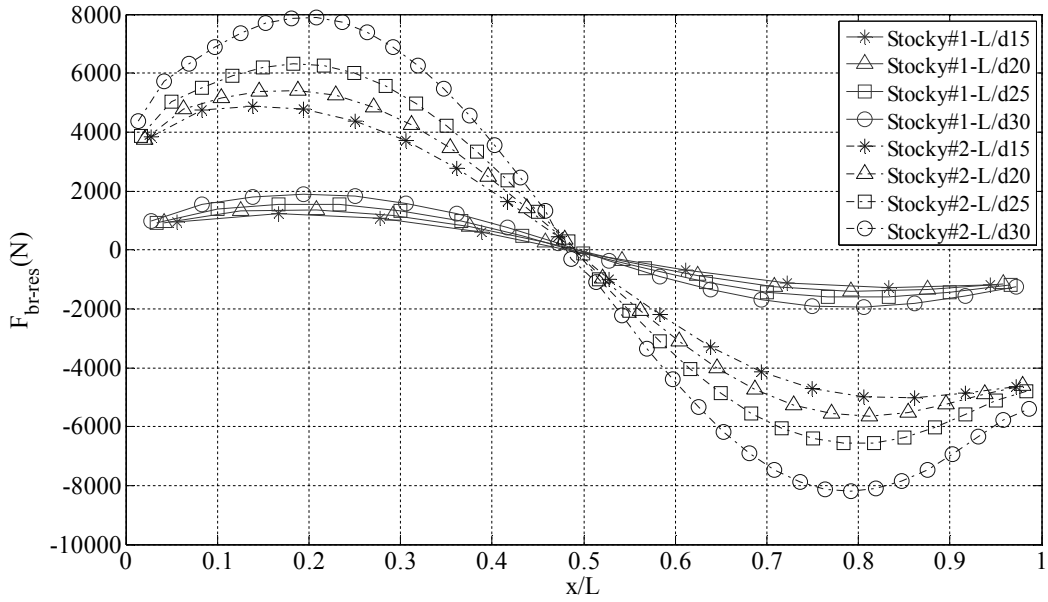

Figure 6.5 Edge fastener resultant brace force ratio distribution

In Figure 6.5 horizontal axis represents the fastener locations through the girder. Horizontal axis covers the full span since the distribution slightly differs with respect to mid-span. Vertical axis represents the resultant brace forces of z and x-directions.

Same as in Figure 6.3 and Figure 6.4; brace forces are separated mainly according to the girder type in Figure 6.5. In addition, each brace force distribution group is also sub-divided by the span-to-depth ratio. According to that observation, resultant brace forces in Figure 6.5 and side-lap fastener brace forces in Figure 6.4 are normalized by the maximum applied beam moment, M_U in Figure 6.6 and Figure 6.7.

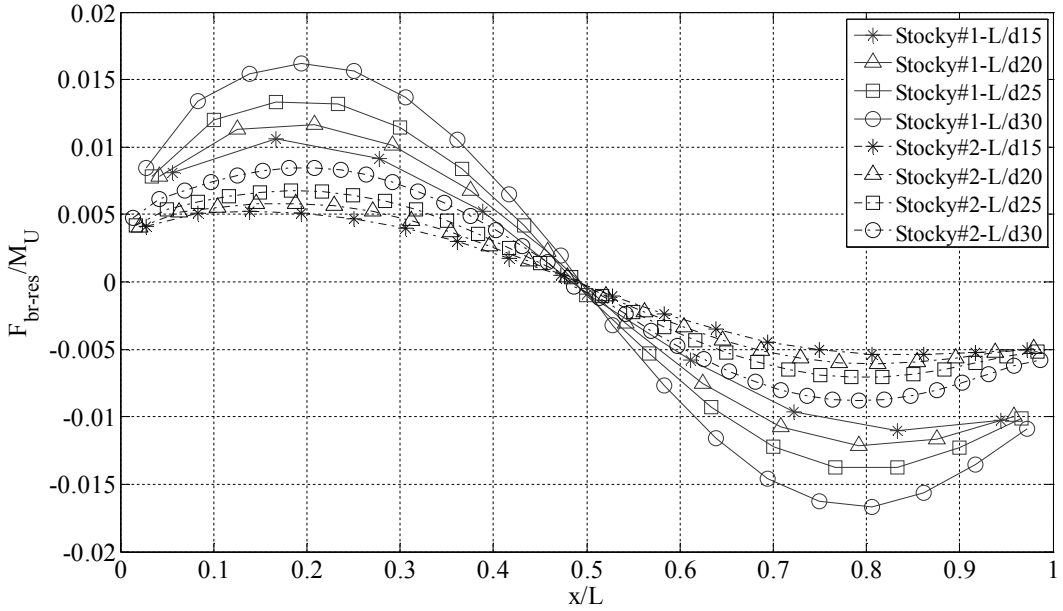

Figure 6.6 Stocky sections edge fastener normalized resultant brace force ratio distribution-Step 1

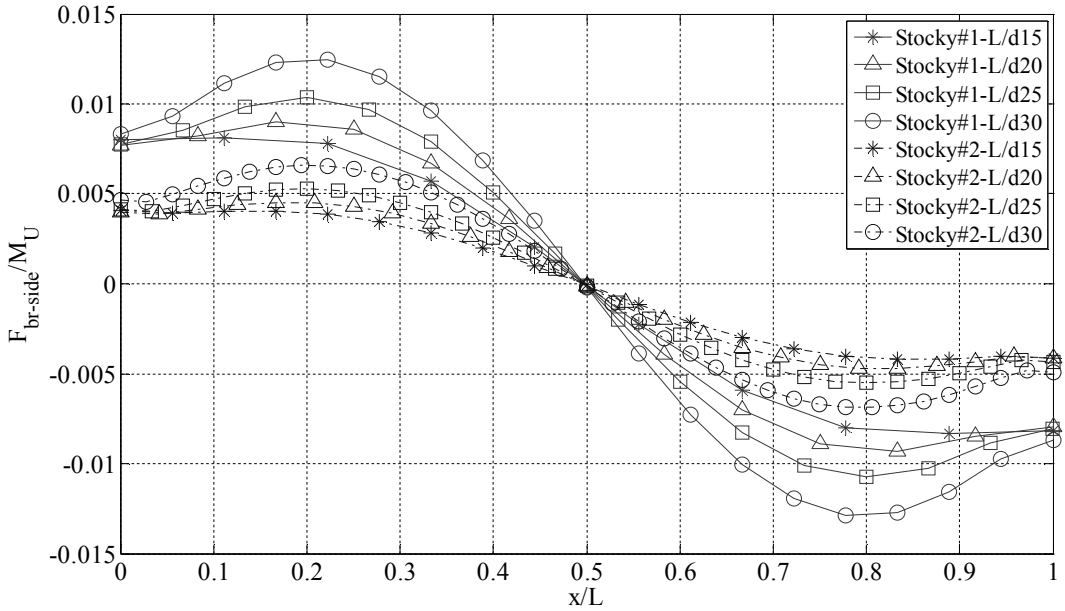

Figure 6.7 Stocky sections side-lap fastener normalized brace force ratio distribution-Step 1

In Figure 6.6 vertical axis represents the normalized resultant brace forces of z and x-directions. Resultant brace forces were normalized by the maximum applied beam moment, $M_{U.}$ Figure 6.7 presents the normalized side-lap fastener brace forces with respect to Figure 6.4. Similar to the Figure 6.6, all the stocky section analysis

results with the standard configuration are demonstrated in Figure 6.7. Horizontal axis covers the full span since the distribution slightly differs with respect to mid-span. Horizontal axis represents the side-lap fastener locations through the girder. Vertical axis represents the brace force of a single side-lap fastener in z-direction that normalized by the maximum applied beam moment, M_U. Markers located at x=0 indicates the normalized brace force value of a single fastener on sheet and the girder connection located transversely to twin girder-diaphragm system at both ends. Its noticed in Figure 6.6 and Figure 6.7 that normalizing the brace forces approached the brace force distribution of Stocky#1 and Stocky#2 but the distributions are still dominated by L/d ratio. According to that, normalized brace forces in Figure 6.6 and Figure 6.7 are normalized again by the span-to-depth ratio, L/d in Figure 6.8 and Figure 6.9.

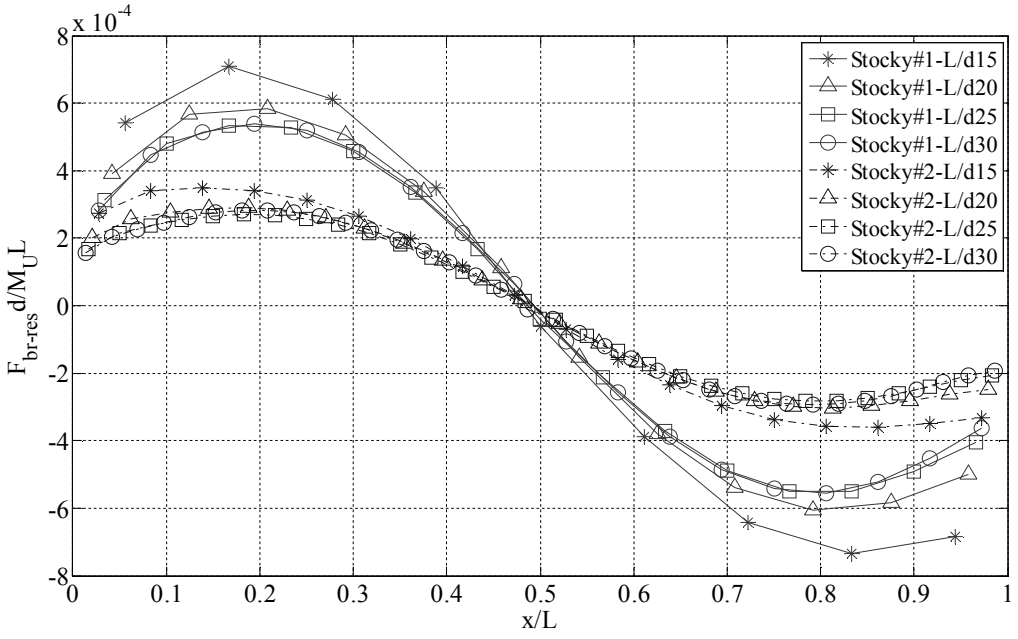

Figure 6.8 Stocky sections edge fastener normalized resultant brace force ratio distribution-Step 2

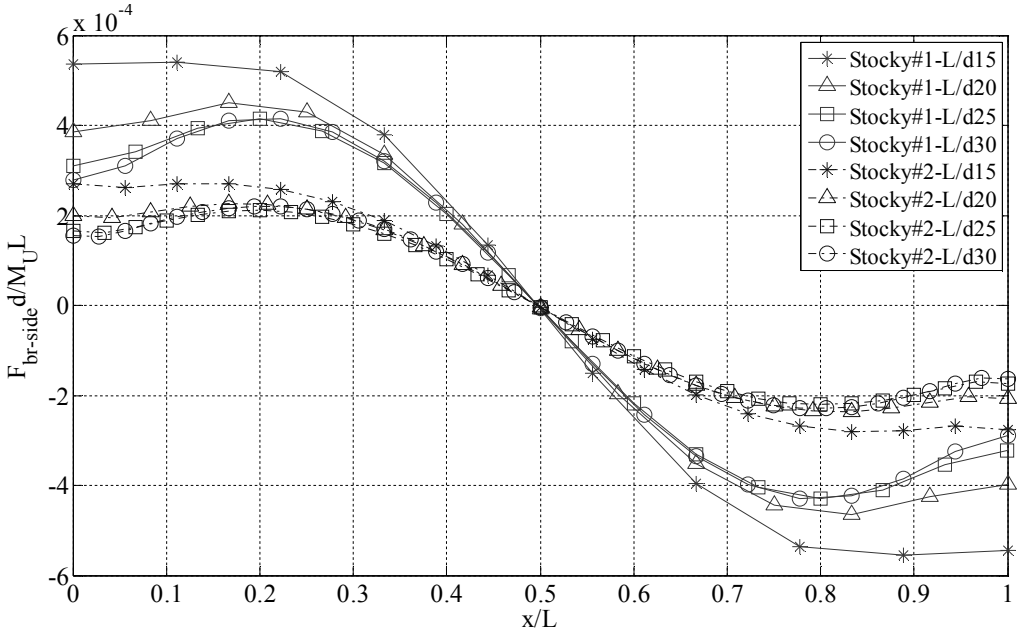

Figure 6.9 Stocky sections side-lap fastener normalized brace force ratio distribution-Step 2

Its noticed in Figure 6.8 and Figure 6.9 that normalizing the brace forces approached the brace force distribution of different L/d ratio but the distributions are still dominated by section type. According to that, normalized brace forces in Figure 6.8 and Figure 6.9 are further normalized with girder cross sectional depth, d in Figure 6.10 and Figure 6.11.

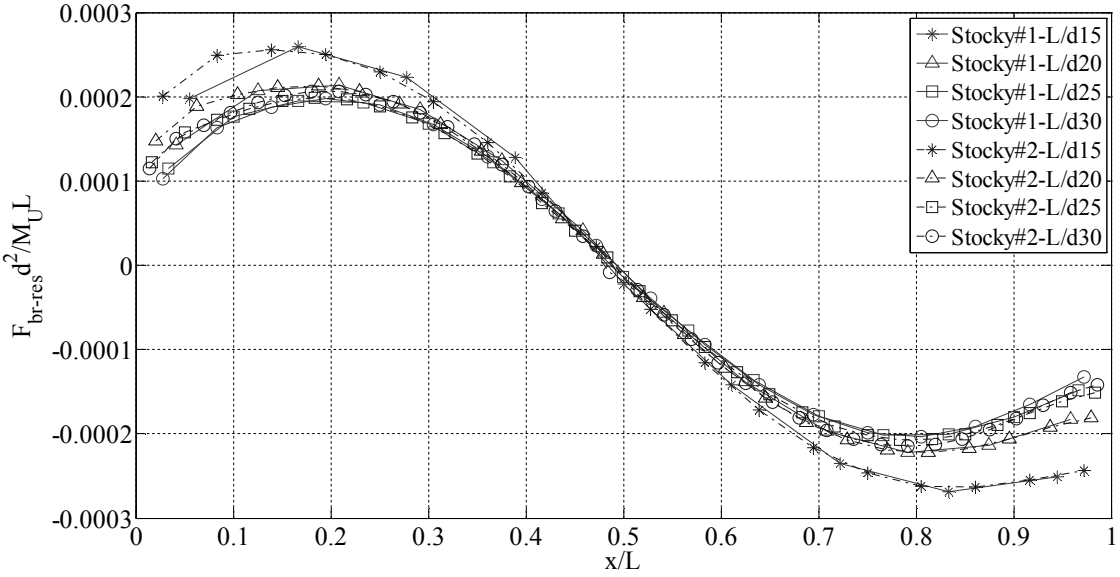

Figure 6.10. Stocky sections edge fastener normalized resultant brace force ratio distribution-Step 3

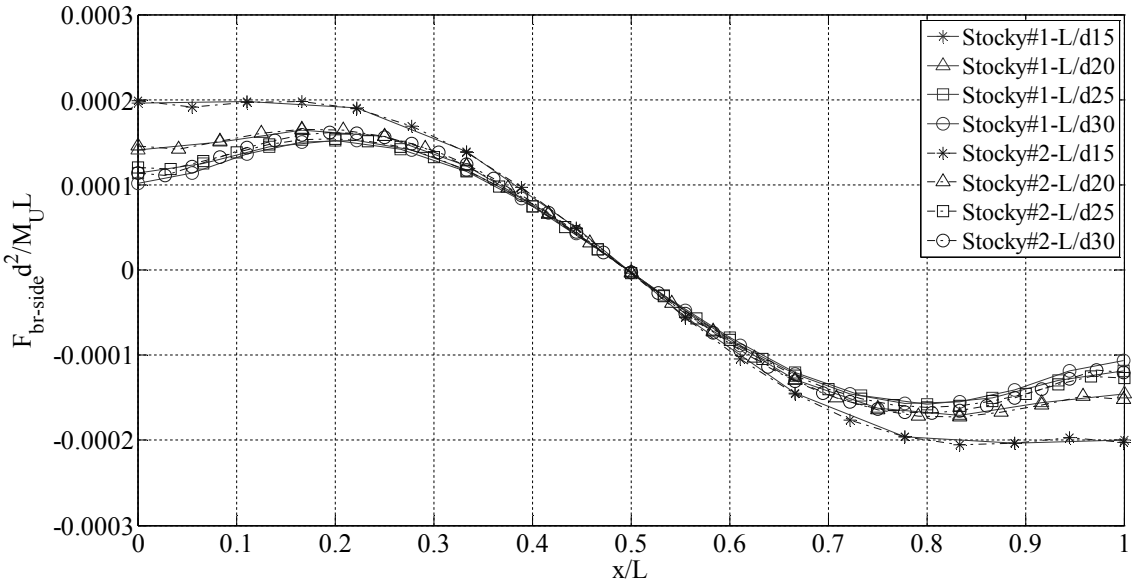

Figure 6.11. Stocky sections side-lap fastener normalized brace force ratio distribution-Step 3

It is noticed in both Figure 6.10 and Figure 6.11 that normalized force distribution curves for L/d ratios of 20, 25 and 30 coincide with each other. It is clear that in both figures normalized brace force value maximizes around the 20% portion of the girder end. Maximum normalized force ratio values are 0.00025 and 0.00020 for edge and side-lap fasteners, respectively. For L/d ratio of 10 these values tend to increase by approximately 20% for both graphs.

6.4. Results on Slender Doubly Symmetric Sections

In this part results are presented for slender doubly symmetric sections. Figures presented in this part consider the same trend with the figures on stocky sections.

6.4.1. Fastener Force Distribution

In Figure 6.12 edge fastener resultant brace force distribution of slender doubly symmetric sections is presented. Only the results of Slender-100#1 L/d 15 and Slender-160#2 L/d 15 configurations were plotted. In the figure, Slender-100#1 L/d 15 section is

represented with asterisk. Circle markers represent the Slender-160#2 L/d 15 section series.

Figure 6.12 indicates that Slender-160#2 L/d 15 section with overall section depth of 1830 mm analyses resulted with higher brace forces with respect to Slender-100#1 L/d 15 with overall section depth of 1464 mm.

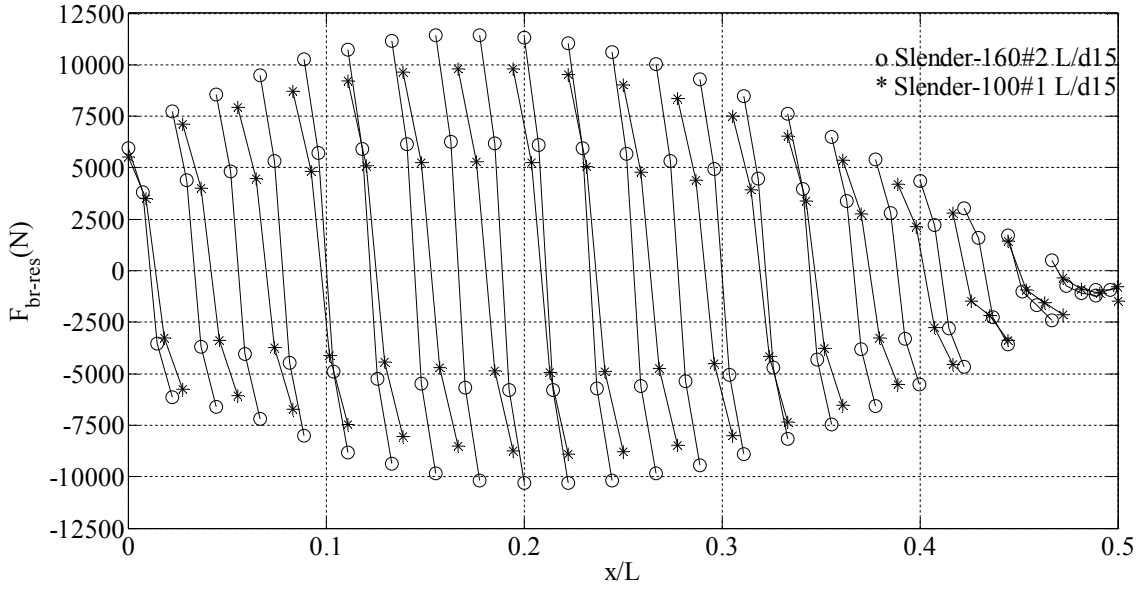

Figure 6.12. Slender doubly symmetric sections edge fastener resultant brace force distribution

Figure 6.13 presents the side-lap fastener brace force distribution of slender doubly symmetric sections. Only the results of Slender-100#1 L/d 15 and Slender-160#2 L/d 15 configurations were plotted in order to provide continuity with Figure 6.12. Similar to the previous figure, Figure 6.13 indicates that Slender-160#2 section with L/d of 15 results with higher brace forces with respect to Slender-160#2 section with L/d of 15.

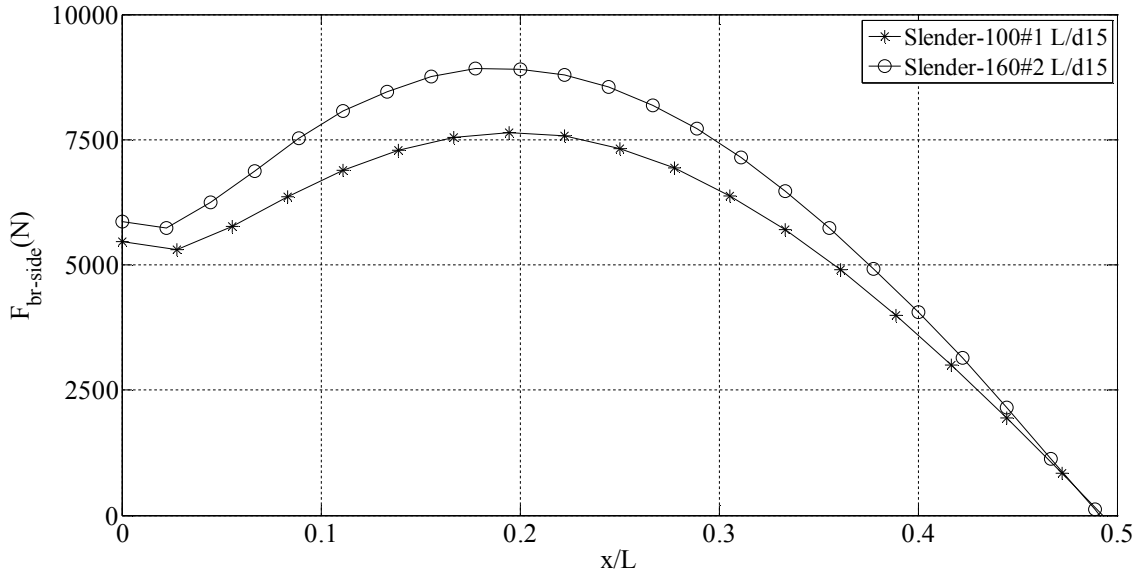

Figure 6.13. Slender doubly symmetric sections side-lap fastener brace force distribution

6.4.2. Normalized Fastener Force Distribution

Figure 6.14, Figure 6.15 demonstrates the edge fastener normalized resultant brace force ratio distribution and the normalized side-lap fastener brace force ratio distribution of slender doubly symmetric sections respectively.

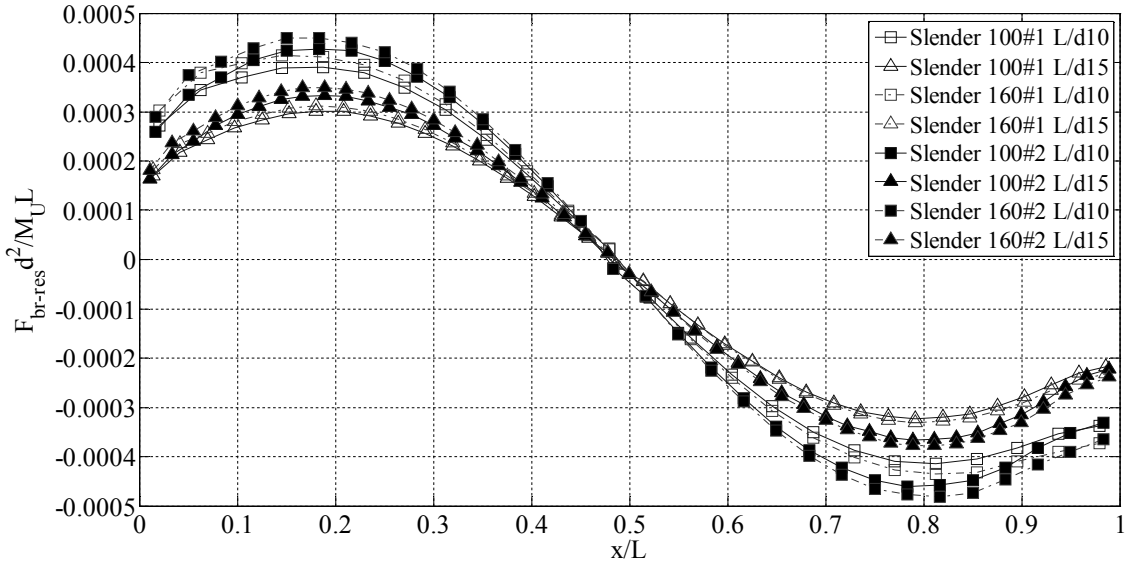

Figure 6.14. Slender doubly symmetric sections edge fastener normalized resultant brace force ratio distribution

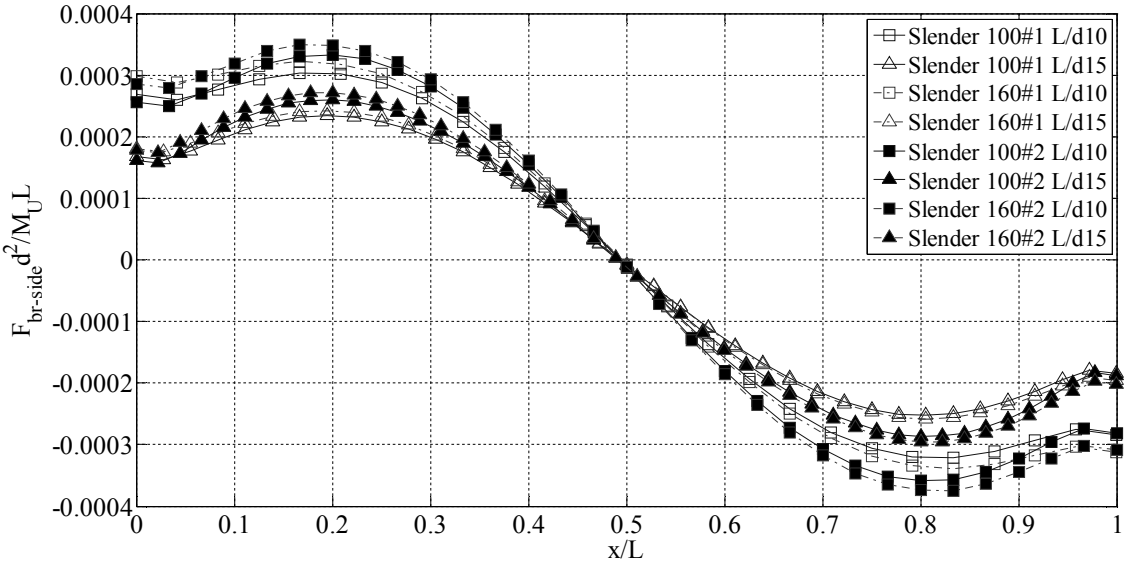

Figure 6.15. Slender doubly symmetric sections side-lap fastener normalized brace force ratio distribution

In Figure 6.14 and Figure 6.15, analyses with L/d ratio of 10 and 15 are indicated with square and triangle markers respectively. It can be seen in both figures that analyses with lower L/d ratio result with higher normalized brace force ratios. Another observation that can be made from both figures is that cross sectional depth makes a clear distinction on the normalized brace force ratio results. Sections with higher depth have higher brace forces.

Analyses with web slenderness ratio of 100 and 160 are illustrated with continuous and dashed lines, respectively, in Figure 6.14 and Figure 6.15. It can be seen in both figures that analyses with lower web slenderness ratio results with higher normalized brace force ratios.

For L/d ratio of 15 the maximum normalized brace force ratio values are 0.00040 and 0.00030 for edge and side-lap fasteners, respectively. For L/d ratio of 10, these values tend to increase by approximately 27% for both graphs.

6.5. Results on Slender Singly Symmetric Sections

In this part results are presented for slender singly symmetric sections. Figures presented in this part show the same trend with the previous figures on stocky and slender doubly symmetric sections.

6.5.1. Fastener Force Distribution

In Figure 6.16 edge fastener resultant brace force distribution of slender singly symmetric sections is presented. Only the results of SS-100#19 L/d 15 and SS-100#39 L/d 15 configurations were plotted. In the figure SS-100#19 L/d 15 is illustrated with asterisk markers. Circle markers represent the SS-100#39 L/d 15 section series.

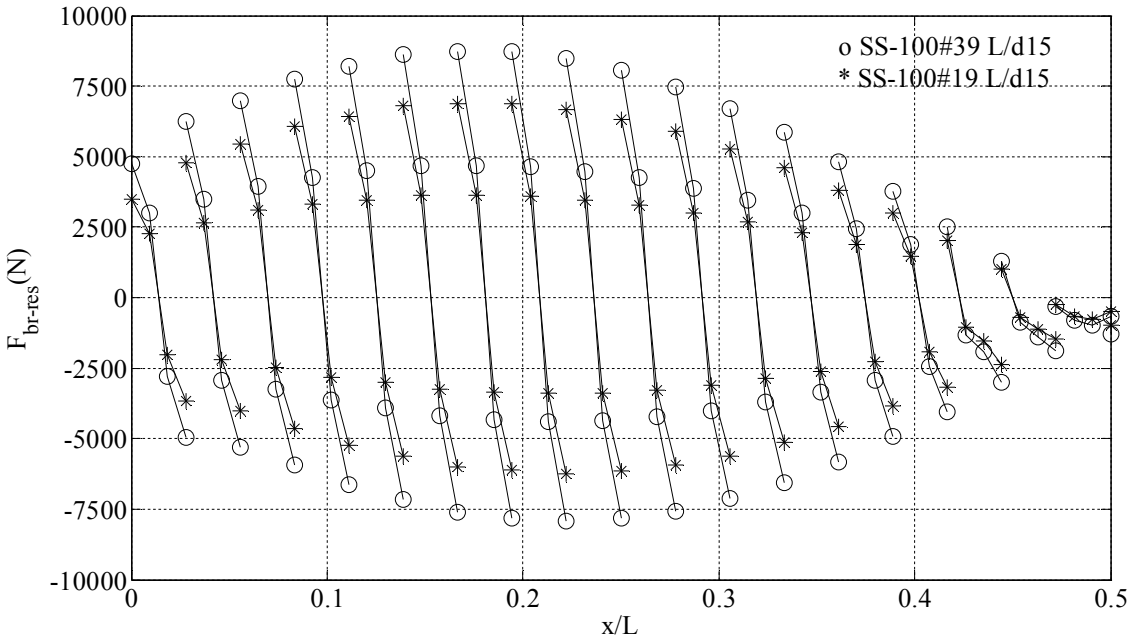

Figure 6.16. Slender singly symmetric sections edge fastener resultant brace force distribution

Figure 6.17 presents the side-lap fastener brace force distribution of slender singly symmetric sections. Only the results of SS-100#19 L/d 15 and SS-100#39 L/d 15 configurations were plotted in order to provide continuity with Figure 6.16. In the figure SS-100#19 L/d 15 is represented with asterisk. Circle markers represent the SS-100#39 L/d 15 series.

Similar to Figure 6.16, Figure 6.17 indicates that the brace forces in section SS-100#39 with an L/d of 15 are higher than those of section SS-100#19 L/d 15.

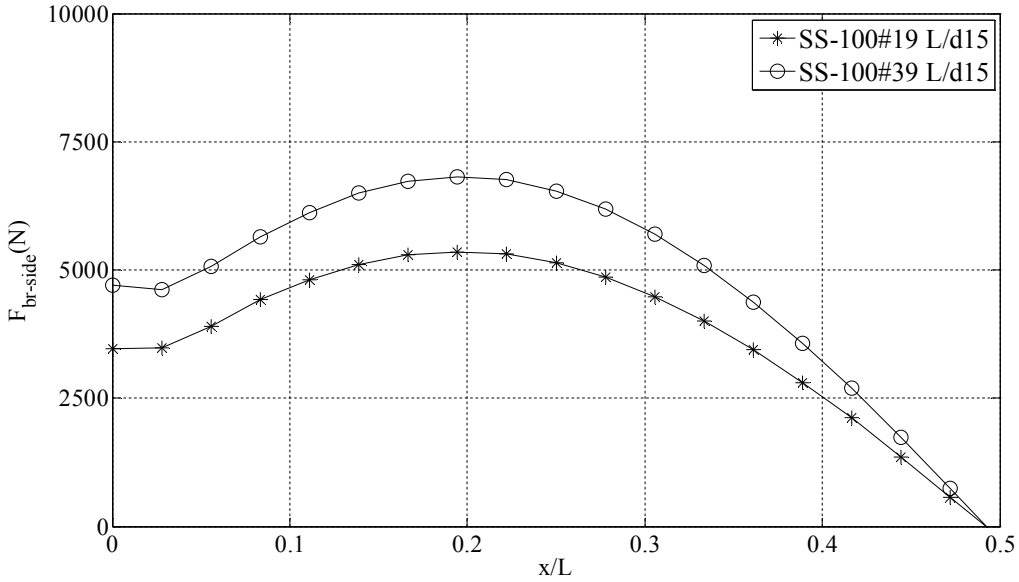

Figure 6.17. Slender singly symmetric sections side-lap fastener brace force distribution

6.5.2. Normalized Fastener Force Distribution

Figure 6.18 and Figure 6.19 demonstrate the edge fastener normalized resultant brace force ratio distribution and the side-lap fastener normalized brace force ratio distribution of slender singly symmetric sections, respectively.

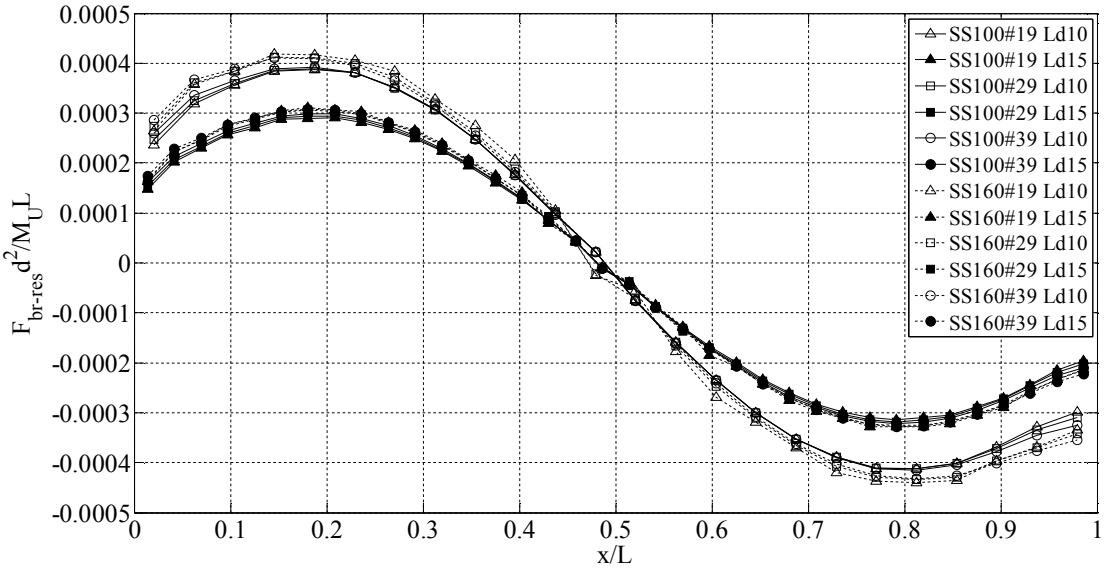

Figure 6.18. Slender singly symmetric sections edge fastener normalized resultant brace force ratio distribution

In Figure 6.18 and Figure 6.19, analyses with L/d ratio of 10 and 15 are represented with normal and filled markers respectively. Similar to the slender doubly symmetric sections results, it is seen in both figures that L/d ratio separates results in a major way. Analyses with lower L/d ratio results with higher normalized brace force ratios.

Analyses with web slenderness ratio of 100 and 160 are represented with continuous and dashed lines respectively in Figure 6.18 and Figure 6.19. It is figured out from both figures that analyses with lower web slenderness ratio results with higher normalized brace force ratios.

It is also noticed in both Figure 6.18 and Figure 6.19 that normalized force ratio distribution curves related to each analysis tend to coincide on each other for L/d ratio of 10 and 15. It is clear that in both figures normalized brace force value maximizes around the last 20% portion of the girder. Maximum normalized brace force ratio values are 0.00035 and 0.00030 for edge and side-lap fasteners respectively. For L/d ratio of 10 these values tend to increase by approximately 34% for both graphs.

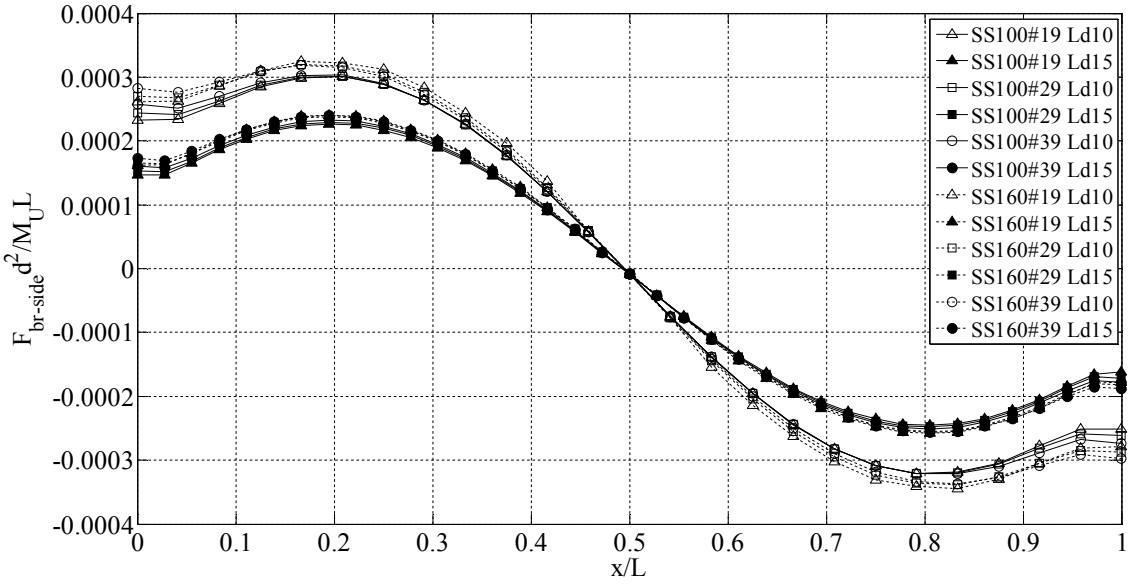

Figure 6.19. Slender singly symmetric sections side-lap fastener normalized brace force ratio distribution

6.6. Effect of Deck Thickness on Brace Forces

Figure 6.20 and Figure 6.21 demonstrates the edge fastener brace force distribution and the side-lap fastener brace force distribution of Slender-100#1 section L/d 15 analyses with 16, 18 and 20 gauge thick decks.

On both Figure 6.20 and Figure 6.21, analysis with 16-gauge thick deck is represented with asterisk marker series. 18 and 20-gauge deck analysis are represented with cross and circle markers respectively.

Figure 6.20 and Figure 6.21 presents large displacement analysis results with three different deck thicknesses with an equal amount of deck shear rigidity, 12507 kN/rad. Major difference between the three large displacement analyses is the amount of diagonal truss element area that corresponds to an equal deck shear rigidity. Diagonal truss element area was calculated according to the test frame analyses with different deck thicknesses. The difference in test frame analyses between different deck thicknesses is the appropriate stiffness of edge and side-lap fasteners.

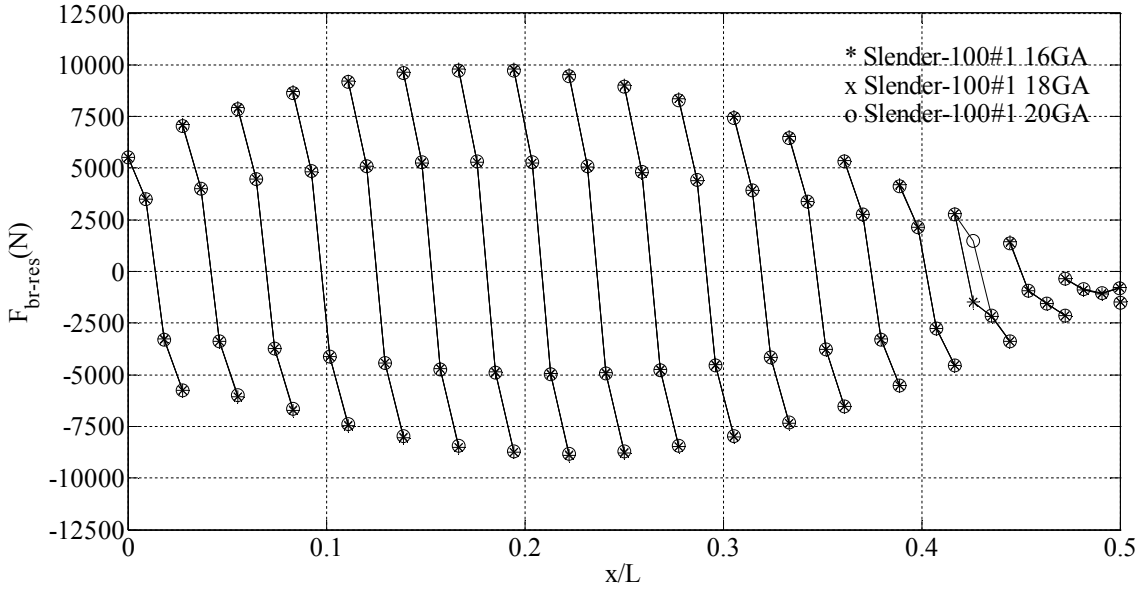

Figure 6.20. Deck thickness effect on edge fastener resultant brace force distribution

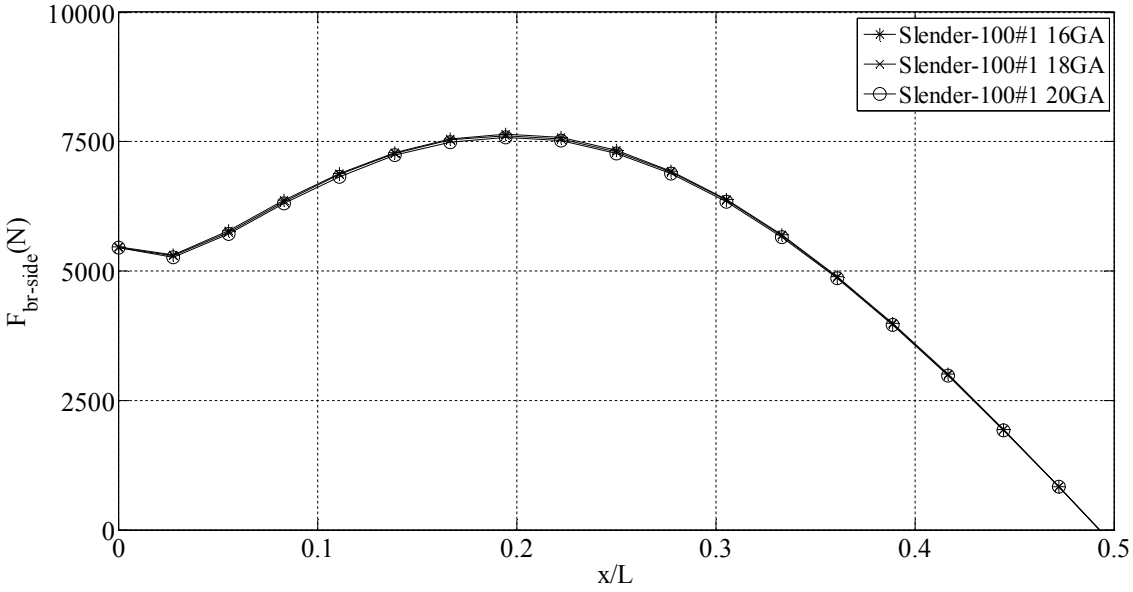

Figure 6.21. Deck thickness effect on side-lap fastener brace force distribution

According to the figures above, deck thickness does not have a major effect on brace forces as long as equal deck stiffness is provided.

6.7. Effect of Deck Width on Brace Forces

Figure 6.22 and Figure 6.23 demonstrate the edge fastener brace force distribution and side-lap fastener brace force distribution of Slender-100#1 section L/d 15 analyses with 610 mm wide and 1220 mm wide decks.

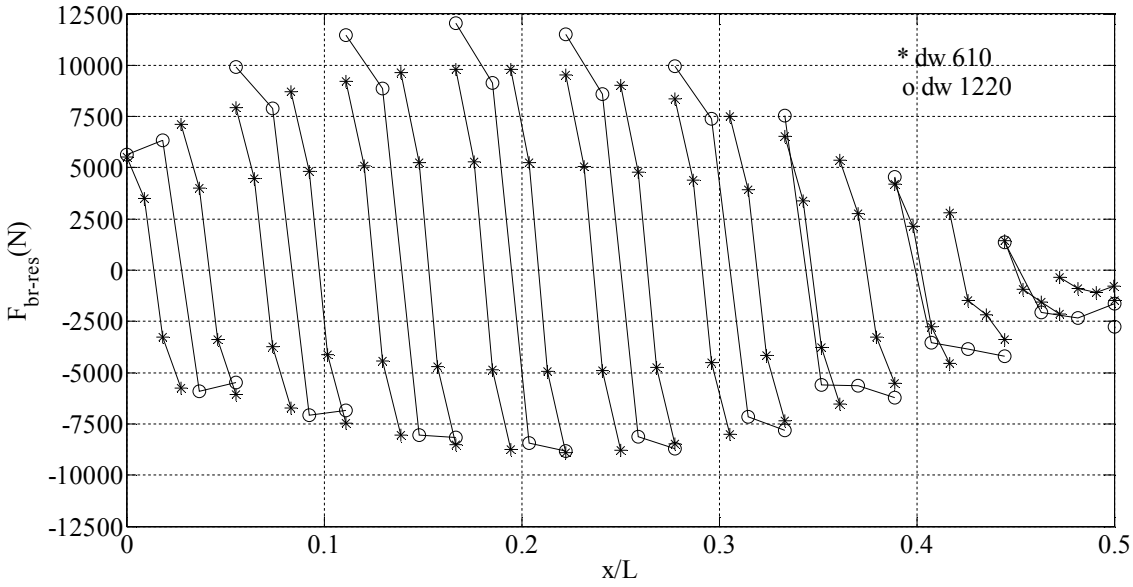

Figure 6.22. Deck width effect on edge fastener resultant brace force distribution.

On both Figure 6.22 and Figure 6.23, analysis with 610 mm wide deck is represented with asterisk marker series. Analysis with 1220 mm wide deck is represented with circle markers.

Figure 6.22 and Figure 6.23 presents large displacement analyses results with two different deck widths with an equal amount of deck shear rigidity, 12507 kN/rad. Diagonal truss element area values that provide the specified deck shear rigidity were calculated according to the test frame analysis with corresponding deck widths.

According to the Figure 6.22, edge fastener brace forces increase by about 25% with a 1220 mm deck. On the other hand, deck width did not have a major effect on side-lap fastener brace forces according to the brace force distribution curves which are almost coincident in Figure 6.23.

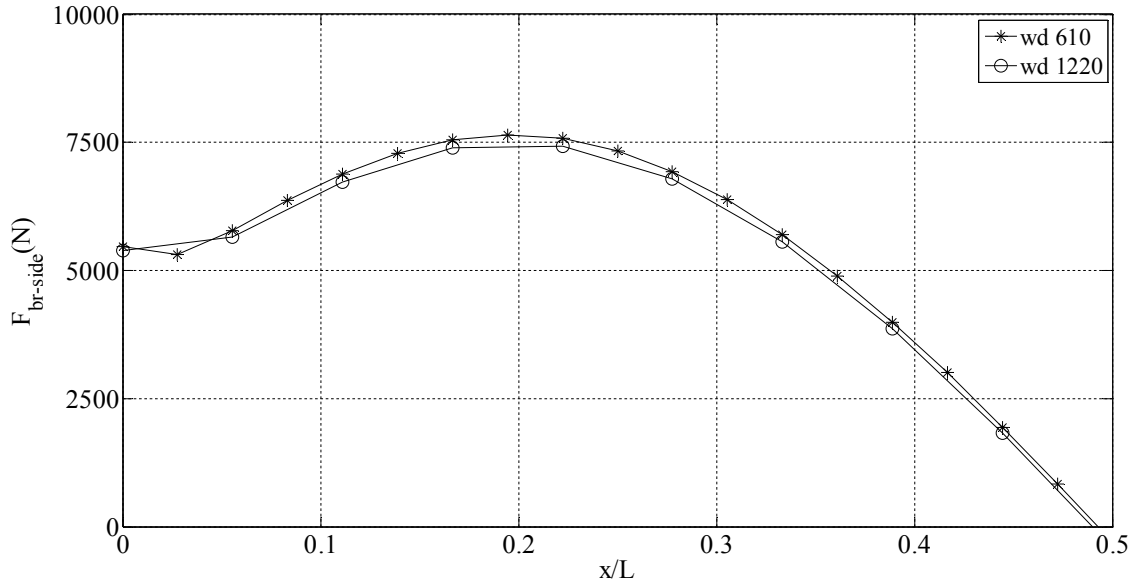

Figure 6.23. Deck width effect on side-lap fastener brace force distribution

6.8. Effect of Number of Edge Fasteners on Brace Forces

Figure 6.24 and Figure 6.25 demonstrate the edge fastener resultant brace force distribution and side-lap fastener brace force distribution for Slender-100#1 section L/d 15 analyses with 3, 4 and 5 edge fasteners on sheet and girder connection.

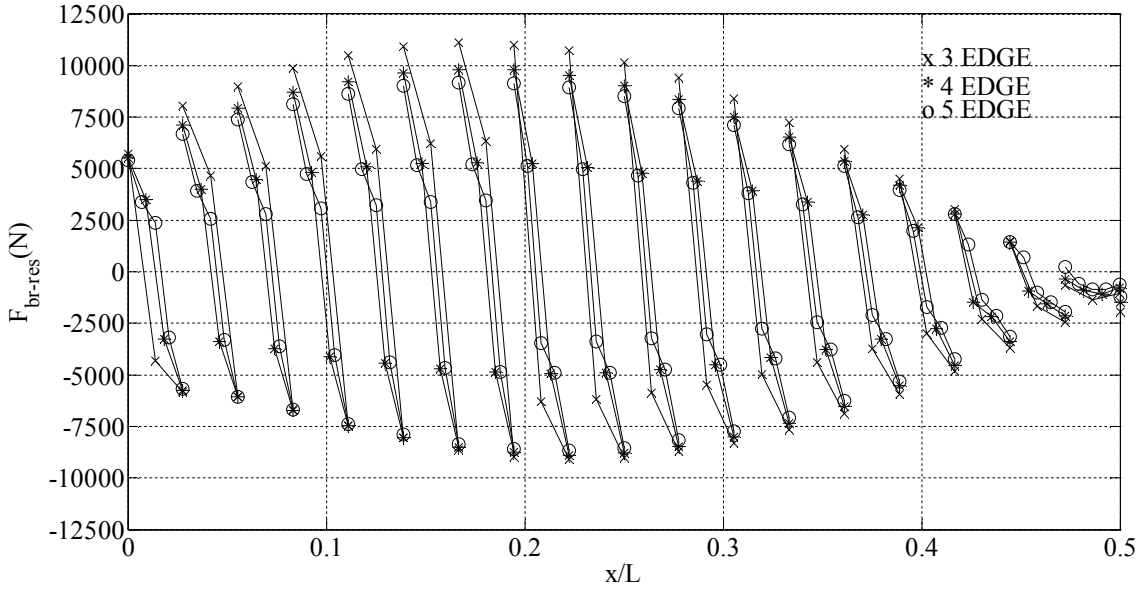

Figure 6.24. Number of edge fastener effect on edge fastener resultant brace force distribution

On both Figure 6.24 and Figure 6.25, analysis with deck sheet-girder connection by 3 edge fasteners is represented with cross marker series. Analysis with 4 and 5 edge fasteners are represented with asterisk and circle markers, respectively.

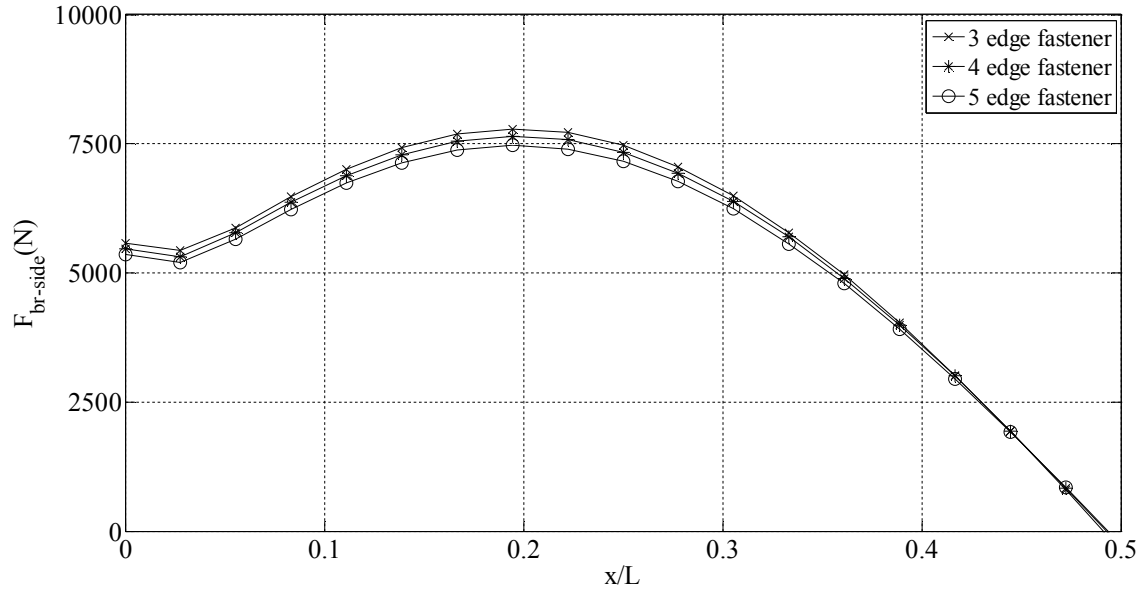

Figure 6.25. Number of edge fastener effect on side-lap fastener brace force distribution

Figure 6.24 and Figure 6.25 presents large displacement analyses results with three different deck sheet-girder connection configurations with an equal amount of deck shear rigidity, 12507 kN/rad. Similar to the deck thickness and deck width effect

investigations, diagonal truss element area values that provide the specified deck shear rigidity were calculated according to the test frame analysis with corresponding deck configurations.

According to the figures above, an increase in the number of edge fasteners does not affect the brace forces generated in the side-lap fasteners. On the other hand the increase in the number of edge fasteners decreases the brace force level in each edge fastener in case of equal deck stiffness. According to the Figure 6.24, providing 3 fasteners in deck sheet-girder connection resulted with a resultant brace force of 11100 N. in each fastener. Further increasing the amount of fasteners decreased the resultant force level to 9805 N., 9194 N. for 4 and 5 fasteners respectively.

6.9. Effect of Number of Side-Lap Fasteners on Brace Forces

Figure 6.26 and Figure 6.27 demonstrate the edge fastener resultant brace force distribution and the side-lap fastener brace force distribution of Slender-100#1 section L/d 15 analysis with 4, 5 and 6 fasteners on sheet to sheet connections.

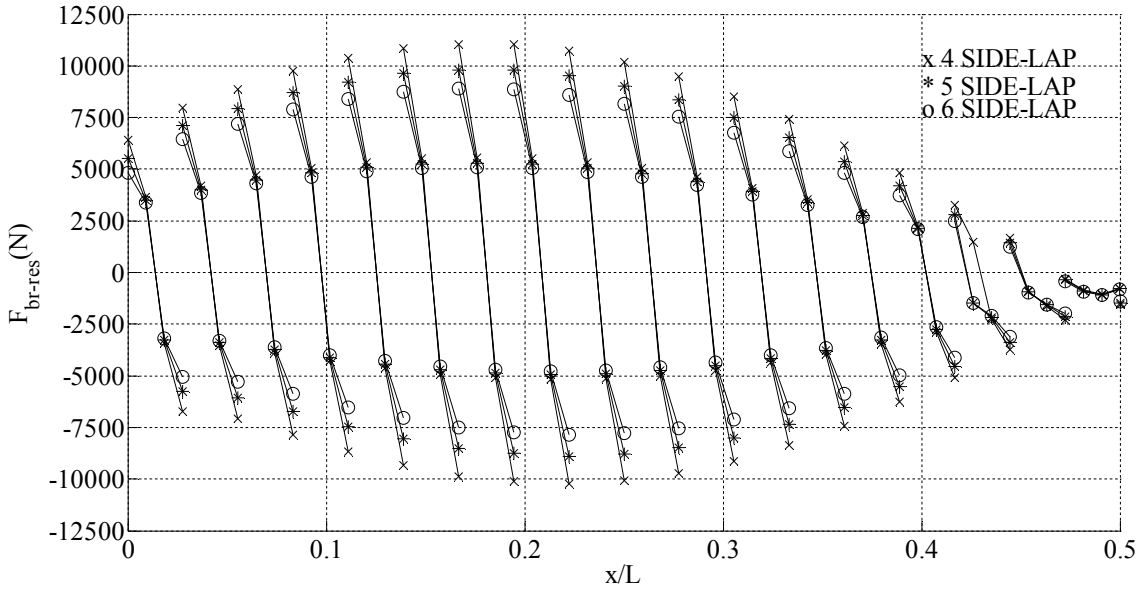

Figure 6.26. Number of side-lap fastener effect on edge fastener resultant brace force distribution

On both Figure 6.26 and Figure 6.27, analysis with sheet to sheet connections by 4 side-lap fasteners is represented with cross marker series. Analysis with 5 and 6 side-lap fasteners are represented with asterisk and circle markers respectively.

Figure 6.26 and Figure 6.27 presents large displacement analyses results with three different sheet to sheet connection configurations with an equal amount of deck shear rigidity, 12507 kN/rad. Similar to the deck thickness and deck width effect investigations, diagonal truss element area values that provide the specified deck shear rigidity were calculated according to the test frame analysis with corresponding deck configurations.

According to the Figure 6.26 and Figure 6.27, an increase in the number of side-lap fasteners decreases the brace forces generated in a single side-lap fastener. On the other hand an increase in the number of side-lap fasteners decreases the brace force level in each edge fastener in case of equal deck stiffness.

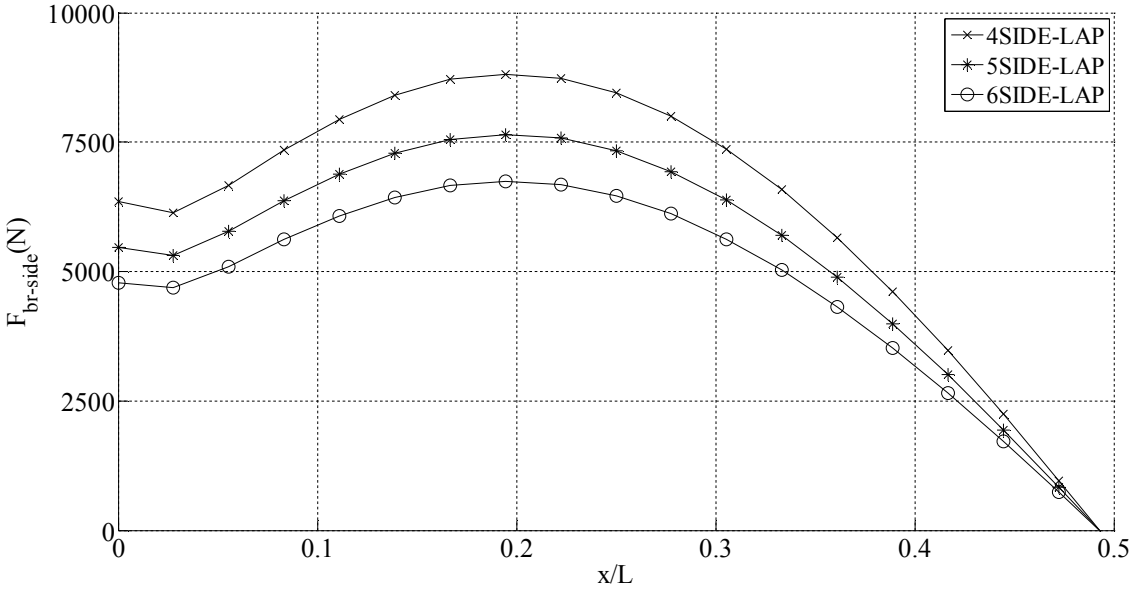

Figure 6.27. Number of side-lap fastener effect on side-lap fastener brace force distribution

According to the Figure 6.26, providing 4 fasteners in sheet to sheet connections resulted with a resultant brace force of 11030 N. in each deck sheet-girder connection fastener. Further increasing the amount of fasteners decreases the resultant brace force level to 9805 N., 8886 N. for 5 and 6 fasteners respectively.

According to the Figure 6.27 providing 4 fasteners in sheet to sheet connections resulted with a brace force of 8817 N. in each side-lap fastener. Further increasing the amount of fasteners decreases the side-lap fastener brace force level to 7641 N. and to 6740 N. for 5 and 6 fasteners respectively.

6.10. Comparison of the Results with Previous Studies

Figure 6.28 presents the deck brace moment, M_{br} comparison of section Stocky#2 with the Section#3 of Helwig (2008-II) with various span-to-depth ratios under 345 MPa bending stress level. Section#3 is an I-shaped steel girder section with a web height of 762 mm and a 12.7 mm web thickness. In Figure 6.28 horizontal axis represents mid point location of each deck through the girder. Vertical axis represents the deck brace moment.

In the figure Stocky#2 section is represented with standard markers. Filled markers represent the Section#3 results. In Figure 6.28 horizontal axis is limited to the half-span according to the data from Helwig (2008-II).

Deck moments were calculated according to the Section 6.2. According to Figure 6.28 results are satisfactorily close to the results by Helwig (2008-II).

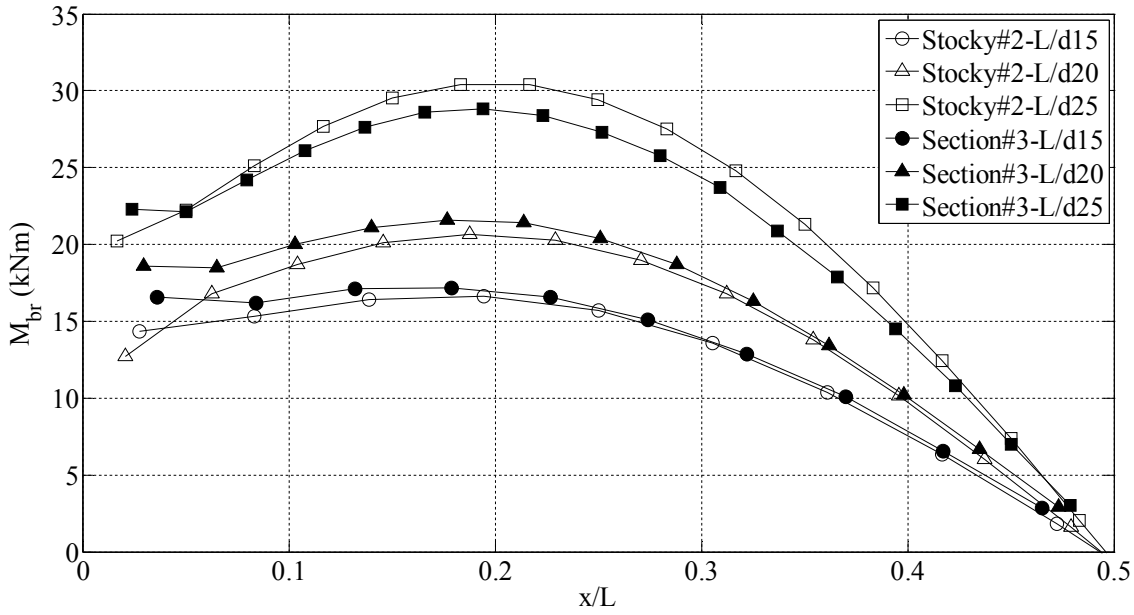

Figure 6.28. Moment calculation and comparison with a previous study

6.11. Strength Requirements

Normalized brace force ratio graphs for stocky, slender doubly symmetric and slender singly symmetric sections in the preceding pages demonstrated the distribution of the normalized brace force ratios. It was observed in these figures that most of the curves representing several large displacement analysis coincided on each other for both

edge and side-lap fastener results. In addition it was also observed that some curves for specific L/d ratios coincided on each other but diverged from the majority.

Vertical axis of the graphs can be named as normalization factor X_{br} that corresponds to the ratio of, $X_{br} = \frac{F_{br}}{M_{u-210}} \times \frac{1}{\left(\frac{L_b}{d^2}\right)}$. By using this ratio, brace forces can be obtained by Equation 7.1.

$$F_{br} = X_{br} * M_{u-210} * \left(\frac{L_b}{d^2}\right) \tag{7.1}$$

where,

F_{br} = Fastener brace force level;

X_{br} = Normalization factor;

$M_{u\text{-}210}$ = Mid-span moment of steel girder or beam under 210 MPa flexural stress;

L_b = Unbraced length of the steel girder or beam;

d = Depth of the beam.

Normalized brace force ratio distribution in the figures is like a sine wave. Peak points of these curves indicate the maximum brace force that occurred in the analyses. Different peak points were observed from the normalization figures for stocky, slender doubly symmetric and slender singly symmetric sections. Consecutive values for edge and side-lap fasteners are demonstrated in Table 6.3.

Table 6.3 Normalization factors for fastener brace forces

4 EDGE, 5 SIDE-LAP FASTENER $4Q_i$ / 210 MPa w_d=610 mm		X_{br} **NORMALIZATION FACTOR**	
Cross Section Type	Cross Section properties	Edge Fastener Resultant Force	Side-Lap Fastener Force
DOUBLY SYM.	$\lambda_w \leq 60$ $L/d \leq 15$	0.00030	0.00020
	$\lambda_w \leq 60$ $L/d > 15$	0.00025	0.00020
	$\lambda_w > 60$ $L/d \leq 10$	0.00050	0.00040
	$\lambda w > 60$ $L/d > 10$	0.00040	0.00030
SINGLY SYM.	$\lambda_w > 60$ $L/d \leq 10$	0.00045	0.00035
	$\lambda w > 60$ $L/d > 10$	0.00035	0.00030

Note that X_{br} values in the Table 6.3 are obtained directly from the peak values of the brace force normalization graphs. Since those graphs are the results of large displacement analyses with standard configurations, normalization factor values are directly applicable to the systems with standard configurations as indicated in the upper left cell in Table 6.3.

Standard deck-girder configuration implies to the systems with:

- Maximum flexural stress level of 210 MPa at the extreme fiber of the girder cross-section,
- 4 times the ideal deck stiffness,
- 610 mm deck sheet width,
- 4 fasteners in the deck sheet and girder connection, 5 fasteners in the adjacent sheet over laps.

For systems with different configurations a correction factor, can be proposed according to the brace force distribution graphs in Section 6.6 to Section 6.9. Correction factor, C_{br} is simply the ratio between the peak values of standard configuration and shifted configurations. Correction factors are listed in Table 6.4. Note that Table 6.4 can be directly used for configurations with 18 or 20-gauge thick decks as long as the necessary deck stiffness is provided.

Table 6.4. Correction factors for fastener brace forces

	C_{br}	
Configuration type	**For Edge Fasteners**	**For Side-lap Fasteners**
3 edge fastener	1.15	1.00
4 edge fastener	1.00	1.00
5 edge fastener	0.95	1.00
4 side-lap fastener	1.13	1.15
5 side-lap fastener	1.00	1.00
6 side-lap fastener	0.90	0.90
$w_d = 610$	1.00	1.00
$w_d = 1220$	1.25	1.00

CHAPTER 7

CONCLUSIONS

7.1. Summary and Conclusions

In this study strength requirements of shear diaphragms used for stability bracing of steel I-beams and girders is investigated with a parallel companion study on the stiffness requirements of the shear diaphragms as well. Three-dimensional finite element analysis program ANSYS Mechanical APDL (2007) was used in order to perform parametrical studies. Parametrical studies were conducted on a twin girder-shear diaphragm system finite element model. Finite element model was verified according to a full-scale twin-girder shear diaphragm buckling test conducted by Egilmez et al. (2005). Shear displacement analyses were conducted on a test frame model in order to perform large displacement analyses on the twin girder-shear diaphragm system with adequate stiffness values. Afterwards large displacement analyses were conducted on twin girder-shear diaphragm systems with various configurations. Distribution of the brace forces through the girders is illustrated for both edge and side-lap fasteners according to the large displacement analyses. In order to capture a general response for girders with several cross sections, brace forces were normalized according to the girder characteristic dimensions.

According to the brace force graphs the findings are as follows;

- Along the length of the beam maximum brace forces occur around quarter span, where the shear deformations are maximum.
- Higher brace forces develop in sections which could sustain higher flexural moments, therefore higher compression forces, due to larger moment of inertias.
- Increasing the span to depth ratio resulted with larger brace force values.
- Maximum brace force of the edge fasteners in a single deck generates within the first and the last fasteners.

- The side-lap fastener forces are higher than the edge fastener connections and the capacity of side-lap connections is smaller than that of the edge fastener connections,

According to the normalized brace force graphs the findings are as follows;

- For the stocky sections; normalized force distribution curves for L/d ratios of 20, 25 and 30 coincide with each other. Curves for L/d of 10 again coincided on each other but diverged from the majority.
- For the slender sections, curves were coincident depending on the L/d ratio. Lower L/d ratio lead to higher normalized brace force ratios. In addition, lower web slenderness ratio resulted to lower ratios. For the slender singly symmetric sections, curves were coincident depending on the L/d ratio as well. Lower L/d ratio lead to higher normalized brace force ratios. In addition, lower web slenderness ratio resulted to lower ratios.

The findings are as follows according to different deck configurations rather than the standard;

- Deck thickness does not have a major effect on brace forces as long as equal deck stiffness is provided.
- Edge fastener brace forces increased with a wider deck. On the other hand, deck width did not have a major effect on side-lap fastener brace forces.
- Increasing the number of edge fasteners did not affect the brace forces generated in the side-lap fasteners. On the other hand, the increase in the number of edge fasteners decreased the brace force level in each edge fastener in case of equal deck stiffness.
- Increasing the number of side-lap fasteners decreased the brace forces generated in a single side-lap fastener. On the other hand, an increase in the number of side-lap fasteners decreased the brace force level in each edge fastener in case of equal deck stiffness.

In conclusion, according to the normalization process an equation is proposed to estimate the fastener brace forces for various types of deck and girder configurations in the design phase of steel decks bracing steel girders. Proposed equation is scaled with a correction factor that serves for different systems rather than standard deck and girder configurations.

REFERENCES

Akbaba, A. (2015). *Stiffness Requirements of Shear Diaphragms Used to Brace Steel I-Beams.* Unpublished M.S. Thesis, Department of Civil Engineering; Izmir Institute of Technology, to be submitted February 2015

American Association of State Highway and Transportation Officials. (2012). *AASHTO LRFD bridge design specifications, customary U.S. units*. Washington, DC: American Association of State Highway and Transportation Officials.

American Institute of Steel Construction. (2001). *Load and resistance factor design specification for structural steel buildings*. Chicago, Ill: American Institute of Steel Construction.

American Institute of Steel Construction. (2005). *Specification for structural steel buildings*. Chicago, Ill: American Institute of Steel Construction.

American Institute of Steel Construction. (2010). *Specification for structural steel buildings*. Chicago, Ill: American Institute of Steel Construction.

ANSYS Inc. (2011). Elements Reference. *Release 14.0 Documentation for ANSYS.*

Cordeck Building Solutions (2014). Floor Decks. Retrieved December 28, 2014, from http://www.cordeck.com/metal-deck-products/form-deck

Davies, J. M., & Bryan, E. R. (1982). *Manual of stressed skin diaphragm design*. London: Granada.

Egilmez, O. Ö. (2005). *Lateral Bracing of Steel Bridge Girders by Permanent Metal Deck Forms.* Ph.D. Dissertation Department of Civil and Environmental Engineering; State University of Houston.

Egilmez, O. Ö., Helwig, T. A., Jetann, C. A., & Lowery, R. (2007). Stiffness and strength of metal bridge deck forms. *Journal of Bridge Engineering*, *12*(4), 429-437.

Egilmez, O. Ö., Helwig, T. A., & Herman, R. (2009). Lateral stiffness of steel bridge I-girders braced by metal deck forms. *Journal of Bridge Engineering*, *14*(1), 17-25.

Egilmez, O. Ö., Helwig, T. A., & Herman, R. (2012). Buckling behavior of steel bridge I-girders braced by permanent metal deck forms. *Journal of Bridge Engineering*, *17*(4), 624-633

Egilmez, O. Ö., Akbaba, A., & Vardaroglu, M. (2014). Stiffness and strength of shear diaphragms used for stability bracing of slender beams. *Proceedings of the Annual Stability Conference Structural Stability Research Council,* Toronto.

Errera, S., & Apparao, T. (1976) Design of I-shaped beams with diaphragm bracing. *J. Struct. Div.*, ASCE, 102(4), 769–781.

Galambos, T. V. (1998). *Guide to stability design criteria for metal structures*. New York: John Wiley.

Helwig, T. A. (1994). *Lateral Bracing of Bridge Girders by Metal Deck Forms.* Ph.D. Dissertation Faculty of the Graduate School; State University of Texas.

Helwig, T. A., Frank, K. H., & Yura, J. A. (1997). Lateral-torsional buckling of singly symmetric I-beams. *Journal of Structural Engineering*, *123*(9), 1172-1179.

Helwig, T. A., & Frank, K. H. (1999). Stiffness requirements for diaphragm bracing of beams. *Journal of Structural Engineering*, *125*(11), 1249-1256.

Helwig, T. A., & Yura, J. A. (2008). Shear diaphragm bracing of beams. I: Stiffness and strength behavior. *Journal of Structural Engineering*, *134*(3), 348-356.

Helwig, T. A., & Yura, J. A. (2008). Shear diaphragm bracing of beams. II: Design requirements. *Journal of Structural Engineering*, *134*(3), 357-363.

Helwig, T. A. (2013). *2013 NASCC presentations: Steel Bridge Design Handbook Session* [Video]. Retrieved from http://media.aisc.org/NASCC2013/B3.mp4.

Kitipornchai, S. & Trahair, N. (1980). Buckling Properties of Monosymmetric I-Beams. *Journal of the Structural Division*, ASCE, *106*(STS), 941-957.

Lawson, R., & Nethercot, D. (1985). Lateral stability of I-beams restrained by profiled sheeting. *The Struct. Engr.*, London, 63B(1), 3-13.

Luttrell, L. D., & Steel Deck Institute. (2004). *Diaphragm design manual*. Canton, Ohio: Steel Deck Institute.

Nethercot, D., & Trahair, N. (1975). Design of diaphragm-braced I-beams. *J. Struct. Div.*, ASCE, 101(10), 2045–2061.

New York State Department of Transportation. (2009). *US Route 219: Southern Expressway*. Retrieved December 28, 2014 from https://www.dot.ny.gov/regional-offices/region5/projects/us-route-219-section5/photos

Owen, T. (2013, April 29). Composite floor system [Web log post]. Retrieved December 28, 2014, from http://tanya1.myblog.arts.ac.uk/2013/04/29/task-8-ludwig-mies-van-der-rohe-alumni-hall/

Texas Department of Transportation (2014). *Bridge Standards.* Retrieved December 28, 2014, from http://www.dot.state.tx.us/insdtdot/orgchart/cmd/cserve/standard/bridge-e.htm

Timoshenko, S., & Gere, J. M. (1961). *Theory of elastic stability*. New York: McGraw-Hill.

U.S. Department of Transportation Federal Highway Administration. (2013). *LRFD Steel Girder Super Structure Design Example.* Retrieved December 28, 2014, from http://www.fhwa.dot.gov/bridge/lrfd/us_ds3.cfm

Wang, L., & Helwig, T. A. (2005). Critical imperfections for beam bracing systems. *Journal of Structural Engineering*, *131*(6), 933-940.

Weeks, J. (2014, December 28). John James Audubon Bridge LA-10 Mississippi River crossing at New Roads [Web log post]. Retrieved December 28, 2014, from http://www.johnweeks.com/river_mississippi/pages/lmiss19.html

Winter, G., (1960) Lateral bracing of columns and beams. *Trans Am. Soc. Civ. Eng.*, 125, 809-825.

Ziemian, R. D. (2010). *Guide to stability design criteria for metal structures*. Hoboken, N.J: John Wiley & Sons.

APPENDIX A

TABLES

Table A.1. Cross sectional properties with finite element ratios

SECTION DESIGNATION	Web aspect ratio	Top flange aspect ratio	Bottom flange aspect ratio
Stocky#1	2.34	2.90	2.90
Stocky#2	1.17	1.45	1.45
Slender-100#1	1.74	1.36	1.36
Slender-160#1	1.74	1.36	1.36
Slender-100#2	2.19	1.36	1.36
Slender-160#2	2.19	1.36	1.36
SS-100# 19	1.75	1.94	1.36
SS-100# 29	1.74	1.69	1.36
SS-100# 39	1.74	1.51	1.36
SS-160# 19	1.75	1.94	1.36
SS-160# 29	1.74	1.69	1.36
SS-160# 39	1.74	1.51	1.36

Table A.2. A List of conducted finite element analyses

SECTION DESIGNATION	# of edge fasteners	L/d	# of side-lap fasteners	σ (MPa)	nQ_i	Deck thickness (Ga)	w_d (mm)
Stocky#1	4	15	5	210	2-3-4-5	16	610
		20					
		25					
		30					
Stocky#2	4	15	5	210	2-3-4-5	16	610
		20					
		25					
		30					
		15		345	4		
		20					
		25					
Slender-100#1	4	10	5	210	2-3-4-5	16	610
		15					
	3-5	15	5	210	4	16	610
	4	15	4-6	210	4	16	610
	4	15	5	210	4	16	1220
	4	15	5	210	4	18-20	610
Slender-160#1	4	10	5	210	2-3-4-5-6	16	610
		15			2-3-4-5		
Slender-100#2	4	10	5	210	2-3-4-5	16	610
		15					
Slender-160#2	4	10	5	210	2-3-4-5	16	610
		15			2-3-4-5-6		
SS-100#19	4	10	5	210	2-3-4-5	16	610
		15					
SS-100#29		10					
		15					
SS-100#39		10					
		15					
SS-160#19		10					
		15					
SS-160#29		10					
		15					
SS-160#39		10					
		15					

APPENDIX B

DESIGN EXAMPLE

Girder Properties:

- Stocky #2 girder
- n, Number of girders: 4
- t_d, Deck thickness: 20 cm
- s_g, Girder spacing: 3.50 m
- L_b, Unbraced length = 14.64 m
- A, Cross sectional area: 18432 mm^2
- $S_{x\text{-}x}$: 4431999 mm^3

1. Design Load calculation:

- Steel girder self weight:

$$18432 mm^2 \times 7.6518 \times 10^{-5} \frac{N}{mm^3} = 1.41 \frac{N}{mm} = 1.41 \frac{kN}{m}$$

- Concrete slab:

$$23.6 \frac{kN}{m^3} \times 3.5m \times 0.20m = 16.52 \frac{kN}{m}$$

- Construction live load $\left(40 \quad \frac{lb}{ft^2}\right) = \left(1.9052 \quad \frac{kN}{m^2}\right)$

$$1.9052 \frac{kN}{m^2} \times 3.5m = 6.67 \frac{kN}{m}$$

Design load: $w = 1.41 + 16.52 + 6.67 = 24.60 \quad \frac{kN}{m}$

Design moment: $M = \frac{w \times L_b^{\,2}}{8} = 659 \quad kNm$

Use a Load Factor=1.3 for the construction condition;

Maximum bending stress: $\sigma = 1.3 \times \frac{M}{S_{x-x}} = 193 \quad MPa$

2. Check girder buckling capacity:

According to the AISC (2010) limit state of lateral torsional buckling is can be checked according to the limiting laterally unbraced length, Lr which is defined below within the Equation B.1. Capacity of a girder alone can be checked with Equation 2.3 as well.

$$L_r = 1.95 * r_{ts} * \frac{E}{0.7F_y}\sqrt{\frac{Jc}{S_{x-x}h_0} + \sqrt{\left(\frac{Jc}{S_{x-x}h_0}\right)^2 + 6.76\left(\frac{0.7F_y}{E}\right)^2}} \quad \text{(B.1)}$$

where,

L_r = Limiting laterally unbraced length for the limit state of inelastic lateral-torsional buckling, mm

r_{ts} = Effective radius of gyration $= \frac{\sqrt{I_y C_w}}{S_x} = 72.89$ mm;

E = Modulus of elasticity of steel, 200 000 MPa;

F_y = Specified minimum yield stress, 345 MPa;

J = Torsional constant, 1489536 mm^4;

c = coefficient, 1 for doubly symmetric I-shapes;

S_x = Elastic section modulus taken about the x-axis, 4431999 mm^3;

h_0 = Distance between the flange centroids, 714 mm;

I_y = Moment of inertia about the principal axis, 65956224 mm^4;

C_w = Warping constant, 8406035382639 mm^6;

Limiting laterally unbraced length, L_r is calculated as 7107 mm. $L_b > L_r$. Limit state of lateral-torsional buckling applies. Lateral torsional buckling capacity of a girder alone is not sufficient enough to resist a 210 MPa bending stress level. Brace is needed.

3. Determine diaphragm properties:

According to the Chapter 5, a deck with four times the ideal stiffness has to be chosen. Ideal deck stiffness can be obtained by an eigenvalue buckling analyses. In this design example Equation 2.15 is used for ideal deck stiffness calculation.

According to the Equation 2.2 M_{cr} is calculated as 349.98 kNm.

Coefficient "m" is picked as 0.5 from Table 2.1 for top flange loading without an intermediate brace. C_b^* is 0.80. M_u for 210 MPa bending stress is 930.72 kNm.

According to the data above, Q_{req}, Q_i is 1777.96 kn/rad. A total deck stiffness of 7111.84 kN/rad is needed. Applying Equation 2.7

$$s_d = \left(\frac{n-1}{n}\right) * s_g = \frac{3}{4} * 3.50 = 2.625 \text{ m.}$$

$$G' = \frac{Q}{s_d} = ' \frac{7111.84}{2.625} = 2709 \text{ kN/m/rad.}$$

A suitable diaphragm can be selected by using Luthrell (2004).

4. Calculate brace forces according to the Equation 7.1:

$\frac{L_b}{d} = 20$ and $\lambda_w = 58 < 60$. $X_{br-edge} = 0.00022$, $X_{br-side} = 0.00018$

C_{br} is 1.0 for a standard deck configuration.

According to the data;

$$F_{br-edge} = 0.00022 \times 930.72 \times \left(\frac{14.64}{0.732^2}\right) \times 1.0 = 5.65 \quad kN$$

$$F_{br-side} = 0.00017 \times 930.72 \times \left(\frac{14.64}{0.732^2}\right) \times 1.0 = 4.32 \quad kN$$